ESO/STC-324a

20.03.2003

UV – VIS – J+H band, Intermediate Resolution, High Efficiency Spectrograph for the VLT

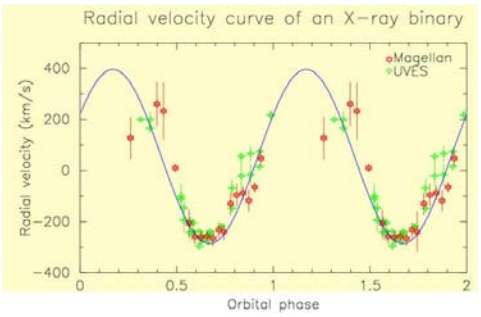

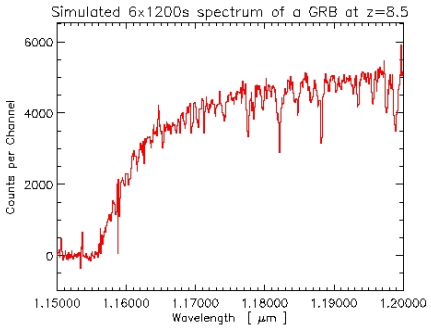

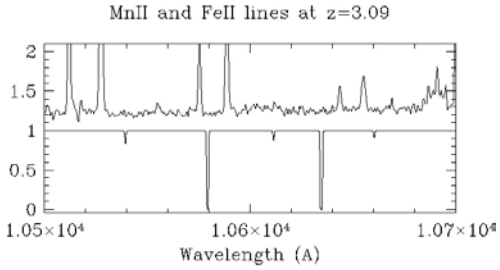

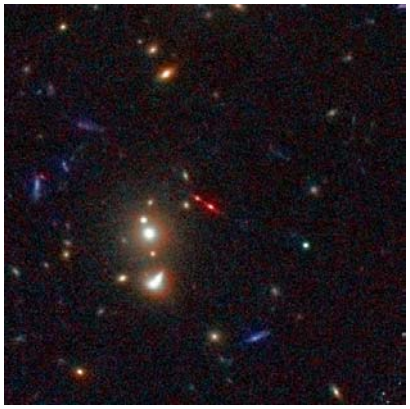

Lensed emission line galaxy at z =3.4

Part 1 – Science Case

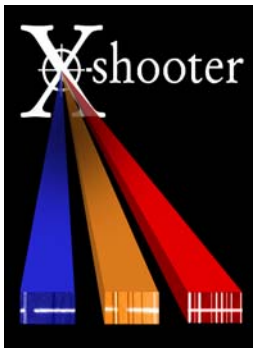

UV – VIS – J+H band, Intermediate Resolution, High Efficiency Spectrograph for the VLT

A Proposal for a 2nd Generation Instrument presented by

Lex Kaper, Astronomical Institute, University of Amsterdam, The Netherlands,
Per Kjærgaard, Copenhagen University Observatory, Denmark,
Roberto Pallavicini, INAF, Astronomical Observatory Palermo, Italy,
Sandro D'Odorico , ESO

Part 1 – Science Case

The X-shooter Science Team:

Jens Hjorth (Copenhagen): chairman and editor of Part 1, Michael Andersen (Potsdam), Piercarlo Bonifacio (Trieste), Andrea Cimatti (Arcetri), Fernando Comeron (ESO), Stefano Cristiani (Trieste), Sandro D'Odorico (ESO), Sara Ellison (ESO), Bob Fosbury (ESO), Claes Fransson (Stockholm), Johan Fynbo (Aarhus and Copenhagen), Paul Groot (Nijmegen), Lex Kaper (Amsterdam), Palle Møller (ESO), Roberto Pallavicini (Palermo), Elena Pian (Trieste) and Bjarne Thomsen (Aarhus)

20.03.2003

Contents

CHAPTER 1

Faint Object Spectroscopy with X-shooter

Spectroscopic observations of astronomical objects is, in its broadest definition, the foundation on which we build or discard astrophysical models of the universe and its inventory. The breathtaking progress in astrophysics within the last century can be traced directly back to the advances in spectroscopic techniques and instrumentation throughout the electromagnetic spectrum. Spectroscopy is a crucial tool for progress in astrophysics.

A number of very important astrophysical questions cannot be properly addressed with the current or near-future spectroscopic instrumentation for the UV to the NIR spectral range at the VLT. X-shooter is being proposed to fill this gap. To properly identify the requirements for this new instrument and to evaluate its potential impact on a variety of astrophysical topics we have studied a number of key science programs. A few synthetic snapshots of the X-shooter science case are presented in Section 1.1. The various trade-offs in spectroscopy of faint objects are discussed in Section 1.2. The main requirements on the performance of X-shooter are derived in Section 1.3. In Chapter 2, X-shooter is compared with other instruments at the VLT and at Keck. Its complementarity to other major facilities which will be operating in the same time frame is discussed in Section 2.4. Chapter 3 outlines the plans for the possible use of the guaranteed time and Chapter 4 gives the composition of the X-shooter Science Team. Individual science cases are presented in Chapters 5 through 7. Appendix A illustrates the Exposure Time Calculator that the Consortium has developed to quantify the expected performance of the instrument. In Part 2 of this X-shooter study we outline in detail the instrument concept and demonstrate its feasibility. We also include estimates of manpower, cost and schedule for the realization of the project. The name of X-shooter was chosen to reflect its capabilities of obtaining, in a highly efficient way, high quality spectra over a broad wavelength range of faint targets.

SECTION 1.1

Snapshots of the Science Case

X-shooter will have a broad and varied usage ranging from nearby intrinsically faint stars to bright sources at the very edges of the Universe. Below we summarize four key programs which are outlined in more detail in Chapters 5 to 7. The applicability of X-shooter will obviously be far wider than the cases presented in this document. Besides, history has shown that opening a new observing capability in observational astronomy will always lead to its own, unexpected results. We are confident that X-shooter will play a fundamental role at the VLT to quantify the evolution of stars and galaxies in our Universe.

1.1.1 Brown Dwarfs

The discovery of brown dwarfs has sparked much interest in the last five years. Brown dwarfs bridge the gap between stars and planets in mass and atmospheric properties. The unexplained existence of the

'brown dwarf desert' (no apparent brown dwarf companions to low-mass stars, in contrast to both planets and other low-mass stars), shows that our understanding of the formation of brown dwarfs is lacking in crucial areas. To understand and study brown dwarfs a detailed analysis of their atmospheres is needed. These are the most complex in the complete stellar and sub-stellar domain: molecule formation, stratification, 'weather' and zonal band due to convection (such as seen on Jupiter and Saturn) will likely cause an appearance similar to the Solar system's giant planets, but without irradiation from a central source. Brown dwarf spectra peak in the near-infrared and are dominated by molecular bands, broad alkali element absorptions and in the coolest objects very broad collision-induced H_2 absorption. The existence of 'weather' will cause strong spectroscopic variability, necessitating simultaneous broad-band observations to understand the physics and chemistry in brown dwarf atmospheres. The study of brown dwarfs requires a spectrograph that is highly efficient, has a broad wavelength coverage, especially including the non-thermal NIR, and a spectral resolution of R=5 000–10 000, which will allow a measurement of the brown dwarf rotation rates that are so important in layering the atmosphere. This resolution is also needed to resolve the night sky emission lines in the NIR region. The ability to resolve these lines is key in obtaining the required science.

1.1.2 Supernovae Type Ia Progenitors

Supernovae Type Ia are the signposts of cosmic acceleration, and determining their physics and origin is of paramount importance to understanding our Universe. Although it is generally agreed that SN Ia progenitors are exploding white dwarfs in binary systems, the type of binary system is still undetermined. Possible candidates range from merging detached white dwarfs to interacting binary white dwarfs and white dwarf-red dwarf pairs to symbiotics and super soft sources. The way to identify SN Ia progenitors is to understand the population characteristics (space densities, mass and orbital period distributions) and evolutionary histories of the possible progenitor populations. From this we can compare calculated explosion rates with observed SN Ia explosion rates. Most of the progenitor populations share that they are intrinsically faint (requiring a high efficiency spectrograph), in binaries (with orbital velocities $\geq$ 100 km s^{-1}), of composite spectral types (white dwarfs, accretion disks and secondary stars), variable (requiring simultaneous observations) and rare (<1 per square degree). A spectrograph with a wide wavelength coverage (U-H), high throughput and good spectral resolution (R=5 000–10 000) is absolutely essential to make the VLT the prime instrument for SN Ia progenitor research.

1.1.3 Gamma-Ray Bursts

Gamma-ray bursts remain a puzzle to this day. Evidence is mounting that they are closely linked to regions of star formation, but their origin remains shrouded in clouds. They have now been identified up to a redshift of $z = 4.5$, and no limit to the highest redshift is expected. Do they follow the overall star-formation rate in the Universe, or are they even good, unbiased tracers of the star-formation rate? Are they ultimately linked to the existence of very massive stars? When did these first occur? A burst at $z = 8.5$ is expected to be only one magnitude fainter than a $z = 3$ burst. Detecting these very high redshift GRBs will require an efficient spectrograph with NIR capabilities. The extremely rapid decline of the optical/NIR afterglow on a timescale of hours to days requires a fast and simultaneous observing campaign. GRBs offer a unique opportunity to study their host galaxies because the afterglows themselves fade from view over time. During the short afterglow phase, GRBs can also be used as lighthouses, illuminating the intergalactic medium and as such they serve as excellent, unbiased probes of the intergalactic structure. They hold the promise to do this up to very high redshifts ($z > 7$) in a way that is unavailable for any other astrophysical object. To study GRB afterglows in detail one therefore needs a highly efficient spectrograph that will make them observable to large redshifts during the burst phase (since they hardly ever reach $V < 18$ after a few hours), and that allows the chance to study their hosts in detail after the decline; a spectral resolution of R=5 000–10 000 is required to

study the circumburst and intergalactic environments, and a wide wavelength coverage will allow e.g. Lyα studies from $z = 1.6$ to $z = 15$, i.e. we will be able to study the GRBs with one setup without knowing their exact redshift.

1.1.4 The Metal Enrichment of the Early Universe

Quasar absorption line studies provide a unique opportunity to study metal abundances throughout the evolution of the Universe by the spectral absorption imprint left by all material between us and the source. With the introduction of the powerful echelle spectrographs HIRES at Keck and UVES at VLT, quasar absortion line studies have been providing a steady stream of new results on the properties of the IGM at high redshifts. While many questions have been answered and an overall scenario of the distribution of N(HI) and enriched material at high redshifts starts to emerge, many problems remains unanswered. Two significant examples are the structure of the IGM on scales up to a few Mpc and the abundances of the interstellar medium associated with galaxies at high redshifts as tracers of the star formation history at early epochs. In order to make a significant progress, we need to be able to study lines of sight toward QSOs significantly fainter than the current limits of HIRES or UVES (V$\sim$19). This is possible with a spectrograph of high efficiency, wide spectral range down to the atmospheric cutoff and intermediate resolution. Access to the non-thermal NIR will allow the simultaneous abundance analysis on rest-frame optical and UV transitions, a capability currently not possible on any other spectrograph.

SECTION 1.2

Optimizing Faint Object Spectroscopy

At low resolution (R$\leq$1 000), a spectrograph on an 8-m telescope is completely sky limited within a typical exposure time (a significant fraction of an hour) throughout the optical/near-IR spectral range. Thus, the resolution can be increased without loosing signal-to-noise per wavelength unit. At high resolution (>20 000), however, it is not possible to obtain sky continuum limited observations within a typical exposure time. Below we argue that there are several considerations that favor an intermediate resolution in the range 5 000–10 000 to fully exploit the spectroscopic capabilities of the VLT for the observations of faint objects.

1.2.1 The OH Night Sky Limit

The wavelength region from the R-band through the I-, J- and H-bands is dominated by intense and narrow (<1 km/s), and highly variable, OH emission lines, as shown in Fig. 1.1. For faint objects observed at low resolution this forest of night sky lines will be unresolved and the resulting spectrum will suffer from unquantifiable systematic errors, due to low-level irregularities in the detector pixel geometries and the slit jaws. In this situation it is not possible to ascribe a credible estimate of the noise associated with the individual spectral bins, effectively preventing the quantification of the significance of a detected spectral feature. At low resolution, the residual sky errors therefore impose a hard limit on the magnitude that can be reached and in particular on the detection of spectral features in absorption or emission, quite independently of the collecting area of the telescope. Using a large telescope at low spectral resolution has the advantage that the spectra of many objects in the field can be packed on the detector (e.g. the MOS modes of FORS2 or VIMOS) but it is not the optimal way to record the spectrum of a single faint object.

1.2.2 The Continuum Night Sky Limit

At high spectral resolution, where night sky emission lines only affect one in about 10^3 spectral elements, night sky lines are not a problem. At intermediate resolution, R=5 000–10 000, 80–90 % of all spectral elements are unaffected by strong sky lines. For a faint object observed at this resolution, spectral

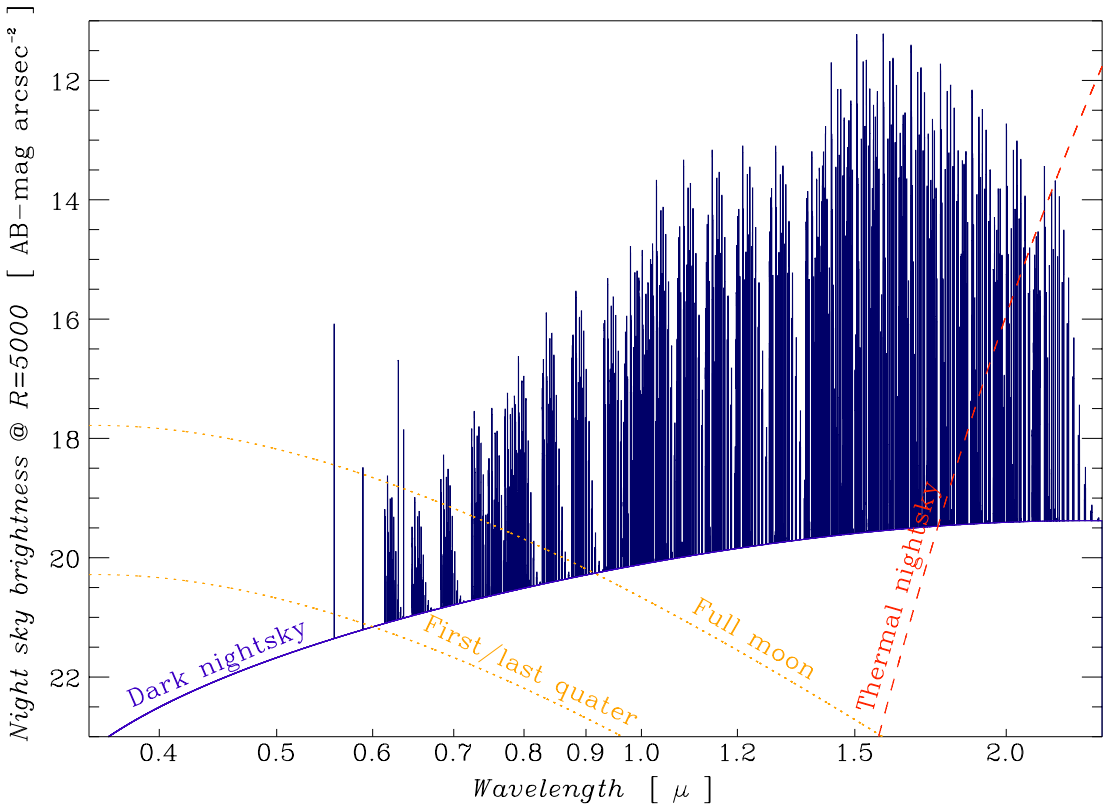

Figure 1.1 The night sky emission from the U-band to the K-band. For simplicity, atmospheric absorption bands are ignored. Under dark sky conditions the main components are airglow and OH emission. The model airglow + OH-spectrum is based on the observed broadband sky brightness and the compilation of OH lines by Rousselot et al. (2000). For the thermal emission a temperature of 273 K and an emissivity corresponding to the typical observed sky brightness, $K_{AB} = 14.3$ arcsec^{-2}, are assumed. The bright sky component from the full Moon is only including Raleigh scattering of sunlight from a grey Moon. Mie scattering on aerosols, which is difficult to quantify due to the variable aerosol content of the Earth atmosphere, would add a long wavelength tail, suggesting that the continuum sky beyond 1 μm may be affected by the Moon.

elements affected by sky lines would, when compared to spectral elements in the night sky continuum, not carry any significant information, as the night sky lines typically are several to many magnitudes brighter than the continuum (see Fig. 1.1). They are therefore best ignored (suppressed) in the reduction. Following the OH suppression, the line free spectral bins (about 85 % of the total) may be rebinned in order to increase the S/N. Through OH-suppression, the problem with systematic errors in the sky subtraction are bypassed. Note that when the OH sky lines are removed, the integrated night sky flux is reduced by about 0.2, 1.2, 3.5 and 4.5 magnitudes in the R-, I-, J- and H-bands respectively.

1.2.3 The Sky-Limited Resolution

Using an 8-m telescope and state of the art detector technology, a spectrograph working at $R = 5\,000$–$10\,000$ is completely sky limited at optical wavelengths within a typical exposure time of one hour. For a 30-min exposure at a resolution of about 5 000 through a $1''$ slit on a dark night, the signal-to-noise decreases by less than 10% due to read out noise, provided the noise is below 2.5–3 e^- in the optical and 6 e^- in the near-IR J- and H-bands respectively. These values are fully compatible with modern detectors.

SECTION 1.3

Science Requirements on X-shooter

From the above considerations it emerges that with 8-m telescopes we are now in a situation where for typical exposure times there is an overlap between the resolution at which the spectra are limited by the shot and flat-fielding noise of the sky continuum and the resolution required for efficient OH-suppression. This opens a window for spectroscopy of the faintest objects with optimum sky rejection and at a resolution which coincides with a vast number of astrophysical applications. Working at a resolution of 5 000–10 000, X-shooter is placed right in the center of this window. As compared to the previous generation of 4-m telescopes, this represents a transition into a new regime.

The core goal of X-shooter is to unleash the scientific potential of this transition, using the VLT. X-shooter should record the best possible spectrum of a single faint object, irrespectively of its magnitude (i.e. deeper limiting magnitudes can hardly be reached by a low dispersion spectrograph due to the sky background) using available technology. This is a core consideration which has to drive the X-shooter design.

1.3.1 Spectral Resolution

Apart from the technical considerations described above there are astrophysical requirements (hinted at in Sec. 1.1) that favor a spectral resolution of $R = 5\,000$–$10\,000$: Most spectra are obtained with the purpose of measuring spectral lines in absorption or emission. The favorite targets of X-shooter will be faint objects where high resolution, such as that provided by UVES, is unfeasible. There is a broad class of objects where intermediate resolution is fully adequate, but where low ($R \leq 1\,000$) resolution is inadequate. Three examples extracted from the science cases are:

- Emission lines from high redshift galaxies: These usually have a width of 100–300 km/s, and thus require a resolution of 1 000–3 000 to match the width of the lines. In the presence of bright night sky lines, an emission line of a faint object should be well resolved in order to avoid that the line is masked out by a night sky line. Working at a resolution $\geq 5\,000$ is therefore the only way to ensure that a possible emission line is detected.

- Intergalactic absorption lines: Absorption lines, such as those seen in faint quasars and GRBs contain vital information about the composition and structure of the intergalactic medium. These absorption lines have widths typically corresponding to a velocity dispersion of 5–20 km/s, often with multiple components mimicking a broader line with a velocity dispersion of more than 50

km/s. This corresponds to a line width of 10–100 km/s, or a resolution of 3 000–30 000. A resolution in the range 5 000–10 000 would be a workhorse resolution for IGM studies.

- Spectral lines in binary systems: Discrete emission or absorption components in reasonably close systems move at radial velocities typically with an amplitude of the order of 100–400 km/s. To resolve these binary motions a minimum velocity resolution of ∼60 km/s is needed. Therefore, a resolution of at least $R = 5\,000$ is needed to resolve these velocity fields. Almost all potential targets will be faint, V>19, so it will not be possible to work at much higher resolution.

1.3.2 Spectral Coverage

The spectral window, where the night sky continuum emission is very low, starts at the atmospheric UV-cutoff and ends around 2 μm with the onset of thermal emission from the atmosphere and the telescope (see Fig. 1.1). As there is a wide range of applications that will benefit from an instrument with a very broad spectral coverage, X-shooter will, for the first time ever, combine the UV, visible and near-IR (U–H band) and pull down the 'artificial walls' separating these wavelength ranges. Particularly the coverage of the UV and the NIR makes X-shooter unique. Two examples highlighting these capabilities are:

- **UV coverage**: The redshift range from 1–2.6 is of high astrophysical interest because it carries the key to the understanding of the formation of the Hubble sequence. Unfortunately this important redshift range is largely inaccessible to the VLT due to the lack of high-throughput instrumentation working below 4000 Å, where this epoch can be viewed in Lyα. In fact, there is not a single UV instrument in the world which can work in the sky limit at a resolution of 5 000 – this is pristine territory. There is therefore ample reason to extend the coverage of X-shooter as far into the UV as feasible. An 8-m ground-based telescope collects photons as fast as HST at 3000 Å, at a fraction of the cost, making it mandatory to cover at least down to this wavelength. In fact, as demonstrated by the comparison of the UVES and STIS observations of the same targets, the VLT competes well with HST in cost per photon down to about 2850 Å.

- **Near-IR coverage**: One obvious application, which has very much been driving the conceptualization of X-shooter is the determination of the redshifts of GRBs from their afterglow emission. The redshift of a GRB is *a priori* unknown and can be anywhere in the range $0 < z < 15$. All available evidence suggests that GRBs trace star formation throughout the universe and it thus appears feasible to determine the star formation history of the universe to redshifts of 15 using GRBs. In this context it is of utmost importance that there is continuous wavelength coverage up to the long wavelength end of the H band at 1.9 μm, since for the most interesting GRBs, at redshifts beyond 10, it will usually not be possible to derive a photometric redshift.

The capability of simultaneously covering the entire 0.3–1.9 μm wavelength range is a major advantage in photometrically and spectroscopically variable objects such as brown dwarfs, close binaries, accretion disks, supernovae and gamma-ray bursts. The coverage of the UV to the H-band minimizes variable slit losses, inter-instrument calibration errors and the need to schedule two telescopes at the same time when simultaneous observations are needed. For non-blackbody (multiple temperature) spectra, such as encountered in gamma-ray bursts, close binaries, accretion disks, QSOs and high redshift galaxies, the complete coverage allows the disentanglement of various contributors to the spectrum. As an example, the study of Lyα in high-redshift galaxies will be possible with X-shooter in the redshift range of $1.5 < z < 15$ in one and the same instrument.

The rationale in covering the full 0.3–1.9 μm range is driven by scientific requirements, but also imposed by the VLT operational model, which requires instruments to be permanently mounted. By covering this broad wavelength range with X-shooter, it is ensured that the optimum single-target instrument is always available at the VLT at any wavelength in the 0.3–1.9 μm range.

1.3.3 Efficiency

X-shooter is optimized for pushing the spectroscopic capabilities of the VLT to its limits. By dividing the light between three arms, X-shooter will have a throughput of $\gtrsim$25 % over most of the wavelength range. With this the limiting magnitudes will be (signal-to-noise=10 per spectral element in 60 min under typical conditions) 22.0, 22.6, 21.9, 21.7, 21.4, 20.7 and 20.0 in the U, B, V, R, I, J and H bands respectively (see Table A.1). By rebinning the OH-suppressed spectrum to low resolution, X-shooter can observe fainter objects than any other instrument at the VLT at any wavelength across the U to H spectral range. As an example, rebinning to a resolution of 500, after suppressing the spectral bins affected by OH emission, the limiting magnitudes for a signal-to-noise of 5 in 10 hours are 25.3, 26.0, 25.4, 25.3, 24.9, 24.0 and 23.3 in the U, B, V, R, I, J and H bands respectively (see Table A.1). This is achieved with an instrument which, having only one main configuration, is also operationally efficient.

1.3.4 Summary

The current and near-future instrumentation suite at the VLT is far from optimal for a broad range of astrophysical questions: there is a lack of a highly efficient (allowing access to the faintest of objects), medium resolution (R=5 000–10 000), broad band (300–1900 nm) spectrograph. Although such an instrument is already lacking, the need for this will become even more urgent when current first generation VLT instruments (especially FORS and ISAAC) will retire. To answer our astrophysical questions and to fill this vacuum in the VLT instrumentation we propose to build X-shooter.

CHAPTER 2

Comparison with Other Instruments

X-shooter will not only fill an important gap in the VLT instrumentation suite, it will also have unique capabilities among instrumentation at large telescopes worldwide. In this chapter we compare the instrument with existing VLT spectrographs and with ESI and NIRSPEC at the Keck telescopes.

SECTION 2.1

Overview of X-shooter Performance

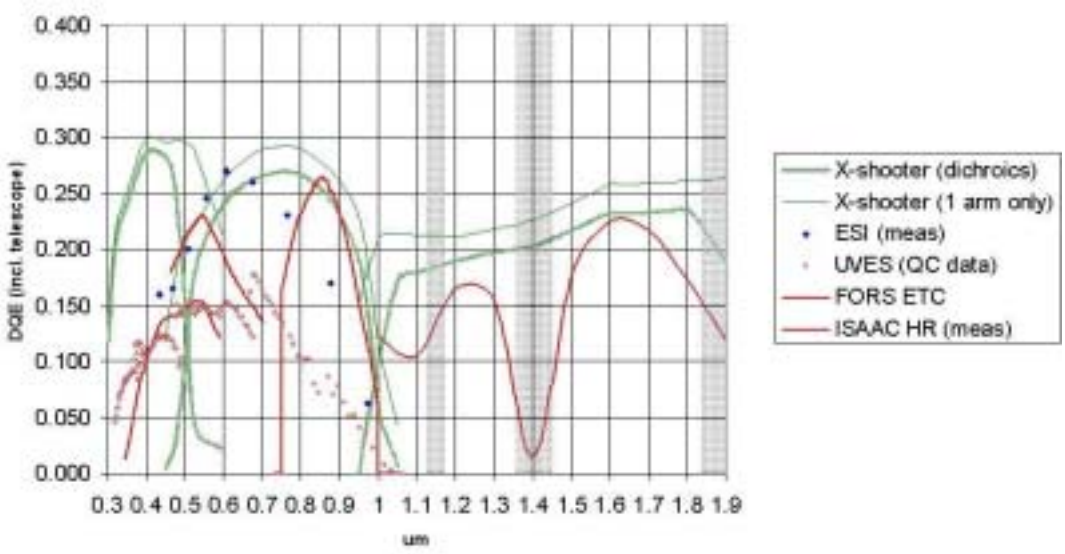

Figure 2.1 Predicted efficiency of the three arms of X-shooter compared with other instruments of the VLT and ESI at Keck 2. Telescope reflections are included, atmosphere is not. For the UV and Visual arms, values of blaze peaks in the echelle orders are used for a consistent comparison with UVES and ESI. In the IR, echelle order average efficiencies are compared with the ISAAC first order grating values (see Sec 4.10 of Part 2 for more details).

In Fig. 2.1 a comparison is given of the predicted system efficiency (top of the telescope to detected photoelectrons) of X-shooter with the measured values for UVES, ESI (Keck), FORS and ISAAC (in modes that compare closest to X-shooter). The IR values are order averages for easy comparison with the measured ISAAC data. The FORS data are from the ESO Exposure Time Calculator predictions selecting the most efficient (volume phase holographic, high dispersion) grisms in FORS2. In terms of detected quantum efficiency, X-shooter is expected to have a unique performance in the UV-Blue region. At visual and red wavelengths it matches ESI, the echellette spectrograph in operation since 2001 at Keck 2 and the peak efficiency of FORS2 with the volume phase holographic grisms (the latter,

however, at lower resolution). In the J- and H-bands, the average efficiency of X-shooter is similar to the peak efficiency of ISAAC and of NIRSPEC.

The data on efficiency have to be complemented by those on resolution and spectral coverage. These are presented in Fig. 2.2. The spectral coverage of each instrument in a single exposure is also highlighted. The comparison shows that, in resolution, X-shooter fills the gap between the high resolution instruments such as UVES and CRIRES and the low resolution instruments FORS and VIMOS. The Low Resolution mode of FLAMES has a similar resolving power. FLAMES has the advantage of multiplexing in fields with a high target density, but with a very restricted spectral coverage per exposure, no UV efficiency and a lower visual and red efficiency.

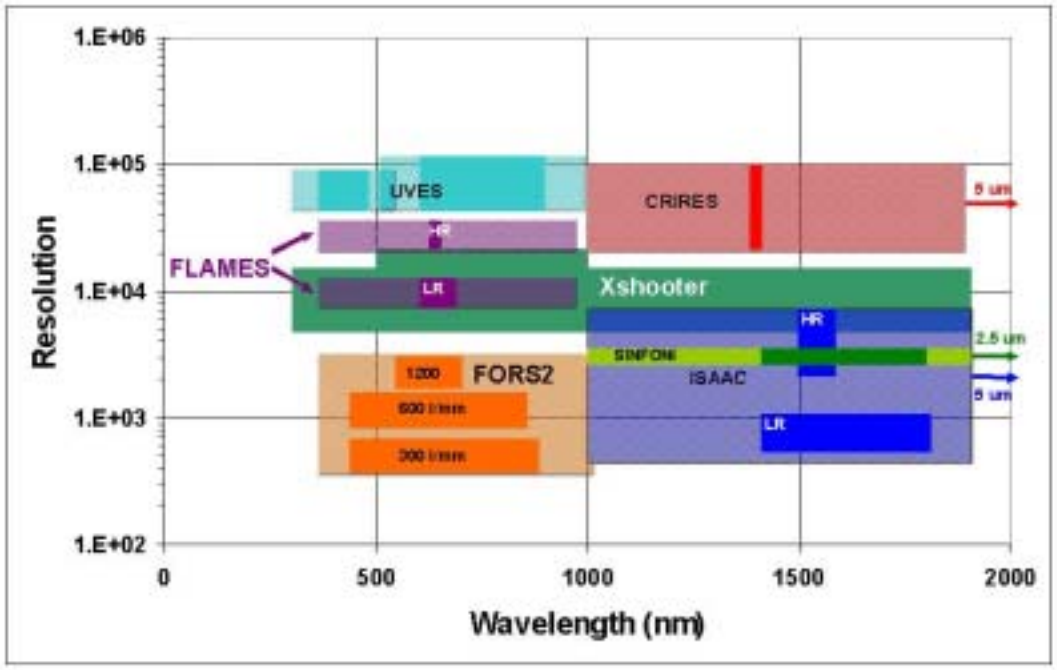

Figure 2.2 First generation VLT spectrographs in the resolution versus wavelength plane, for the region of interest to X-shooter. Widths of the darker stripes approximately identify the spectral coverage of a single observation. VIMOS (not shown) approximately overlaps with FORS. Note that by the time X-shooter will be implemented ISAAC and the FORSes will be long beyond their expected lifetime. X-shooter is unique among instrumentation at 8–10m telescopes in providing full coverage from the UV to the H band in one shot.

SINFONI, the integral field spectrograph operating in the J-, H- and K-band coupled with Adaptive Optics, to be installed at the VLT in 2004, will provide spectra covering either the J- or H-bands in a single exposure. The throughput of SINFONI and X-shooter is similar, with some additional losses in SINFONI expected by the use of the AO module. The limiting resolution of SINFONI is $R = 4\,500$, while the X-shooter NIR-arm can reach $R = 8\,000$ with 2-pixel sampling of a $0\farcs6$ slit. SINFONI can work in a seeing limited mode and in an adaptive optics (AO) mode. The Laser Guide Star AO system for SINFONI, which due to its almost complete sky coverage is the reasonable base for comparison with X-shooter, is expected to give a Strehl ratio of 30 % in the K-band in average seeing. Using Marechal's criterion, the corresponding Strehl ratios in the H and J bands will be of the order of 13 % and 3 %, respectively. Therefore, when working at the detector noise limit, AO will not lead to a significant improvement in the instrument's performance in the J and H bands that are in common with X-shooter. With a pixel scale of $0\farcs125$/pix in non AO-mode ($0\farcs30$/pix for X-shooter) SINFONI will, with its current detector, never reach the sky limit, and would, if upgraded with a state-of-the-art detector, take about 1.5 times longer than X-shooter to reach the sky limit at a somewhat lower spectral resolution. X-shooter will cover both the J- and H-bands in a single exposure, while SINFONI requires two exposures.

We can therefore conclude that in the J- and H-bands X-shooter gains a factor of ∼two in both spectral coverage, spectral resolution and actual sensitivity for faint objects. This reflects the fact that SINFONI is optimized to obtain spectroscopic data at sub-arcsecond resolution (driven by a set of key scientific programs which require this capability) while X-shooter is designed to obtain the best spectroscopy of the faintest stellar targets.

X-shooter has comparable or superior efficiency in the visual and red band with respect to ESI at Keck 2. When this is convoluted with the larger collecting area of that telescope, the overall performance in terms of limiting magnitudes should be just slightly lower. X-shooter will have the additional benefit of simultaneous observations in the U-, J- and H-bands as well.

There are two 2nd generation instruments for the VLT currently under study that potentially have a partial overlap with the X-shooter capabilities, namely KMOS and MUSE. Although the final characteristics of these instrument are far from being established we can carry a preliminary comparison.

The KMOS spectrograph is intended as a powerful multi-object machine to work in the 1–2.3μm spectral region. Its location at Nasmyth and the need of additional subsystems to observe several objects in the field will necessarily lead to a lower detection efficiency on single objects with respect to the NIR arm of X-shooter. The need to store several spectra on the detectors will reduce the spectral coverage in a single exposure to at most one single NIR band. Even if X-shooter would include the K band, the two instruments will remain largely complementary. KMOS should offer an unique performance in the NIR observations of targets with moderate to high spatial density on scales of a few arcminutes. X-shooter should provide spectra of a single object to a fainter limit and with a larger spectral coverage in a single exposure. It would be the preferred choice for the observations of isolated targets or sparse samples of astrophysical targets.

The MUSE spectrograph should also be located at one Nasmyth focus of the VLT. The instrument will be optimized for deep field ($\sim 1' \times 1'$) spectroscopy in the range 500–950 nm. If it will be possible to manufacture the field slicer unit to the required efficiency, the average MUSE efficiency over the spectral range of operation should be comparable to that of the visual arm of X-shooter even if the instrument is located at Nasmyth. The differences in parameter space between the two instruments (MUSE privileging spatial information over a more extended spectral coverage) translate into very different science drivers for the two instruments even in the overlapping spectral region. It would be a waste of the instrument capability to use MUSE for the observations of a point-like target. It would be inefficient to produce 3D mapping with X-shooter. The astrophysical output of the VLT will be maximized by the availability of both facilities.

SECTION 2.2

The Power of X-shooter

As an additional way to compare X-shooter with the other optical/NIR spectrographs, we have defined a quality parameter to characterize the global spectrograph performance. This is a combination of throughput, spectral resolution and wavelength coverage. The "power" of the spectrograph is defined as follows:

$$P = \frac{R\frac{\lambda_2}{\lambda_1}}{t}. \tag{2.1}$$

Here R is the resolution through a $1''$ slit, λ_1 and λ_2 are the lower and upper wavelengths of the instantaneous wavelength coverage and t the integration time needed to reach a S/N=10 on a R=22.0, U= 22.0 or H=19.5 magnitude object at an airmass of 1.0 and through a $1''$ slit in $0''.8$ seeing and in dark time.

X-shooter requires 3000, 5400 and 4800 seconds to reach a S/N of 10 per Å at U=22.0, R=22.0 and H=19.5 respectively, at a resolution of R_U=5000, R_R=7000 and R_H=5000. For X-shooter the power therefore becomes: P_U = 10.5, P_R=8.2 and P_H = 6.6.

Table 2.1 lists the power of X-shooter compared to other spectrographs. The power is computed in

three wavelength regions: at U (3500 Å), R (6500 Å) and $H(1.6\mu\mathrm{m})$, characteristic of the three arms of X-shooter. *Measured with this yardstick, X-shooter will be more powerful by a factor $\gtrsim$10 than any existing or planned ESO spectrograph, and will still outperform ESI and NIRSPEC by a factor of 2* (including the larger collecting area of Keck). The large increase of power for X-shooter compared with other spectrographs is mainly due to the large wavelength region covered by X-shooter in one shot, and the optimization in the design that was possible due to the fixed spectral format of X-shooter.

Table 2.1 also shows the power multiplied by the multiplexing for multi-object spectrographs. It is evident that X-shooter in this comparison is not competitive with VIMOS and FLAMES (because X-shooter is optimized for single-object spectroscopy). It is however interesting that X-shooter compares well to FORS1, FORS2, and SINFONI even if multiplexing is factored in.

Table 2.1 The power of X-shooter compared with other instruments.

Instrument		R ($1''$slit)	λ_2/λ_1	t (s)	Power (single object)	Power (MOS)
ESO (U-band)	X-shooter	5 000	1 900/300	3 000	10.55	
	FORS1[a]	666	592/347	3 175	0.35	6.65
	FORS2[b]	666	623/316	2 200	0.60	11.40
	UVES[c]	16 200	388/302	150 000	0.14	
ESO (R-band)	X-shooter	7 000	1 900/300	5 400	8.2	
	FORS1[d]	1 200	743/521	8 413	0.2	3.8
	FORS2[e]	2 166	726/573	4 019	0.7	13.3
	UVES[f]	14 800	707/600	32 400	0.5	
	FLAMES[g]	43 800	620/520	243 000	0.2	1.6
	GIRAFFE[h]	9 750	652/574	10 930	1.0	130.0
	VIMOS[i]	6 830	710/500	10 975	0.9	450.0
Keck	ESI[j]	3 900	1 009/390	2 300	4.4	
ESO (NIR)	X-shooter	5 000	1 900/300	4 800	6.6	
	ISAAC[k]	3 200	1 690/1 609	120 000	0.03	
	SINFONI[l]	1 125	1 900/1 400	15 500	0.1	3.2
	CRIRES[m]	20 000	1 662/1 638	540 000	0.04	
Keck	NIRSPEC[n]	10 750	1 808/1 413	3 600	3.8	

[a] GRIS_600B grism
[b] GRIS_600B grism
[c] CD1 blue arm, 2x3 binning, t calculated as 42 exposures of 1 hour each
[d] GRIS_600R grism
[e] GRIS_1200R
[f] CD3 red arm template, R=22, 2x3 binning, 9 one hour exposures are needed
[g] CD4 template, no binning, 67.5 one hour exposures
[h] Low resolution LR05, MEDUSA fiber mode
[i] R2130-631 grism
[j] Echellete mode; from Shenis et al. 2002
[k] MR mode, t calculated as 34 one hour exposures
[l] See Section 2.1
[m] From CRIRES web page
[n] From NIRSPEC Manual; echellete mode

Comparisons of instruments based on a single number (e.g. the power defined above) evidently cannot take into account all the capabilities that each individual instrument offers or indeed the qualitative effects of changing the specifications of an instrument. For example increasing the resolution by a small factor would in some cases mean a quantum jump in scientific knowledge gained.

A general way of comparing spectrographs, not taking into account the wavelength coverage, is to calculate the sensitivity to a single spectral feature. This has been done for X-shooter and existing 1st generation VLT instruments, for which the ESO ETC can be used. The template spectrum is assumed to be a power law spectrum with a slope of 0.75, $f_\nu \propto f^{-0.75}$, normalized to an AB magnitude of 22.0 at 1 μm. The corresponding UBVRIJH broadband magnitudes are 22.1, 22.8, 22.5, 22.2, 21.7, 20.9 and 20.2, comparable to the spectrum of a typical faint quasar or GRB afterglow. As this source is too faint for high resolution spectroscopy, UVES has not been included in the comparison. The spectral feature is assumed to be a fully absorbed line with a width of 30 km s^{-1}, resembling a moderately strong IGM absorption line of intermediate width. Using a 1 arcsec slit, this line will not be resolved with X-shooter or any of the instruments included in the comparison. The exposure time required to detect this line at a given level of significance scales with the inverse square of the signal-to-noise per resolution element and the inverse square of the resolution, as long as the line is not resolved.

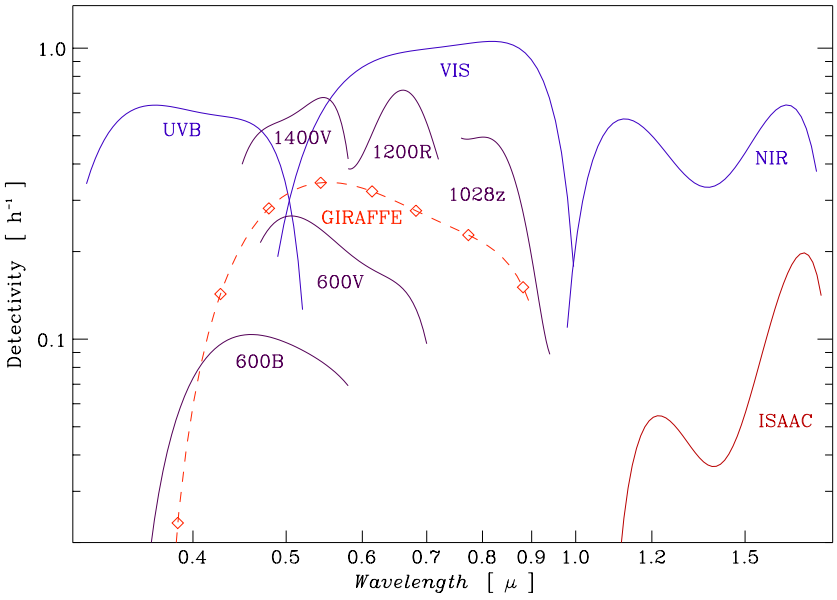

Figure 2.3 The sensitivity of X-shooter FORS, GIRAFFE and ISAAC to a 30 km s^{-1} wide absorption line, as a function of wavelength. For GIRAFFE the diamonds indicate the central wavelength of the individual intermediate resolution spectral orders.

In Fig. 2.3 we plot the detectivity, defined as the inverse of the number of hours needed to detect the absorption line at a signal-to-noise of 5. X-shooter reaches a near uniform detectivity across the entire 0.3–1.8 μm wavelength range, showing that it is optimally suited to observe the 'lighthouses of the universe' throughout this broad wavelength range. The diagram also visualizes the lack of VLT instrumentation which is capable of working with high efficiency in the UV part of the spectrum. There is no competition below 3500 Å and even below 4500 Å X-shooter gains very significantly over existing VLT instrumentation. The high resolution VPH grisms of FORS2 competes quite well with X-shooter but are due to their short wavelength coverage in general not very useful for absorption line studies. Given that GIRAFFE is fibre coupled, the medium resolution mode of GIRAFFE performs well, largely

within a factor of 5 of X-shooter, but suffers from the short wavelength coverage. The difference between ISAAC and X-shooter essentially reflects that the ISAAC detector in terms of noise and dark current is not comparable to current state-of-the-art IR detectors.

SECTION 2.4

Synergy with Other Facilities

As the ultimate spectrograph for quantitative studies on faint targets at the VLT in the decade 2007–2017, X-shooter will complement and benefit from other major facilities in observational astrophysics operating in the same period. Here we give a brief outline, which is certainly not exhaustive, of possible synergies with X-shooter.

2.4.1 Optical/NIR from Ground: OmegaCAM/VST & VISTA

The wide field cameras at ESO, OmegaCAM/VST for the optical and VISTA for the near-infrared, will start to operate in 2004 and 2006 respectively. These survey facilities are especially designed for deep, wide field observations over major portions of the sky. They will, in particular, be extremely important to increase samples of faint, rare populations. Examples are $z > 6$ galaxies and QSOs, old white dwarfs and the RR Lyrae in the extreme outer Galactic halo. While large field, low resolution MOS instruments will be used to confirm the nature of many of the faint candidates discovered in these surveys, X-shooter will be required to study in detail the kinematics, physical properties and metallicity of the most interesting targets (e.g. is there a metallicity gradient in the outer Galactic halo?). We see the OmegaCAM/VST+ VISTA + X-shooter combination as essential for the success of ESO as the prime observatory for observing the faint and the rare.

2.4.2 Optical/NIR from Space: HST, JWST, SNAP

HST will remain in operation well into the X-shooter era, after which it will be succeeded by the James Webb Space Telescope (JWST). After the installation of the Cosmic Origins Spectrograph (COS) in 2005, HST COS observations, combined with X-shooter observations will be a very powerful tool to observe the complete wavelength region from 1100 Å to 1.9 μm. For quasar absorption line studies this will enable a direct comparison of systems at low redshift observed with COS and at high redshift observed with X-shooter. In future multi-wavelength surveys such as the current GOODS survey, X-shooter will play a pivotal role in providing a broad, one-shot, high quality spectrum in the optical/NIR region.

X-shooter's NIR-arm will be an excellent complement to JWST's NIRSpec for those targets that require higher resolution than the maximum $R = 1\,000$ currently planned for NIRSpec. Although the VLT + X-shooter will be in no competition with JWST in terms of sensitivity, applications needing $R > 1\,000$ such as detailed line shape studies in high redshift QSO's and resolved orbital motions in binaries, will remain the domain of X-shooter in the JWST era.

The Supernova Acceleration Probe (SNAP) is proposed to observe 2 000 supernovae Type Ia in the redshift range $0.3 < z < 1.7$ in 22 fixed fields near the north and south ecliptic poles. Its on-board spectrograph will cover a wavelength region 300–1700 nm, very similar to X-shooter, but at a resolution of only ∼100. These spectra will be used to establish the SN redshift and identify it as type Ia from the tell-tale Si λ6150 and S λ5350 features. Due to the overlap in wavelength coverage between X-shooter and SNAP, X-shooter will be able to observe *every SNAP SN Ia, irrespective of its redshift*, that has a sufficient brightness and accessible position. Because of its high efficiency and higher resolution, X-shooter will be ideal for the ground-based follow-up to study the physics of these SN Ia during their own evolution and that of the Universe. The complementary capabilities of X-shooter and SNAP will lead to a better understanding of the physics of SN Ia.

2.4.3 Sub-mm and FIR: SIRTF/APEX/ALMA/Herschel/Planck

The near future will see a revolution in the (sub)-mm/FIR wavelength region. SIRTF, a powerful space telescope for imaging and spectroscopy in the thermal IR, is expected to be launched this year. When toward the end of the decade ALMA, Planck and Herschel will come into operation a very large number of new FIR/sub-millimeter point sources will become available with accurate positions. In many cases, e.g. very high redshift object candidates or lensed galaxies, an optical/NIR spectrum will be needed to confirm their identity. Since most of these sources will be optically faint and with unknown UV/optical/NIR spectral energy distributions, X-shooter will be the instrument to use for this follow-up. The availability of X-shooter will put the VLT in the center of this revolutionary field of astronomy. One key-project we envision for X-shooter is the follow-up of point sources from Planck that have sub-mm spectra indicative of being at very high redshift. These galaxies may or may-not be fully optically obscured.

2.4.4 LOFAR

A similar situation to ALMA will occur when the Low Frequency Array (LOFAR) becomes available, shortly after the start of X-shooter. This new generation radio telescope will revolutionize radio astronomy at the low frequencies (< 100 MHz). Its unprecedented resolution and sensitivity will no doubt lead to important new results, among others on galaxies at even higher redshifts than will be found with ALMA. Spectroscopic follow-up of these high redshift candidates will be obtained with X-shooter. The ability of *LOFAR* for post-observation beam-formation will allow a continuous record of the complete sky. This will be ideal for identifying those gamma-ray bursts with prompt radio emission (<1 day after the γ-rays). This ability will complement high-energy GRB detectors. Although LOFAR will most likely be located on the Northern Hemisphere, there will be a considerable overlap in observable sky with the VLT.

2.4.5 High-Energy Astrophysics: Chandra, XMM-Newton, Integral, Swift, GLAST

At this moment Chandra and XMM-Newton are revolutionizing X-ray astronomy. Resolving the hard X-ray background, hundreds of X-ray sources in globular clusters, Ultra-luminous X-ray Sources in Local Group Galaxies and X-ray selected quasars behind dense stellar fields are just a few of the exciting results becoming available now. With the recent addition of Integral these will be extended to even higher X-ray energies. All three facilities are envisioned to continue to work well into the X-shooter era. For many of these X-ray sources, optical and NIR spectra will be needed to ensure a maximum scientific output. Here we only mention the X-ray binaries in quiescence that will be discovered in the Galactic plane. Many of these will contain stellar mass black holes and neutron stars. Although these are considered to be among the 'holy grails' of X-ray astronomy, their actual masses can only be obtained through a combination of X-ray observations and optical/NIR spectroscopy. Due to the optical/NIR faintness of these sources, their concentration toward the Galactic center and the spectral resolution required, X-shooter will be the instrument to use for this.

The launch of Swift at the end of this year promises new breakthroughs in gamma-ray burst astronomy. With 140 yearly GRB positions with arcsecond accuracies over the minimum two year life time of Swift, and its sensitivity to short GRBs, Swift will start to answer the questions on the origin of short GRBs, as well as the (different) properties of the environments of short and long duration GRBs. Although Swift and X-shooter may have only a short overlap in time unless the Swift lifetime is extended, this is not so in the case of Integral or the *Gamma-ray Large Area Space Telescope*: GLAST, that will operate in the X-shooter era (launch is foreseen in 2006). With its unprecedented large collecting area (50 times more sensitive than EGRET at 100 MeV), it will be a highly important mission in the identification of gamma-ray bursts and X-ray transients, as well is being able to resolve the gamma-ray sky and deliver gamma-ray point source positions with accuracies as small as $30''$. The optical identifi-

cation of GLAST point sources and establishing their nature will be an important task for X-shooter. X-ray transients discovered with GLAST will be the hunting ground for stellar-mass black holes and the masses of neutron stars in close binaries. Determining black hole and neutron star masses requires an optical/NIRspectrograph such as X-shooter on the VLT.

The capabilities of Swift, Integral and GLAST combined with the availability of REM, TAROT-2 and X-shooter at ESO will further strengthen ESO's key role in GRB research.

2.4.6 LISA: Opening the Window onto General Relativity

The *Laser Interferometer Space Antenna; LISA* will be the beginning of a new era in astronomy, when we will be able to detect, for the very first time ever, gravitational waves from astrophysical objects. Among the top candidates for LISA are detached and interacting white dwarf binaries. Especially the recently discovered ultrashort AM CVn systems with periods less than ten minutes will be among the strongest and most secure LISA sources. However, those we currently know of (only three) will be the very tip of a gigantic iceberg that LISA will uncover. To characterize these systems and to understand the nature of the gravitational wave signal, electromagnetic observations will remain a key element. White dwarf binaries are best studied in the optical and X-ray regimes, and in the optical X-shooter will be the instrument of choice, since a medium resolution spectrograph of high efficiency will be needed to resolve the orbital velocities of these ultrashort period systems. One of the main aims of LISA will be the observations of supermassive-black hole mergers in the Universe. Even though at this point it is unclear if these mergers will leave any trace in the electromagnetic domain, the properties of their host galaxies will be extensively studied. Without a doubt, X-shooter will be the instrument of choice for this if these galaxies are faint and distant.

CHAPTER 3

Scientific Programs for the Guaranteed Time

Based on the estimated cost and manpower commitment for X-shooter, we can expect around 70 nights to be available to the institutes participating in the Consortium. The Consortium would like to use this time for a small number of key programs, each requiring of the order of 20 nights of VLT time. In such a way, early in the lifetime of X-shooter we will be able to use the unique capabilities of X-shooter to make substantial scientific breakthroughs. A decision on the subject of these programs has not been made (and cannot be made) at this time. X-shooter is an instrument with a very broad science case, ranging from the nearest objects to the outer reaches of the Universe. Many of the fields in which X-shooter will make a difference, are developing rapidly. We envision that about a year before the installation of X-shooter we will make a call for GTO programs within the Consortium to identify the key projects. At this stage we would like to list a number of *possible* projects. These should be seen as a guideline to the flavor of key projects we envision.

- **Old White Dwarfs.** To constrain the distribution and space density of old white dwarfs in our Galaxy, thereby shedding light on the earliest phases of massive star formation in our Galaxy, we wish to observe a sample of ∼200 old white dwarfs distributed over the observable sky. To obtain this sample with X-shooter will require ∼20 nights (see Section 5.3).

- **Gamma-Ray Bursts.** X-shooter will not only allow a detailed study of GRB afterglows, but also of their host galaxies. One of the spearpoints of GRB research with X-shooter will be to characterize GRB host galaxies with respect to e.g. star formation rate and metallicity and to compare them with the total galaxy population in the same redshift range. We would like to dedicate ∼20 nights on the GRB afterglow and host galaxy research (see Section 6.2).

- **Quasar Absorption Lines.** UVES has provided unique results in this field in three years of operation at the VLT, but many topics related to absorption line systems at high redshift require observations of QSOs fainter than the limiting magnitude of the instrument). X-shooter promises a real breakthrough in this field. It will explore the UV-Blue and NIR parts of the spectrum to which its current counterpart at Keck, ESI, has no access. In 20 nights we will be able to observe around 150 faint QSOs, with an expected major impact on a variety of open issues (see Sections 7.4 and 7.5).

- **Planck Compact Source Catalog.** The *Planck* Compact Source Catalog will be a breakthrough in sub-mm point sources. We expect, among others, obscured and very high redshift galaxies to be a prime source of the Planck point sources. These may constitute the Planck Extreme Source Sample. Optical and NIR observations, establishing the identity and redshift of these sources will among others clarify whether the star formation in the early universe really takes place primarily in highly obscured galaxies or not. We estimate to be able to identify of the order of 100 Planck extreme point sources in 20 nights of X-shooter observations (see Section 7.3)

- **High-Redshift Objects.** X-shooter will be the instrument to use to identify and study high redshift $1.5 < z < 2.5$ and extremely high redshift objects ($z > 6$) that will become available from e.g. SDSS, OmegaCAM, VISTA and sub-mm observations. Although at this stage it is difficult to predict the number of these candidates that will be observable with X-shooter, 20 nights of observations will make a major impact and will turn X-shooter into the instrument to study the very high redshift universe (see Sections 7.1, 7.2, 7.3, 7.4).

CHAPTER 4

The X-shooter Science Team

The X-shooter Feasibility Study Science Team consisted of the following people:

- **Michael Andersen** astronomer at the Astrophysikalische Institut Potsdam (D). Main science interests are in GRBs and their host galaxies. Is the project manager for PEPSI on the LBT. Author of 40 refereed publications.
- **Piercarlo Bonifacio** Astronomer at the Osservatorio Astronomico di Trieste (I). Main science interests are in abundances of primordial elements, abundances in stars and in DLA systems. Member of the AVES and PEPSI science teams. Author of 45 refereed papers.
- **Andrea Cimatti** Associate astronomer at the Osservatorio Astrofisico di Arcetri (I). Main science interests are in observational cosmology, galaxy formation and evolution. Author of 48 refereed publications. Author of the X-shooter science case on *Primordial Massive Galaxies*.
- **Fernando Comerón** Associate astronomer at ESO, head of the User Support Group. Has been support astronomer at the NTT for EMMI and SUSI/SUSI2, at the VLT for ISAAC and UVES and member of the VLT commissioning team. Author of 41 refereed publications. Author of the X-shooter science cases on *Brown Dwarfs* and *Star Formation*.
- **Stefano Cristiani** Senior Astronomer at the Osservatorio Astronomico di Trieste (I). Main science interests are in cosmology, quasar absorption lines, formation and evolution of galactic structures. Author of more than 100 refereed publications. Author of the X-shooter science case on *Tomography of the Intergalactic Medium*.
- **Sandro D'Odorico** Head of Optical Instrumentation Department at ESO. Has been responsible for the definition and procurement of several instruments for the 3.6m, the NTT and the VLT (CASPEC, EFOSC, EMMI, SUSI2, FORS and UVES). Main science interests: absorption systems at high redshifts as detected in QSO spectra and properties and evolution of high redshift galaxies. Author of more than 100 refereed publications.
- **Sara Ellison** ESO-Paranal research fellow. Main science interests are in QSO absorption lines studies. She is the PI on the CORALS program on dust biases in absorption line system selection. Instrumentation experience in moderate resolution and echelle spectrographs. Author of 20 refereed publications. Author of the X-shooter science case on *Metal Enrichment of the Early Universe*.
- **Bob Fosbury** Space Telescope instrument scientist for ESA and Deputy-head of the Office for Science of the Space Telescope – European Coordinating Facility at ESO. Main science interests are in AGNs and their host galaxies and the chemical evolution in the early universe. Is Co-I on the

GOODS project. Instrumentational experience in HST and JWST instrumentation, spectroscopy and (spectro)polarimetry. Leading the JWST NIRSpec Science Operations planning. Author of 94 refereed publications. Author of the X-shooter science case on *Massive Star Formation at Early Epochs*.

- **Claes Fransson** Professor at Stockholm Observatory (S). Main interests: supernovae, supernova remnants, gamma-ray burst-supernova connection, clusters of galaxies, high redshift supernovae. 65 refereed journal papers. Author of the X-shooter science case on *Supernovae*.

- **Johan Fynbo** Research fellow at the Universities of Aarhus and Copenhagen (DK). Main science interests are in GRBs and the host galaxies, the properties of high redshift galaxies, among which damped Lyman α absorbers and Lyα emitters. Author of 30 publications in refereed journals. Author of the X-shooter science case on *Gamma-Ray Bursts as High-Energy Laboratories and Cosmological Probes*.

- **Paul Groot** Assistant professor of astrophysics at the University of Nijmegen (NL). Main science interests are in the structure and evolution of close binaries, old white dwarfs and the identification of supernova Type Ia progenitors. Author of 48 refereed publications and member of the team that received the EU 2002 Descartes Prize. Author of the X-shooter science case on *Close Binaries and Stellar Remnants*.

- **Jens Hjorth (chair)** Associate professor of astrophysics at the University of Copenhagen (DK). Main research interests are in observational cosmology. Author of 68 publications in refereed journals. Member of the team that received the EU 2002 Descartes Prize.

- **Lex Kaper** Assistant professor of astrophysics at the University of Amsterdam (NL). Main science interests are in the physics of gamma-ray bursts, the formation and evolution of massive stars and the equation of state of neutron star matter. Author of 42 refereed publications.

- **Palle Møller** Associate Astronomer at ESO Garching. Main science interests are in the high redshift universe (Damped Lyman Alpha galaxies, large scale structure, QSO host galaxies, cosmology). Author of 44 papers in refereed journals. Author of the X-shooter science case on *Faint Emission Line Galaxies at z =1.6–2.6*.

- **Roberto Pallavicini** Senior Astronomer at the Osservatorio Astronomico di Palermo (I) and member of the Board of Directors of the National Institute of Astrophysics (INAF). Co-PI on PEPSI for the LBT, and leading the optical technology group at Palermo Observatory. Main science interests are stellar X-ray astronomy and high-resolution optical spectroscopy. Author of more than 100 publications in refereed journals.

- **Elena Pian** Permanent staff member (Researcher) at INAF, Astronomical Observatory of Trieste, Italy and member of the REM team. Main scientific interests: high energy astrophysics, with emphasis on multiwavelength variability of blazars and GRBs. Author of 90 papers in refereed journals. Member of the team that received the EU 2002 Descartes Prize. Author of the X-shooter science case on *Gamma-Ray Bursts as High-Energy Laboratories and Cosmological Probes*.

- **Bjarne Thomsen** Associate professor of astrophysics at the University of Aarhus (DK). Research interests are in stellar populations, observational cosmology and the high redshift universe. Author of 28 publications in refereed journals. Author of the X-shooter *Exposure Time Calculator*.

Inputs by L. Testi to Sec. 5.1; S. Benetti, A. Goobar, J. Sollerman, M. Turatto to Sec. 6.1; F. Fiore, N. Masetti, E. Palazzi to Sec. 6.2; and V. D'Odorico to Sec. 7.5 are acknowledged.

CHAPTER 5

Stellar Astrophysics

SECTION 5.1

Brown Dwarfs

5.1.1 Astrophysical Importance

The discovery of cool objects with temperatures below 2000 K (L and T dwarfs, the majority of which are brown dwarfs) has been the main driver for intense observational and theoretical efforts over the past decade. Brown dwarfs bridge the gap between stars and planets in terms of mass and atmospheric properties. A physical understanding of the atmospheres of brown dwarfs is the current challenge, as these are the most complex in the whole stellar and substellar domains. Many different processes act together (formation of molecules and grains, large-scale convection, sedimentation of grains below the photosphere, raindown of chemical species, formation of clouds and large-scale weather patterns) resulting in a large complexity.

Observationally, this means that the spectral features of brown dwarf atmospheres must display considerable time variability. Photometric monitoring of T dwarfs has indeed revealed aperiodic brightness variations with amplitudes of up to 0.3 mag and characteristic timescales ranging from several hours to a few days, attributed to the formation and evolution of cloud decks. The evolution of weather patterns also implies that observations at different spectral ranges obtained at different times provide separate snapshots of the probed features. These probably sample the same object under different conditions. Complex time variations complicate the interpretation of the observed spectra in the theoretical framework, as the correlation between features observed in two different domains may be distorted by such variability.

In broad terms, the spectra of brown dwarfs are relatively simple in appearance in the visible-red range (Fig. 5.1). The molecular bands that dominate the visible spectra of M-type stars weaken towards lower temperatures as the component species become locked in grains, producing a monotonically rising spectrum dominated by very prominent and broadened lines of alkali elements. The features in the near-infrared JHK bands as well as at longer wavelengths are dominated by molecular bands primarily due to water, methane and also ammonia at the lowest temperatures, in addition to broad features due to collision-induced H_2 opacity. The chemical stratification of the atmosphere, with cloud decks of different compositions as a function of height, and the existence of zonal convection patterns and possible azimuthal structures, probably results in an overall appearance similar to those of the giant planets of our Solar System. However, important differences are expected that arise from the absence of a powerful external source of radiation in the case of isolated brown dwarfs. The observed spectrum of a brown dwarf is thus the blend of a variety of spectra arising from different regions across the unresolved disk of the object that probe chemistries located at a range of depths in the atmosphere, and more or less exposed to view depending on the local weather patterns that are likely to vary with time.

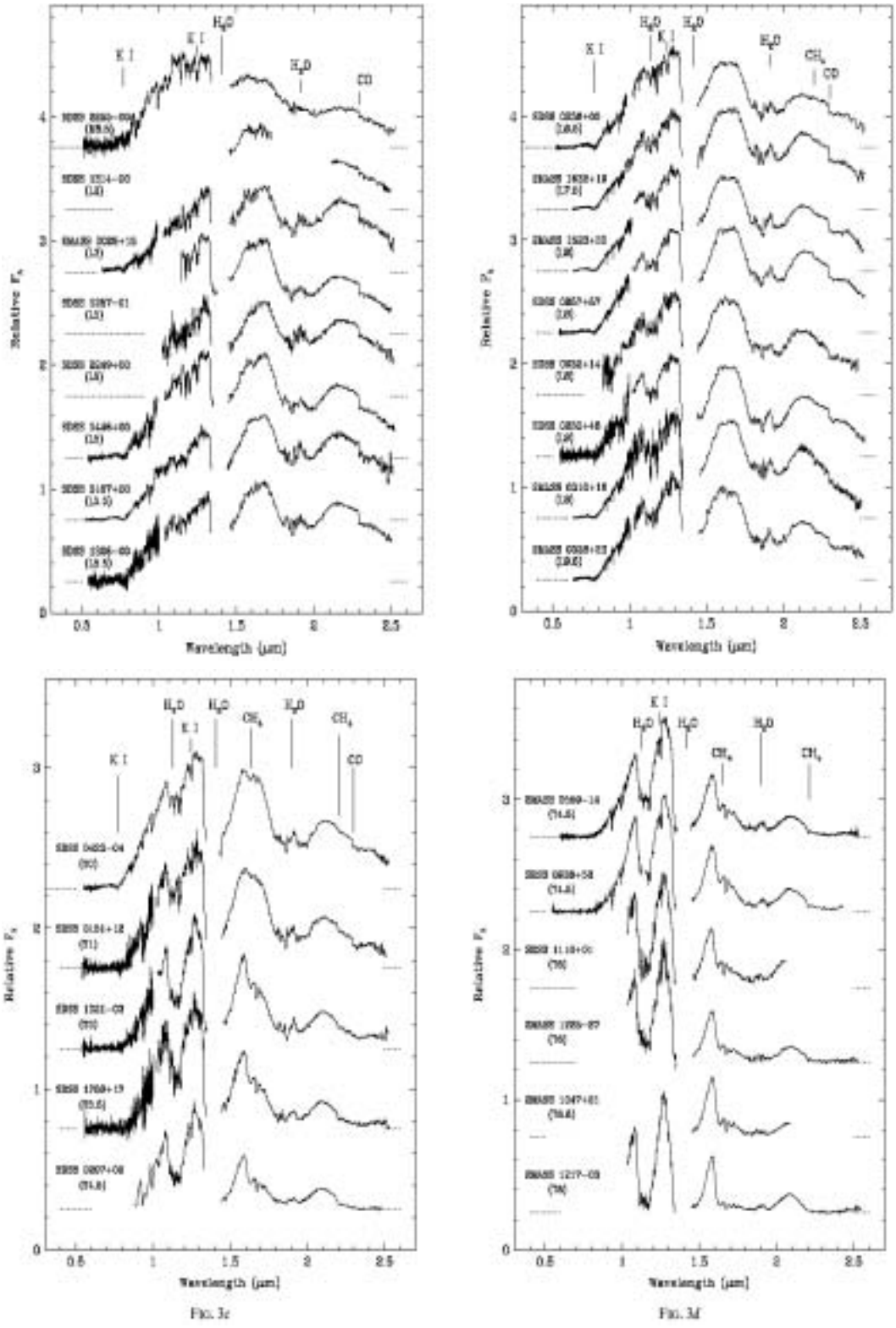

Figure 5.1 Spectral atlas of L (top) and T (bottom) dwarfs, covering a large fraction of the wavelength range accessible to X-shooter plus the K band. Some of the most prominent atomic and molecular features are indicated. Note that the spectra cover the whole visual to near-infrared wavelength domain (from Geballe et al. 2002).

5.1.2 Instrument Requirements

Simultaneous spectroscopy at medium resolution, high signal-to-noise, and a long wavelength baseline extending from the visible-red to the infrared is of prime importance to provide proper observational input to the model atmospheres of brown dwarfs. It is essential to remove the fundamental uncertainty introduced by the time variability of weather patterns.

Simultaneous spectroscopy over a large wavelength range, providing a wealth of physical information, will help in addressing the outstanding questions on the origin of the diversity found among the handful of T dwarfs known so far. Tentative spectral sequences for L and T dwarfs have been established, but significant mismatches between visible and infrared classification criteria persist, especially among the T dwarfs. This raises the question which physical factors are probed by the spectral sequence. The answer to this question needs further progress in modeling, but essential to it is a high quality dataset where uncertainties stemming from the use of different instrumentation and non-simultaneous observations can be removed.

5.1.3 Target Selection

The sample of objects for spectroscopic follow-up will be greatly expanded thanks to the planned large-area infrared surveys to be carried out with VISTA from Paranal. A combination of the capabilities of VISTA and X-shooter is thus likely to put European astronomers in a unique position to take the leadership in this field.

5.1.4 X-shooter Performance

The proposed specifications of X-shooter provide a wavelength coverage that ranges from the accessible part of the visible spectrum (where the flux below ~ 6000 Å is virtually zero) to beyond the peaks of emission in the J and H bands, while the VLT provides the light-gathering power needed to obtain high quality spectra. The medium spectral resolution offered by X-shooter is sufficient for detailed chemical abundance analyses and would also allow approximate measurements of rotational velocities, which are an important factor in governing the overall atmospheric circulation in these objects. The comparison among objects of different ages would also yield constraints on the evolution of mass and angular momentum loss. A resolution of $R \sim 10000$ would be needed for useful work in this area, together with high S/N resulting in a good determination of line profiles. Evolved brown dwarfs have been shown to be similar to very low-mass stars in displaying signs of activity, in particular Hα emission. Although the origin is unclear, it is possibly due to the interaction of the magnetic field with the fully convective interior of the object, like in the case of very low-mass stars. The high S/N provided by X-shooter would allow the observation of other lines, such as the Ca II infrared triplet, that also sample chromospheric activity in very low mass stars.

In principle, simultaneous spectroscopy with different VLT instruments having comparable capabilities observing in a coordinated way could overcome the concerns due to time variability. However, operational constraints at the VLT are expected to allow such coordinated observations only on a rather exceptional basis. The possibility of simultaneous observations from the R to the H band can thus in practice be considered as a unique feature of X-shooter.

According to the current VLT 1st generation instrumentation plan, the capabilities of X-shooter overlap with those of four VLT instruments. The relative performances are discussed in each case based on the characteristics of two of the best studied brown dwarfs: the L dwarf Kelu-1 and the T dwarf Gl229B. Broad-band photometry on which the performance estimates here are based is taken from Ruiz et al. (1997) and Matthews et al. (1996). We note that these are bright objects while X-shooter is optimized for faint objects.

The comparisons described below have been made assuming a seeing and a slit width of $0\farcs5$ (or a value close to it) for the existing instruments. The choice of rather good seeing conditions is intended to

produce a comparison fairly favorable to FORS2 and ISAAC; poorer conditions would involve a loss of throughput (through slit losses) for FORS2 and ISAAC to keep the same resolution, while for X-shooter it would be possible to widen the slit without a loss of resolution. A general remark on the comparisons given below is thus that they become more favorable to X-shooter as the external seeing gets worse.

- FORS2: Highest resolution in the red is provided by grism 1028z+29, covering the range 741–947 nm. Using a $0\farcs5$ slit under $0\farcs5$ seeing yields a resolution $R = 4700$, i.e., a resolution element of $\Delta\lambda = 0.17$ nm. The same resolution is obtained by X-shooter when a $1\farcs5$ slit is used, making it easy to observe with a seeing of $1\farcs0$. An on-chip binning of 4 in the spectral direction (and 3 in the spatial direction) is possible. The effective pixel size for the X-shooter is $0\farcs56$, as compared to $0\farcs25$ for FORS2. The resolution element is 2.0 and 2.68 pixels for FORS2 and X-shooter respectively. For Kelu-1 ($I = 16.8$), the required integration time to reach $S/N = 31$ with FORS2 in this setup is 100 s. For the same object and exposure time the X-shooter reaches $S/N = 23$ per binned pixel. It should be noted, however, that the value for FORS2 is given at its maximum value, whereas the X-shooter value is an average over an order. When this is taken into account, as well as the different pixel sizes, the S/N values are practically identical. But it should be noted that the X-shooter obtains this performance with a seeing of $1\farcs0$ instead of $0\farcs5$. In addition comes the full wavelength coverage offered by X-shooter compared to only 200 Å for FORS2 in one shot.

- ISAAC: The performances of ISAAC spectroscopy at medium resolution and X-shooter, in terms of both throughput and resolution, are fairly similar for bright objects. The main difference is that ISAAC needs 10 grating settings to cover the spectral range in the J and H bands that X-shooter will cover in a single exposure. The resolution $R = 6000$ offered by ISAAC in medium resolution spectroscopy mode ($0\farcs6$ slit) can be matched by X-shooter with a $0\farcs5$ slit and 3-pixel post-observation binning. For a T dwarf of $J = H = 16$, a $S/N = 50$ per resolution element in the J band is obtained with ISAAC in 9 min of integration time, vs. 5 min. for X-shooter. At H, the corresponding numbers are 10 min and 6 min, respectively. Thus, X-shooter is more advantageous than ISAAC at mid-resolution spectroscopy, even if only a limited wavelength range that can be covered with a single setting of ISAAC is needed. When considering the gain in simultaneous spectral coverage and throughput, X-shooter is a factor of ~ 20 more efficient than ISAAC. However, operationally the gain is even higher than that, since the comparison of efficiencies that we have described does not take into account the extra overhead added to ISAAC coming from the time needed to move mechanical elements in the instrument to change its settings.

- FLAMES/GIRAFFE: The resolution of X-shooter in the far red is well matched by that of FLAMES/GIRAFFE operating at low resolution. For Kelu-1, a 100 s integration of X-shooter gives $S/N = 15$ on a resolution element of 5 pixels at 800 nm ($R \simeq 6000$), only one third of the time needed by FLAMES/GIRAFFE at the same wavelength. The ratio increases to 4.1 for the case of Gl229B (2000 s needed to obtain $S/N = 10$ with X-shooter at the same resolution and wavelength, vs. 2.3 h with FLAMES/GIRAFFE). Therefore, X-shooter represents an improvement of a factor of at least 3 with respect to FLAMES even without taking into consideration the extended wavelength coverage. The multiobject capability of FLAMES may represent an advantage only in the densest regions of lightly embedded young clusters.

5.2.1 Astrophysical Importance

Observationally, the study of the early stages of star formation is one of the topics where a multiwavelength approach is most important. In a time span of only about 100 000 years a forming star passes from the stage of a cold, rapidly collapsing cloud core detectable only at millimeter and far-infrared wavelengths, to an embedded protostar in hydrostatic equilibrium surrounded by a thick envelope of gas and dust that becomes sufficiently transparent only at near- and mid-infrared wavelengths. Finally it becomes an emerged pre-main sequence star surrounded by a disk where the leftovers of its circumstellar envelopes settle down. Pre-main sequence stars are also often detected by their X-ray emission, resulting from the interaction of their magnetic fields with their convective mantles and with their circumstellar disks. At the beginning of the emerged stage, phase accretion is still going on, giving rise to characteristic signatures in the visible and near-infrared such as emission lines of hydrogen, calcium, and helium, and a featureless continuum that veils the features of the underlying photosphere of the young star. Veiling also occurs at near-infrared wavelengths (longer than $\sim$ 1–1.5 μm) due to continuum emission by dust in the circumstellar disk, heated by the star and by the viscous dissipation of energy within the disk itself. Spectacular signatures of activity in the visible and near-infrared include fast jets, which play an essential role in removing angular momentum from the young stellar object, and probably also in driving turbulence and regulating further star formation at large in the parental cloud.

Young stellar objects over the whole mass spectrum are highly variable objects. Time variability in this case has two dominating origins:

- Accretion from circumstellar material left over from the star formation process and its infall on the surface of the object. This is coupled (in a not fully understood manner) with instabilities in the inner regions of the accretion disk and its connection with the central star through magnetic field lines.
- Rapid rotation and extended convective mantles in stars of a few solar mass and below produce vigorous chromospheric activity resulting in, among other observational manifestations, extended star spot complexes and high-energy emission.

Emission lines in the visible spectrum are the main probes of both accretion and chromospheric activity (Fig. 5.2). The prominence of such emission lines at all masses, makes the entire stellar (and partly substellar) range accessible to the study of its accretion properties. Another important diagnostic tool of the accretion process in the visible is the veiling of the continuum due to emission from hot ionized plasma, probably generated at the base of the accretion columns where the infalling material from the disk is decelerated and heated by shocks as it encounters the surface of the star. While the visible spectrum mainly probes hot gas and physical processes taking place close to the surface of the star, the near-infrared also carries information on the inner parts of the accretion disk. Since diagnostics of both sides of the accretion process have characteristic variability timescales (of the order of days), understanding the correlation between processes taking place in the inner disk and the ultimate incorporation of material to the surface of the star needs simultaneous observations probing both environments over a similar time span.

In the last decade medium- and high-resolution observations of the lines tracing mass accretion, coupled with detailed MHD models of the accretion gas dynamics, have provided solid arguments in favor of the magnetospheric accretion model, in which accretion takes place through columns that connect the inner edge of magnetically truncated disks to the stellar surface along the magnetic field lines. The combination of kinematic observations and models have shown that Hα emission is produced all over the accretion columns, rather than in the boundary layer at the interface between a disk without inner truncation and the surface of the star, as earlier models proposed.

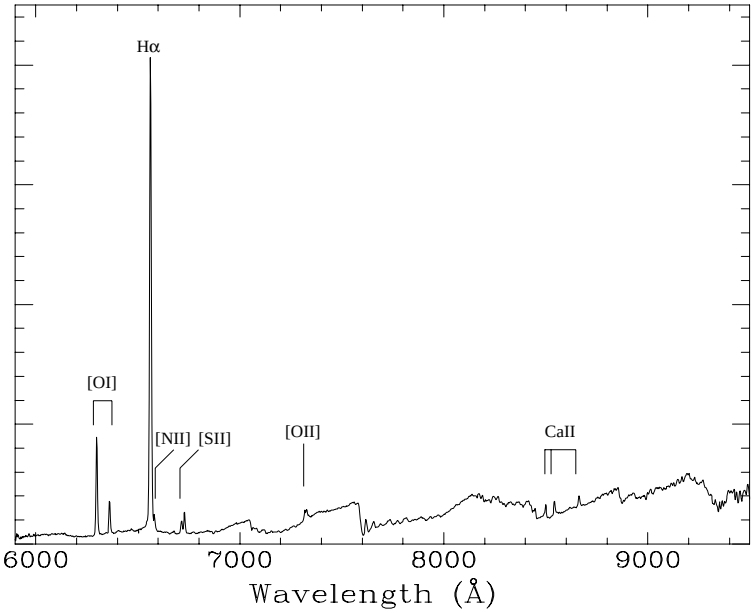

Figure 5.2 FORS2 spectrum of LS-RCrA 1, an object in the stellar-substellar boundary with an exceptionally strong system of emission lines. These lines probe different processes taking place in the circumstellar environment, ranging from inflow at the base of the accretion columns very close to the surface of the star (Hα, CaII) to outflows of diffuse gas producing forbidden lines in the disk wind. This object turns out to be strongly underluminous for its spectral type, which may be due to either an edge-on disk or to accretion-modified pre-main sequence evolution. From Fernández & Comerón (2001).

Besides accretion, mass loss in the form of stellar winds, disk winds and collimated jets is also recognized as a fundamental process in star formation, especially when concerning the removal of angular momentum in the early stages of stellar evolution. This is a highly variable phenomenon, especially regarding the poorly understood process of the generation of jets close to the surface of the star.

5.2.2 Target Selection

The abundant observational signatures of youth nowadays allows the detection of young stellar objects at all masses using a wide variety of techniques spanning over virtually the entire electromagnetic spectrum. Radio continuum emission of ionized gas, millimeter and submillimeter line emission from molecules in outflows, continuum emission from warm, dusty envelopes in the same wavelength range, thermal infrared emission from circumstellar disks, visible and near-infrared variability due to accretion instabilities or azimuthal surface features, narrow-band optical emission in a variety of lines, ultraviolet excess due to veiling caused as accreting material reaches the surface of the star, and X-ray emission due to chromospheric activity or disk flares, are among the techniques used to probe star forming regions in the search for young stellar objects. Some techniques are better suited than others at a given mass or age range, but together they are able to provide complete samples of targets down to the substellar regime for an entire star forming region. Upcoming visible and near-infrared surveys such as those to be carried out by VST or VISTA will be of great importance to provide complete census, but the existing material from all-sky surveys like 2MASS already provides an enormous database whose large potential has not at all been fully exploited yet.

5.2.3 Instrument Requirements

A spectral resolution that will allow to resolve kinematical structure within the emission lines is required, thus giving insight into velocity patterns developing in the accreting gas. The velocity range for such

kinematical diagnostics spans several tens of km/s, requiring a spectral resolution of $R \simeq 10,000$. A similar resolution is needed to reveal kinematical structure arising from mass loss, particularly in the forbidden lines that originate in low density regions and in the lower velocity regions close to the source of jets and outflows. On the infrared side, the ability to resolve structure within the CO bands in the H window may allow to disentangle them from photospheric bands thus giving insight into the short-term time evolution of the disk and its vertical structure.

A broad wavelength baseline is needed to probe accretion, as its signatures extend from the ultraviolet, where the veiling emission can dominate over the photospheric continuum, to the infrared where the disk contribution begins to be important. Similarly, for the determination of the physical properties and structure of outflows it is of fundamental importance to simultaneously probe forbidden lines belonging to different atomic species with different ionization states, hydrogen lines arising from different excited levels (e.g. the entire Balmer and Paschen series of hydrogen, as well as the higher transitions of the Brackett series), and a large number of molecular transitions of H_2 and CO.

5.2.4 X-shooter Performance

The combination of moderate velocity resolution and the enormous wavelength will give X-shooter a unique complementary role with respect to other VLT instruments that are able to address related issues, such as adaptive optics instruments yielding high spatial resolution (ultimately VLTI), high resolution spectrographs able to further study the detailed structure of limited subsets of spectral lines, or thermal infrared instruments probing more distant regions of disks. It will also provide an important complement to ALMA, which will focus on stages taking place earlier in the process of star formation (such as molecular cores and protostars) or further away from the central object (such as circumstellar envelopes).

The visible/near-infrared range covered by X-shooter offers a window extremely rich in information on emerged young stellar objects. This range includes the spectral region where the photospheric continuum of star peaks; the beginning of the range where the emission of the hotter, inner parts of the circumstellar disk becomes comparable in intensity to the photospheric emission; and many of the most important emission lines resulting from accretion, winds, and jets, and chromospheric activity.

As stressed above, both medium spectral resolution and simultaneous broad spectral coverage are the strong points of X-shooter in the area of star formation. We consider for a case study LS-RCrA 1 (Fig. 5.2), a recently discovered object near the stellar/substellar boundary and the first of a class including so far only two known members. LS-RCrA 1 is a member of the young R CrA star forming region with a mid M-type spectrum and an unusually strong emission line spectrum. One of its most surprising characteristics is its low luminosity that, considered jointly with the late spectral type and the distance to the region, is far below what would be expected for other members. Its infrared spectrum (only K-band observations have been published so far) is also unusual in having CO lines much less prominent than expected for its spectral type, no detectable atomic lines, and no signs of near-infrared excess, thus discarding veiling by dust as a possible cause of the lack of spectral features at 2.2 μm. Either edge-on disks or accretion-modified evolution may be responsible for the underluminosity, but arguments based on line ratios disfavor the first explanation. However, stronger support in favor of the accretion-modified evolution may be provided by the kinematical information of the Hα line, unavailable from the low resolution FORS2 spectrum presented in Fig. 5.2. The possible relationship between the unusual spectral features in the visible and the infrared is not yet understood. We take LS-RCrA 1 as an example as it represents at present the faintest known object displaying the full range of T Tauri-like spectral signatures, and also because it may be a representative of largely overlooked population that may provide with new insights into early stellar evolution. The visible and near-infrared magnitudes are taken from Fernández & Comerón (2001) as follows: $V = 21.6$, $R = 19.8$, $I = 18.2$, $J = 15.3$, $H = 14.5$.

The comparisons with the different instruments described below have all been made using the same assumptions and definitions as in Sec. 5.1.4, and the same remarks made there apply.

- FORS1: Many interesting diagnostic lines are in the UV, starting from [OII], in a region where FORS2 is very inefficient as compared to FORS1. Therefore, FORS1 and FORS2 should be considered separately. FORS1 in the blue/UV can achieve a resolution $R \simeq 1200$ using a $0\farcs5$ slit, about 8 times lower than planned for X-shooter in that range and inappropriate for kinematical investigations. This is not compensated by a gain in efficiency: widening the X-shooter slit ($3\farcs8$) to degrade the resolution at 370 nm to $R = 1200$ makes X-shooter more efficient than FORS1 by a factor of 2.8 in terms of time needed to achieve a given S/N. For example, a star with a continuum of $U = 20$ observed for 50 min with X-shooter would yield $S/N = 55$ per resolution element, while 140 min would be needed by FORS1 to achieve the same. More importantly it should be noted that the the DQE of FORS1 drops sharply shortward of 370 nm, whereas the DQE of X-shooter is practically constant between 320 nm and 400 nm. X-shooter thus provides both higher efficiency and resolution than FORS1 at 370 nm, and adds the critical advantage in this field of providing kinematical information on UV lines.

- FORS2: The high-resolution holographic grisms allow a coverage of the V, R, and I bands between 456 and 948 nm with only one small gap of 40 nm around 750 nm and a resolution ~ 3 times smaller than that provided by X-shooter, approximately 5000 when a $0\farcs5$ slit is used. To cover the whole range of emission lines of interest, the red part of the spectrum where the photosphere dominates, and the bluer wavelengths where veiling is most easily detectable, the three high resolution FORS2 grisms (1400V, 1200R, and 1028z) need to be used. The discussion on the relative efficiencies of FORS2 and X-shooter over the V, R, and I bands given in Sec. 5.1.4 largely applies in the present case as well: X-shooter can observe the entire range much faster and in worse seeing conditions.

- UVES: For a detailed modeling of the kinematics of accretion, higher resolution than provided by X-shooter may be needed. The advantage of UVES in providing such high spectral resolution applies however only to strong emission lines. For the study of the continuum X-shooter will be needed. UVES may thus be considered complementary to X-shooter in this field.

- FLAMES/GIRAFFE: For the same reasons described in Sec. 5.1.4, X-shooter is to be preferred over FLAMES concerning spectroscopy of point sources, both due to spectral coverage and to efficiency per resolution element. However, the IFU units of FLAMES may allow the 3-D spectrosocopic mapping of the extended circumstellar environment in some selected objects, and its capabilities can thus be regarded as complementary with those of X-shooter.

- ISAAC: Given the similar expected throughput and resolution of ISAAC-medium resolution and X-shooter to within a factor of 2 (see the comparison between X-shooter and ISAAC in Sec. 5.1.4), the main difference is expected to be in the number of settings (10) needed by ISAAC to cover the same wavelength interval. For a relatively bright object like LS-RCrA 1, a $S/N = 30$ in the J band and 50 H bands is reached in only 1 min (per setting in the case of ISAAC). In the case of X-shooter the longer times to be used in the visible, which determine the duration of the exposure, will yield at no extra cost in time S/N values of a few hundreds that would require a substantial extra investment of time with ISAAC. Likely advantages of such extremely high S/N in the infrared at medium resolution will be detailed kinematical information on the CO bands in the H window and the possibility of studying in detail the excitation conditions of H_2 thanks to the accurate measurement of line ratios in both the J and H windows. Still, the possibility that ISAAC (or some of its modes) may not be available anymore by the time that X-shooter becomes operational may turn X-shooter into the instrument providing the J and H spectroscopy capabilities formerly offered by ISAAC and the VLT workhorse for VLT medium-resolution infrared spectroscopy, perhaps complemented with KMOS.

5.3.1 Astrophysical Importance

White dwarfs

Stars with main-sequence masses less than 8 solar masses produce white dwarfs at the end of their lives. For the most massive stars this is already after ∼200 Myrs. After their formation these white dwarfs cool slowly by radiating away their heat capacity (e.g. Hansen 1999; Bergeron & Leggett 2002). Detecting the coolest, oldest white dwarfs offers us a view into the very earliest epochs of our Galaxy. What is the shape of the old Galactic white dwarf population? What is their mass and space velocity distribution (see e.g. the discussion sparked by Oppenheimer et al. 2001)? What was the inital mass-function of our Galaxy? What is their binary fraction? Old, hydrogen-rich white dwarfs that have cooled to $T_{\rm eff} < 4000$ K, develop strong NIR collision-induced H_2 absorption, making their spectra highly recognizable distinguishable (Harris et al. 1999; 2001). Fig. 5.3 shows the spectrum of one of these cool objects.

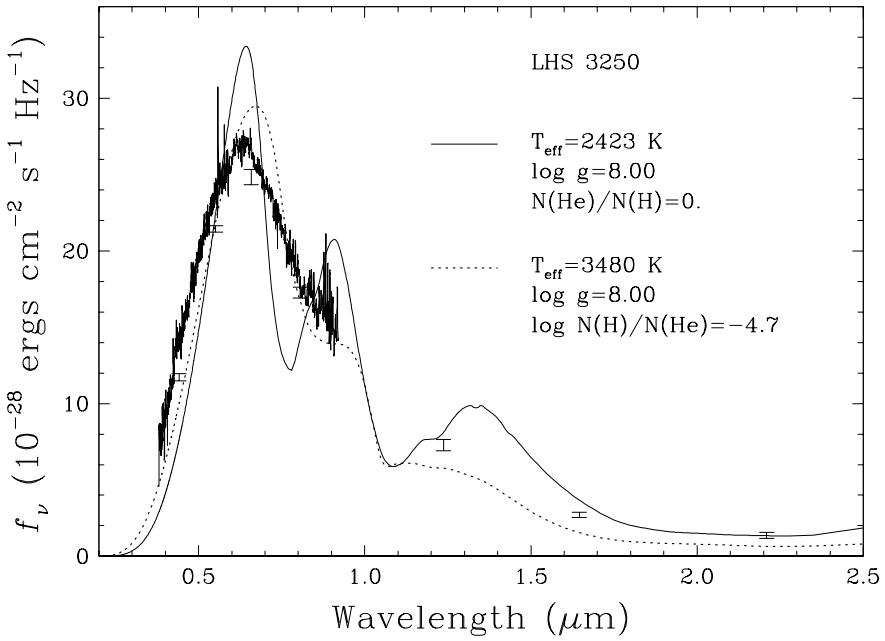

Figure 5.3 The optical spectrum of the ultracool white dwarf LHS 3250, showing the near-infrared absorption, along with two models at different temperatures and composition. A wide band instrument such as X-shooter will be needed to spectroscopically characterize these enigmatic objects. From Bergeron & Leggett (2002).

Supernovae Type Ia are of paramount importance to track the evolution of the Universe (e.g. Riess et al. 1998). However, the nature of SN Ia progenitors is still unknown. The most likely candidates are white dwarfs in binary systems that are driven over the Chandrasekhar limit either by steady accumulation of matter through mass-transfer, or by mergers (Livio 2000). In an alternative scenario the supernova explodes through an off-axis ignition of helium on a CO white dwarf of lower mass. However, which of the candidate white dwarf binary populations (supersoft sources, symbiotics, Cataclysmic Variables, AM CVn stars or detached binary white dwarfs) is the SN Ia progenitor population is unclear. Lacking this knowledge inhibits a further modelling of SN Ia explosions. To distinguish between the candidate populations we need to determine their characteristics, such as space density, orbital period and mass distributions.

The detection of gravitational waves with future satellites such as LISA will mark a breakthrough in

our ability of studying the Universe. Regimes that are hitherto closed, such as the central processes in supernovae, gamma-ray bursts, neutron star and black hole mergers and magnetars, will be opened for investigation. The success of gravitational wave detectors hinges on a good, *before-hand* understanding of the signal shape *and* the expected background signal. The background in the LISA frequency band is expected to be made up mainly of binary white dwarf systems in our Galaxy, both detached as well as semi-detached (AM CVn systems). A small number of AM CVn systems with extremely short orbital periods ($P_{\rm orb} < 10$ min), are currently the best candidates for detection with LISA (e.g. Israel et al. 2002; Warner & Woudt 2002). Our knowledge of the space density of such systems is far from complete and to estimate the LISA background we will have to characterize this population first. Detection and characterisation of these, intrinsically faint, ultra-short binaries is best done in the optical and X-ray regimes.

Equation of state of nuclear matter and the masses of stellar mass black holes

The structure of neutron stars challenges our understanding of particle physics, quantum mechanics and astrophysics. The unique opportunities offered by neutron stars to study environments of extreme density, extreme gravity, extreme magnetic fields and extreme rotation rates are unparalleled. The maximum mass of a neutron star is a strong limitation on the equation of state of neutron stars if this mass exceeds $M_{\rm NS} > 2$ $M_\odot$. Masses derived from radio pulsars are all consistent with 1.4 $M_\odot$ (Thorsett & Chakrabarty 1999). However, milli-second radio pulsars are thought to be the product of a prolonged phase of mass-transfer in a Low-Mass X-ray Binary (LMXB) in which the neutron star is not only spun up to milli-second periods, but also gains an appreciable amount of mass ($\geq 0.1 M_\odot$). Soft X-ray transients are ideal targets to search for such massive neutron stars; during the outburst they are easily identified by X-ray satellites. During quiesence the determination of the radial velocity curve of the mass-donor (typically an F-M type star in a 11 min to ∼days orbit) will yield the mass of the neutron star. Of the eight known LMXB pulsars five have been discovered during the past five years (including the three known millisecond X-ray pulsars; Wijnands & Van der Klis 1998; Markwardt et al. 2002; Galloway et al. 2002). More discoveries are therefore expected. Of these systems only 2A1822−37 has allowed a recent determination of its radial velocity curve with UVES due to the high luminosity of the slightly evolved secondary, V=16 (Jonker & Van der Klis 2001; Jonker, Van der Klis & Groot 2003; Fig. 5.4).

About 70% of all known Soft X-ray Transients have turned out to contain stellar mass black holes with a typical mass of ∼7 $M_\odot$. They have quiescent magnitudes $17 < V < 23$ (Orosz et al. 2002 and references therein). The reason for this strong concentration in the mass distribution is unkown and one of the key questions in black hole and binary evolution research. A study of the companions of these systems can illucidate the binary's evolutionary history. In GRO J1655−40, due to the high intrinsic brightness of the subgiant F-type companion, the abundances on the surface of the companion have been shown to be highly anomolous, leading to the suggestion that black hole soft X-ray transients might be the remnants of hypernovae/gamma-ray burst explosions (Israelian et al. 1999; see Fig. 5.5).

The physics of accretion disks

Accretion disks are one of the most common, and most poorly understood, phenomena in astrophysics. From young stellar objects, to close binaries, to AGNs and GRBs, accretion disks play a deciding role in shaping our Universe. Despite recent progress in understanding the source of viscosity in hot, high density accretion disks (e.g. Balbus & Hawley 2002), their general physics is still very poorly understood. The dependence on mass-transfer rate and X-ray irradiation (e.g. in Soft X-ray transients and dwarf novae outbursts), the structure of the accretion disk atmosphere, the dependence on chemical composition and the nature of the viscosity in the low-mass transfer rate, tenuous disks found in cataclysmic variables and Soft X-ray Transients in quiescence, is virtually unknown (e.g. Menou, Perna & Hernquist 2002).

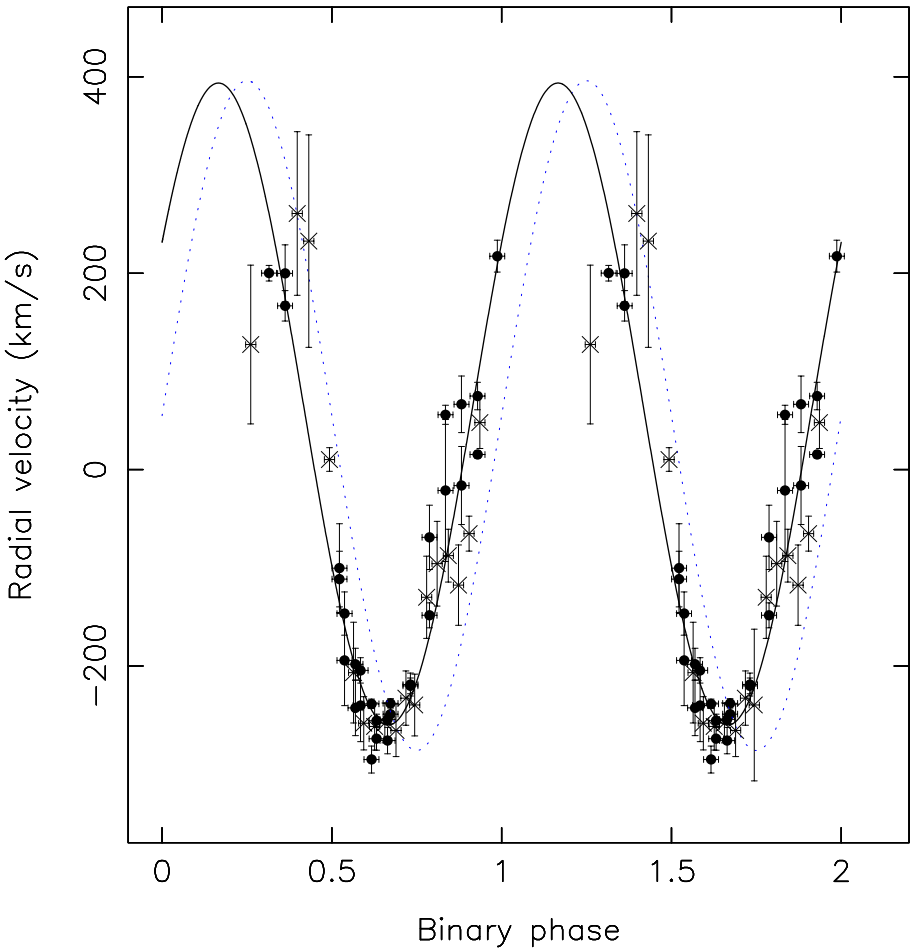

Figure 5.4 The radial velocity curve of 2A1822−37, as obtained with UVES and Magellan. The limits on the mass of the neutron star is still dominated by the errors and scatter in the points, even though this is the brightest of observable LMXBPs (Jonker, Van der Klis & Groot 2003).

Our inability to resolve any accretion disk in systems besides young stellar objects, prevents a direct, detailed study. However, two indirect imaging techniques, Doppler tomography (Marsh & Horne 1988) and eclipse mapping (Horne 1986), offer the possibility of reconstructing spatially resolved accretion disk velocity fields and spectral energy distribution on a micro-arcsecond scale. Results in Cataclysmic Variables so far have shown that the structure of even high mass-transfer rate systems does not conform to standard accretion disk theory (see e.g. Groot et al. 2002).

5.3.2 Instrument Requirements

Old white dwarfs

Due to their intrinsic faintness ($M_V > 14$) appreciable numbers of old white dwarfs are expected only at $V > 20$, requiring a high throughput instrument for spectroscopic follow-up. The broadness of the NIR H_2 absorption makes it imperative to obtain spectra over a broad wavelength range. Resolving binary motion and determining accurate space velocities require a spectrograph with a velocity resolution ≤ 50 km s^{-1}. Characterizing the shape of the WD spectrum, and thereby allowing a more careful modelling and derivation of fundamental parameters (e.g. T, M), requires a high throughput, wide spectral range instrument on a large telescope.

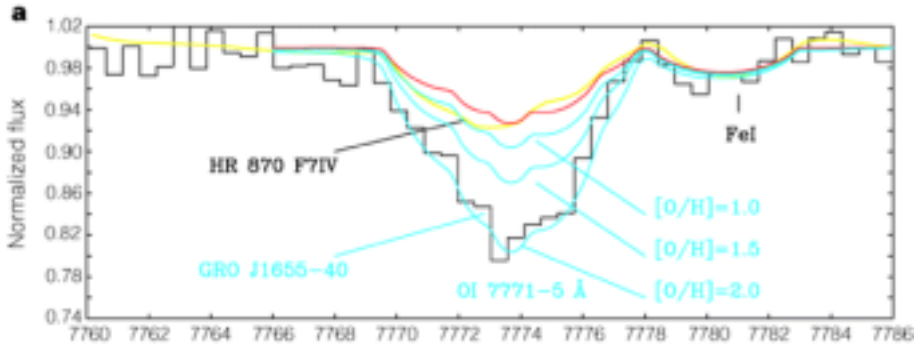

Figure 5.5 The spectrum of GRB J1655−40 compared with model spectra of different metallicity. A metallicity of 10×solar is needed to fit the lines. From Israelian et al. (1999).

Close binary systems

To distinguish between the candidate SN Ia progenitors a combination of wide field imaging and high throughput, medium resolution spectroscopy is needed. OmegaCAM/VST and VISTA provide the ESO wide field capabilities, but to study these, often intrinsically faint, populations an adequate spectrograph is lacking. The faintness of most of the black hole Soft X-ray transient companions (visible after the decline of the initial outburst) excludes a study at the required resolution with current VLT instrumentation.

Medium resolution ($R \geq 5\,000$) is needed to adequately resolve the orbital motion in close binary systems. A broadband wavelength coverage is needed for the crucial simultaneous observations of the multiple components in these systems: the white dwarf in the UVB, the accretion disk in the UVB, optical and NIR, and the secondary in the NIR. Due to erratic photometric variability (e.g. photometric outbursts), and spectroscopic variability (e.g. varying irradiation of the secondary) it is imperative to obtain simultaneous observations over the complete wavelength range. Since the majority of the observable population of these sources lies at V>18 and/or are best studied in extragalactic systems (e.g. the supersoft sources in the LMC/SMC) a high throughput spectrograph is required, especially since the integration times for these systems are in most cases limited at, typically, 1/20th of an orbital period at most to prevent phase smearing of the velocities. For a 4 hour binary this limits the integration times to < 12 minutes.

Accretion disk physics

A breakthrough in accretion disk physics will come from the joint application of Doppler mapping (i.e. velocity resolved studies) with eclipse mapping (i.e. time resolved studies) of accretion disks in close binaries. Since close binary systems are notorious for photometric and spectral variability on all time scales *simultaneous* observations in the optical and NIR bands is crucial. To do this, simultaneity, medium resolution ($R \geq 5000$), wide spectral range (to reconstruct the accretion disk spectral energy distribution) and high throughput is needed. Especially a NIR extension will allow a meaningful correction for (and a study of) the light of the red mass-donor in the low mass-transfer rate systems that harbour the, as yet unexplained, tenuous accretion disks (see e.g. Fig. 5.6).

5.3.3 Target Selection

Targets for the old white dwarfs are expected to come from OmegaCAM/VST, VISTA and the SDSS. To characterize the population we expect to need ~ 200 old white dwarfs. With only a few examples known, estimating a space density is highly uncertain, but we expect less than one per square degree down to V=21. A few hundred to a few thousands are therefore expected from SDSS, and similar numbers from OmegaCAM/VST (due to its deeper limiting magnitude).

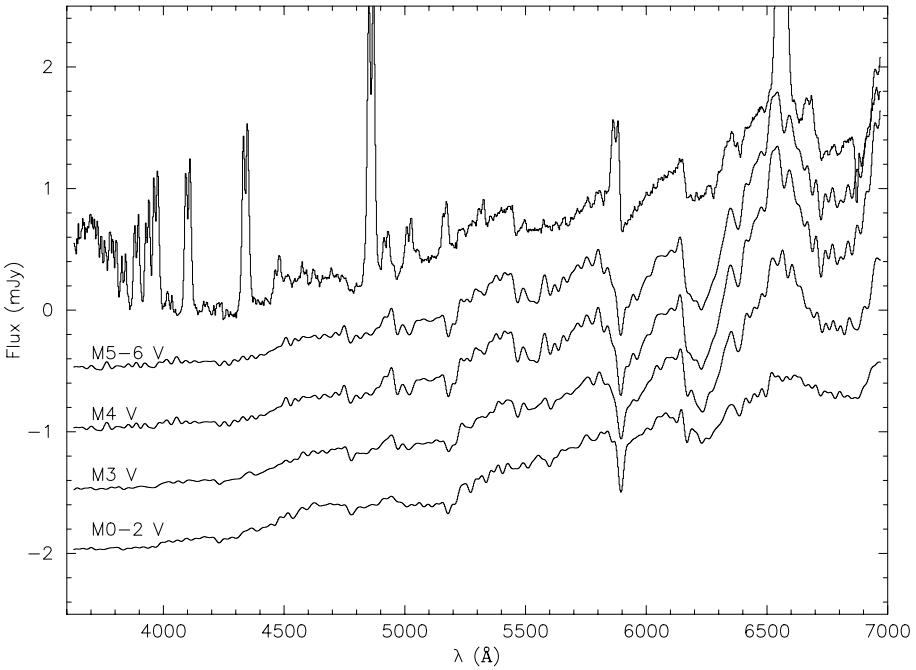

Figure 5.6 The optical spectrum of IP Peg, showing the contributions of the accretion disk (blue continuum and emission lines) and the red mass donor of early M-type. To accurately correct for the contribution of the secondary (which is phase dependent) simultaneous NIR spectra will be essential.

For the supernovae Type Ia progenitors the number of targets depends very much on the possible parent populations. Of detached binary white dwarfs we know a few dozen, none of which so far meets the criterium of having a combined mass exceeding the Chandrasekhar mass and that will merge within a Hubble time. We known 12 AM CVn systems, 5 of which were found in the last three years. This is therefore very much an evolving field.

Soft X-ray transients are found at a rate of $\sim$4 per year. Of these most are black hole systems and the rest are neutron star systems. The best chances of determining neutron star masses is in low mass X-ray binary pulsars. Of the eight known LMXBPs, five were found in the last five years, including the three millisecond X-ray pulsars.

There are over 600 CVs known, 83 of which are eclipsing, and of these $\sim$65% are visible at Paranal. Many of these are also outbursting systems, where time-dependent, simultaneous eclipse mapping and Doppler mapping can be obtained. These systems are the main targets for the accretion disk physics program. With an increase in the observing efforts on faint cataclysmic variables, the number of eclipsing systems is expected to rise at a few per year.

5.3.4 X-shooter Performance

For close binary systems current VLT instrumentation is unsuitable for these observations due to lack of efficiency (UVES), spectral resolution (FORS) or capability of simultaneously observing at the required resolution (FORS+ISAAC).

X-shooter is unique in the combination of three main objectives: high throughput, medium resolution and wide wavelength coverage. For all the fields described above at least two of these characteristics are required. Current VLT instrumentation is not capable of meeting the required demands. For the old white dwarfs the combination of wide spectral range, high throughput and spectral resolution is crucial. For the neutron star and black hole masses the spectral resolution and high throughput. For the accretion disk studies and the time evolution of soft X-ray transients, it is the combination of high throughput, spectral resolution, wide wavelength coverage and simultaneity. X-shooter's combination

of high throughput and spectral resolution will open up the important field of abundance measurements in Soft X-ray transient companions, which may give us direct links to the origin of gamma-ray bursts. With X-shooter we will be able to also obtain the radial velocity curves of LMXBPs down to V=22. To illustrate the X-shooter capabilities we show the result of the X-shooter ETC for an old white dwarf at V=22, and for phase resolved spectroscopy on a V=20 mag binary in a 4 hour orbit, and compare these to existing VLT instrumentation.

To reliably establish the Galactic distribution, space velocities, mass distribution and age distribution of old white dwarfs, we will need to obtain spectra of at least 200 objects. With X-shooter, obtaining a spectrum at V=22, over the full X-shooter wavelength range at a resolution of R≥5000, to a S/N=10 in the continuum, will require 40 minutes per object (see Fig. 5.7), and therefore 30 nights will be needed for the full sample. To cover the complete wavelength range with FORS2 and ISAAC one needs to go to at least one third of the X-shooter spectral resolution, and it then still takes a total of 4 hrs in four settings to obtain similar signal-to-noise (using the FORS2 600B, 600RI and ISAAC SW Low resolution mode, J and H band). To obtain spectra at the same spectral resolution and wavelength coverage is not (and will not be) possible without X-shooter.

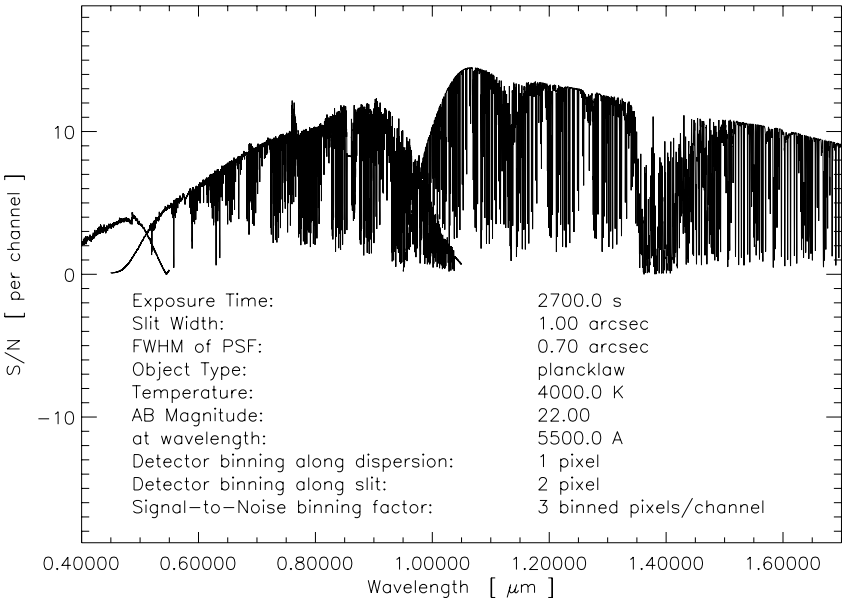

Figure 5.7 X-shooter Exposure Time Calculator for a 4 000 K blackbody at V=22. A S/N>10 is reached in 40 minutes of integration, where 4 hrs is needed with FORS+ISAAC.

In the accretion disk studies in close binary systems the full wavelength range will be needed, but also at the X-shooter resolution of R≥5 000 ($\Delta v \leq$60 km/s). For the radial velocity studies, smaller parts of the wavelength region may be required. As an example we show the S/N requirements for a close binary in a 4 hour orbit where quiescent magnitude is V=20. The 4 hour orbit limits the integration time to $<$ 12 minutes, to prevent phase smearing. At Hα X-shooter will have $R = 7\,000$ (with a $1''$ slit), and the 12 minute integration will yield S/N≥10 at V=20. The closest current alternative is FORS2 using the 1200R grism, but this will only yield half the resolution ($R = 4\,300$), with similar throughput. For most close binary systems this prevents an accurate (<30%) determination of the radial velocity curves and therefore of the neutron star and black hole masses. Although UVES has the required resolution, its efficiency prevents usage for radial velocity studies at magnitude >16.

CHAPTER 6

Cosmic Explosions

SECTION 6.1

Supernovae

6.1.1 Astrophysical Importance

A better understanding of the physics of supernovae (SNe) has fundamental implications in many fields of modern physics and astronomy. Stellar physics, extragalactic astronomy, observational cosmology and nuclear physics, among others, are influenced as our knowledge of SN explosions improves. As the endpoints of the evolution of massive stars, SNe are the most important contributors to the chemical enrichment of galaxies. As such the existence of supernovae is a prerogative for the existence of life as found on Earth. They are used as cosmological distance indicators and the recent association of some peculiar SNe with Gamma-Ray Bursts opens one more window to explore into the multiple dimensions of terminal stellar instability. SNe are broadly divided in SN Ia (exploding white dwarfs) and in core collapse SNe (CCSNe) which include SN II, IIL, IIB, Ib/c (Wheeler & Benetti 2000).

Core-collapse supernovae: the illumination by SN1987A

SN 1987A has made a tremendous impact on the understanding of core collapse supernovae. The two orders of magnitude shorter distance compared to normal supernovae made totally new observations possible. Among the highlights were the first reliable abundance determinations for supernovae, the detection of dust formation and the observation of radioactive isotopes. All these achievements were the result of a broad wavelength coverage with high S/N observations at epochs up to several years after the explosion. The late epochs are of special significance, since the supernova ejecta becomes more and more transparent with time, and the interior regions become accessible to observations. Further, several of the most interesting phenomena, like dust formation and the decay of radioactive elements take place at these epochs. Finally, these nebular spectra are considerably easier to model, and abundances etc. can more reliably be determined compared to the early phases. Although SN 1987A has given us unique information about this explosion, it is only one particular case. For a full understanding of the explosion physics one needs similar information on a larger sample including supernovae of different nature and in different environments.

Abundances

Both the optical and IR range contain a large number of lines useful for determining the abundances of the most abundant elements (for a review see Fransson & Kozma 2002). This includes carbon, oxygen, magnesium, sulphur, calcium and iron and cobalt (Table 6.1).

Not only is the full wavelength range needed, but also a complete time coverage. As the supernova expands, the density decreases and at the same time the radioactive energy input decreases exponentially.

Table 6.1. Important Diagnostic Supernova Lines

Ion	Wavelength (Å)
H I	6 563, ...
He I	5 577, 10 830
C I	8 729, 9 812
O I	5 577, 6 300, 6 364
Mg I	4 571
Si I	10 990, 16 450
S I	10 824, 11 309
Ca II	7 292, 7 325, 8 499–8 663
Fe II	7 155, 12 570, 15 330, 16 400
Co II	15 430

Therefore, the temperature and degree of ionization also decrease. As demonstrated in the case of SN 1987A, this provides extremely useful constraints on the structure of the supernova and the reliability of the derived abundances. Observations to as late time as possible are therefore needed. In particular at an epoch of 500–700 days a dramatic drop in the temperature is expected to take place, connected to the so-called IR-catastrophe. This occurs because a transition from cooling by optical to IR fine-structure lines takes place. As will be discussed below this is also accompanied by molecule and dust formation, which is of special interest.

A related and much discussed issue is the role of hydrodynamical mixing and instabilities in the supernova ejecta. Again, there is much evidence for this in SN 1987A. The most direct way of studying this is through the line profiles of the different elements. Lines of different elements are here expected to probe different regions of the ejecta.

While much work on abundances has been concentrated on core collapse supernovae, Type Ia supernovae are of prime interest in their own right. The details of the explosion mechanism, deflagration versus detonation, is reflected in both the relative strengths of different lines, as well as in the line profiles. In particular, three-dimensional large scale instabilities may result in asymmetries and distinct feature of the line profiles. As in CCSNe, abundances in Type Ia's are best derived in the late, nebular phases.

Radioactivity

After about a month the energy input into the supernova ejecta is dominated by the decay of radioactive isotopes, primarily $^{56}\mathrm{Ni} \rightarrow {}^{56}\mathrm{Co} + \gamma \rightarrow {}^{56}\mathrm{Fe} + \gamma$ and positrons. The gamma-rays and positrons are thermalized, giving rise to the observed optical and IR emission. Besides ^{56}Ni, also radioactive ^{57}Ni and ^{44}Ti isotopes are produced in the explosion. The masses and relative abundances of these isotopes are important diagnostics of the conditions of the supernova explosion during the first seconds.

In SN 1987A all three isotopes were observed from the bolometric light curve, as well as from line emission of Fe II and Co II. The latter is the most direct way of determining the ratio of iron to cobalt in the supernova. In particular, the ratio of the [Co II] 1.547 μ and [Fe II] 1.533 μ lines directly maps the Fe/Co ratio in the supernova.

The decline rate of the late time bolometric luminosity gives a direct measure of the iron group materials synthesized in the explosion that are returned to the ISM. It is important to measure this rate from spectrophotometric light curves, since some of the optical/near IR bands are heavily affected by

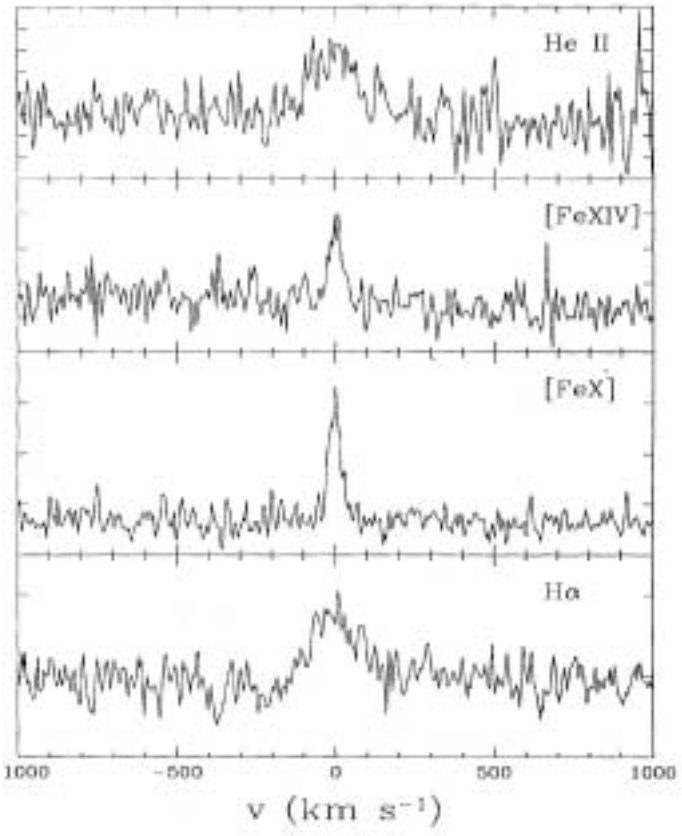

Figure 6.1 Narrow emission lines originating in the circumstellar nebula of SN 1993J (Benetti et al. 1994).

strong spectral features. From the decay time scale of these lines the isotopic ratio in SN 1987A could be determined.

For supernovae other than SN 1987A only the ^{56}Ni isotope has been observed. The transition between the ^{56}Ni and ^{57}Ni decay as the most important energy source occurs at about 700 days, depending on the isotopic ratio.

Dust formation

Asymptotic-Giant-Branch (AGB) stars and supernovae are the main candidates are for the formation of dust. While the dust formation in AGB stars has been fairly well established, this is not the case for supernovae. Only in SN 1987A has there been unambiguous evidence for this. At an epoch of about 500 days there was a marked shift of the peaks of the line profiles of the strongest emission lines in the spectrum. This was interpreted by Lucy et al. (1991) as a result of absorption of the line emission from the supernova ejecta by newly formed dust. The emission from the rear, receding part of the ejecta would then be more absorbed than the emission from the front part, producing a suppression of the red side of the line profile. In SN 1987A this event was accompanied by a general shift in the emission from the optical range to the mid-IR range, again indicative of dust thermalization of the supernova radiation. Although of prime importance for the cosmic formation of dust, this event has sofar only been detected in SN 1987A.

Interaction of supernovae with the circumstellar medium

The interaction of supernovae with the circumstellar medium gives insight in the mass loss history of the progenitor, the ejecta structure and shock wave physics. In the optical and NIR this interaction manifests itself in the form of broad and narrow lines of neutral as well as highly ionized atoms. The

most extreme example of this is in the Type IIn supernovae. While the broad lines come from ejecta ionized by the shock wave, the narrow lines originate in the dense, circumstellar gas ionized by the shock radiation before the shock hits the gas (see Fig. 6.1). The velocity of this gas reflects the acceleration of the stellar wind of the red supergiant progenitor by the burst of radiation at the shock break-out. Because of the dilution of the radiation the velocity is expected to decrease with radius. The velocity width of the circumstellar lines are therefore expected to decrease with time as the supernova shock wave expands to larger radii. Typical velocities are in the range 10–1000 km s^{-1}.

The supernova - gamma-ray burst connection

During the past few years a strong connection between supernovae and GRBs has emerged. GRBs are discussed in detail in Section 6.2. An aspect related to this section, however, is the detailed understanding of different classes of supernovae as candidates for GRBs. In particular, Type Ic supernovae are of special interest. Both theoretical modeling and the observation of the coincidence of the Type Ic SN 1998bw and GRB 980425 have brought this connection to the forefront.

Detailed studies of SN 1998bw showed that it had several unique aspects compared to other supernovae. The ^{56}Ni mass derived from the light curve and line emission was a factor ten higher than for typical supernovae, and the line profiles extended to 60 000 km s^{-1}. The line profiles showed strong evidence for hydrodynamical mixing, and asymmetry has been claimed.

In the next few years this type of studies will become increasingly important. GRBs will be rapidly and accurately localized and the sample of relatively nearby GRBs can be expected to increase. To study these supernova/GRBs the limits will of 8-m class telescopes will be stretched, especially during the important late time decay. A maximum throughput is therefore crucial.

In parallel, more detailed studies of especially the Type Ic supernovae, in terms of masses, abundances, radioactive elements and hydrodynamics, are important. Polarization measurements may provide evidence for asphericity, possibly connected to hydrodynamical jets.

Type Ia supernovae as a cosmological tool

Type Ia supernovae provided the first direct evidence for an accelerating universe. The smoking gun signal of the dark energy would be the study of the early deceleration phase. This requires observations of supernovae at a redshift of $z \sim 1$. Such supernovae are now being discovered, for example in the GOODS transient search. Furthermore, systematic effects are likely to be the next big discussion in supernova cosmology. The large projects that lie ahead to determine the cosmic equation of state will need to understand differences between the local and the distant sample of supernovae in detail.

Early observations and complete coverage of the light curves and the spectral evolution are missing. It will be of paramount importance to sample the rising branch of the bolometric light curve in order to set very tight constrains on models of SN Ia progenitors (Riess et al. 1999). Observationally, the acquisition of type Ia data of sufficient time and wavelength coverage with intermediate ($R \sim 5000$) resolution presents a particular challenge (Fig. 6.2). Supernovae occur unpredictably, making conventional telescope-instrument scheduling very difficult. Yet, when they do occur, they demand fast response and frequent (about once per day) observations over a wide wavelength range. Currently, the quality, temporal and wavelength coverage of SN Ia databases is seriously deficient. In particular, there is a severe shortage of IR observations, and yet this wavelength range is vital for understanding the physics of SNe Ia (Meikle 2000).

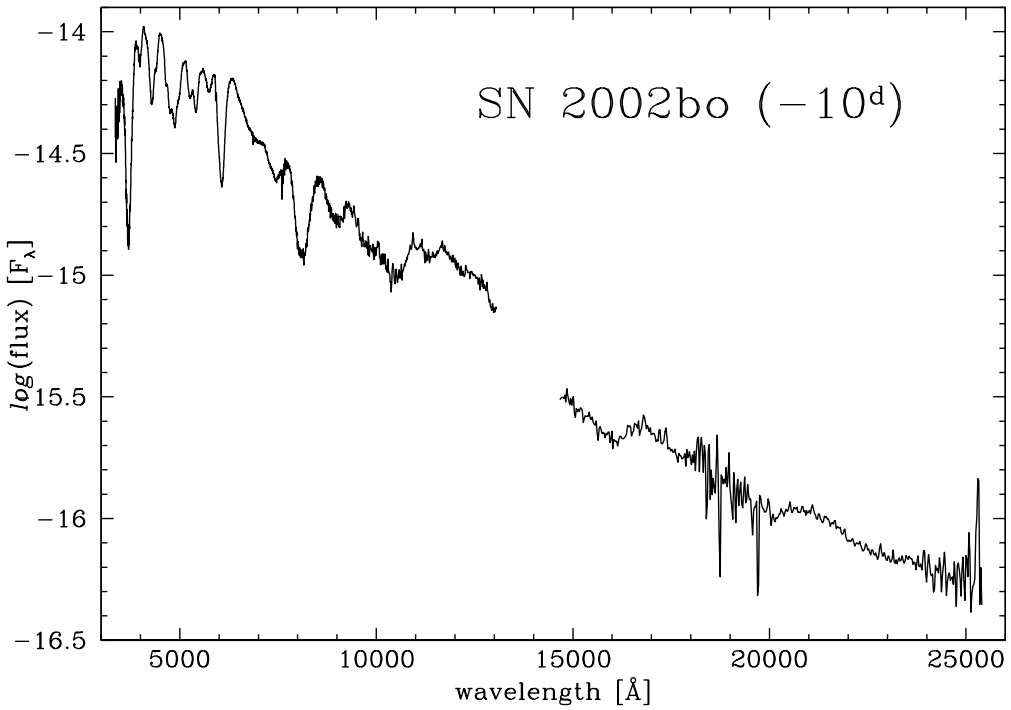

Figure 6.2 The composite optical-NIR spectrum of SN 2002bo 10 days before maximum light.

6.1.2 Instrument Requirements

To observe SNe at all redshifts between 0 and 1.7 with the highest possible quality a number of requirements are to be met:

- Line profiles are best observed in the NIR lines, where line blending is less severe than in the optical. In particular, iron and cobalt have their most isolated lines in the J- and H-bands. Access to these is very important. To resolve these features a resolution of 50–100 km s^{-1} is needed.
- From the wavelength list (Table 6.1) it is obvious that a complete coverage of the optical-NIR is necessary for studying the most abundant elements produced in supernovae.
- In order to determine the Fe/Co ratio access to [Co II] 1.547 μm and [Fe II] 1.533 μm is important.
- Sampling the UV-optical-NIR region of the spectrum is crucial to obtain spectrophotometric light curves.
- A broad wavelength coverage is important in order to see both wavelength dependent extinction effects and also to determine which is the abundance zone in which dust formation takes place. To characterize the circumstellar environment, and to constrain the progenitor model medium resolution ($R \geq 5\,000$) spectroscopy is required.
- Most of the redshift determinations for the distant supernovae come from narrow galactic lines, such as [O II] λ3727. The ability to separate the two components of this line is of utmost importance for secure redshift determinations, as has been shown with ESI at the Keck Telescope. The next generation VLT spectrograph will have to be competitive in this respect. At high redshift the well-known supernova lines move into the near-IR, and a spectrograph with a wide wavelength capability becomes increasingly important. The Si IIλ6150 line, which is the main absorption

feauture used for the classification of SNe Ia, falls out of the optical domain for $z > 0.5$. Access to the H-band will ensure a detection up to $z \sim 1.7$.

For the study of systematic effects (e.g. redshift evolution) high signal-to-noise spectra of distant supernovae are required, especially in the rest frame UV, where metalicity differences become most pronounced. FORS has proven very useful for supernovae Ia at maximum at $z = 0.5$, but to move to higher redshifts of $z = [0.7, 1.0]$ the throughput must be increased. A broad spectral range is also critical for detailed tests for dimming of SNe Ia by intergalactic large grain dust.

6.1.3 Target Selection

Efficient searches for nearby and distant supernovae are being conducted at many facilities on the ground. For example, the CFHT Legacy Survey will find $\sim$ 4000 SNe over the next 5 years, half of which will be too distant to be efficiently studied with current VLT instrumentation. The planned SNAP mission will discover thousands of SNe at high redshift.

6.1.4 X-shooter Performance

X-shooter will provide the required spectral resolution for line profile analysis and faint spectral identification at high redshift, the required sensitivity to faint sources and the needed wide wavelength range, in particular the NIR arm which offers a major advantage over ESI at Keck. It promises to give fundamental contributions to all the above supernova problematics, reaching the stage where the intrinsic rate, details of the explosion mechanism, and nature of the collapsed remnant in these events can be routinely investigated.

Follow-up spectroscopy to classify very distant supernovae has been difficult. For SN 2002hp, discovered at a magnitude of 24.35, a deep VLT/FORS spectrum was sufficient to determine a redshift of 1.3 from the galaxy emission lines, but not deep enough to secure the supernova type. To demonstrate the power of X-shooter we show an ETC calculation of the S/N attained for an Type Ia supernova at maximum light at $z = 1.5$ ($I = 25.4$, $J = 24.0$, $H = 22.0$). The simulation shows that X-shooter can determine the type and redshift of such a distant supernova in an exposure time of 4 hours (and possibly less).

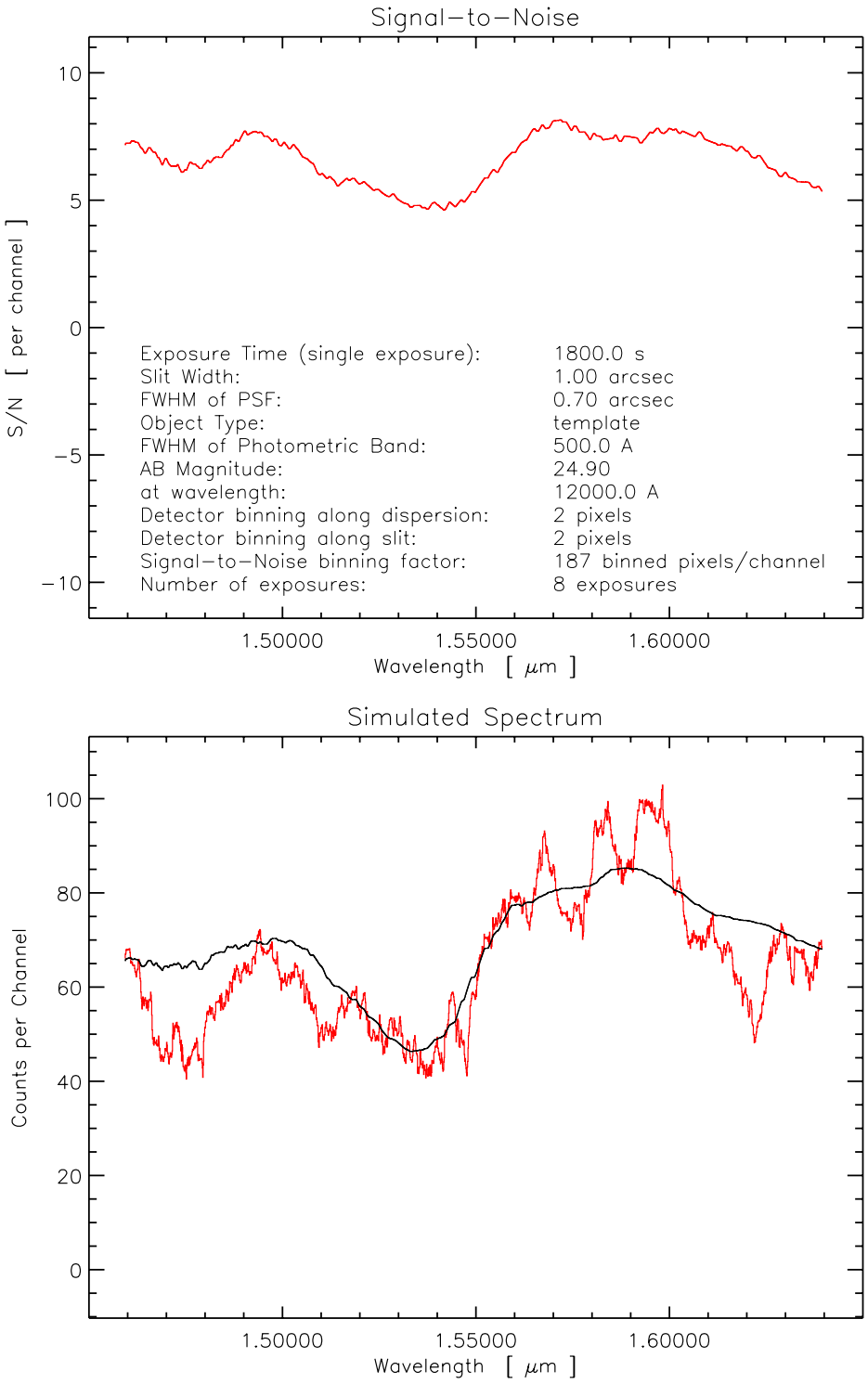

Figure 6.3 X-shooter ETC simulation of a 4 h exposure of a high-redshift Type Ia supernova at maximum light. The upper panel shows the S/N attained by the NIR arm when binned to a resolution of ~ 500 Å. The lower panel shows a simulated X-shooter spectrum on top of the template spectrum (black curve) that has been redshifted and dimmed to a redshift of $z = 1.5$. Before binning both spectra have been weighted by $(S/N)^2$ in order to minimize the contribution from atmospheric absorption and emission lines. The template spectrum is a DFOSC/DK1.5m spectrum of the Type Ia SN 1999ee (Hamuy et al. 2002) at maximum light. The approximate magnitudes of the supernova are $I = 25.4$, $J = 24.0$, $H = 22.9$. The broad Si IIλ6150 feature, indicative of a SN Ia, is clearly identified at 1.54 μm in the simulated spectrum. The continuum emission of the host galaxy may potentially complicate the measurent. If the host galaxy has emission lines, the full X-shooter wavelength range covers Lyα, [OII], Hβ, [OII] and Hα which would be detectable in the unbinned spectra.

6.2.1 Astrophysical Importance

Gamma-Ray Bursts are powerful sources with a spectrum peaking at 100 keV and whose durations are bimodally distributed around 20 s (long GRBs) and 0.2 s (short GRBs). Remnants of the explosion are a long-lived, fading "afterglow", detectable at all frequencies from gamma-ray to radio, and, according to current theoretical expectations, a stellar-mass black hole. The observed rate of GRBs is about 2–3 per day. Optical and infrared spectroscopy of the afterglow of long GRBs has demonstrated that their origin is cosmological, with detected redshifts up to $z = 4.5$, but higher redshifts are expected. If their GRB energy is emitted in a jet, the observed gamma-ray intensities yield energies comparable to the most powerful supernovae. If isotropic, GRBs are by far the most powerful explosions in the Universe. For short GRBs no counterparts have been detected so far, and their redshift distribution remains unknown.

Due to their high redshift and huge energies, GRBs are tracers of the most extreme physical conditions in the universe back to its earliest ages. The three most central aspects of GRBs for astrophysical research are:

- **The GRB progenitors.** A major question in GRB research is the nature of the progenitors. There are two main classes of possible candidates: mergers of two compact objects (e.g. neutron star–neutron star or neutron star–black hole, e.g. Belczynski, Bulik & Rudak 2002) and the collapse of a massive star (e.g. Zhang, Woosley & MacFadyen 2003). The latter class encompasses the so-called 'hypernova' and 'supranova' and 'collapsar' models. The properties of the environment are expected to be very different in these scenarios. In the merger case, the bursts are expected to take place in a uniform, low-density intergalactic medium due to the long time between formation of the compact objects and the merger of the binary. In this time the binary may have travelled a substantial distance through or out of its host galaxy. In the hypernova scenario the burst is coincident with the supernova explosion and its immediate environment is therefore the pre-explosion stellar wind. On the other hand, in the supranova scenario (Vietri & Stella 1998), the burst happens after a certain delay from the associated SN and, as such, it is expected to occur in an evacuated cavity surrounded by a SN shell.

- **The link with star formation.** All progenitor models imply that GRBs should be associated with massive star formation. Also observationally, there is evidence that GRBs preferentially occur in regions of ongoing star formation. Thus GRBs are ideal tracers of massive star formation throughout the evolution of the universe. A great advantage of GRBs over other star formation tracers is that GRB-selection does not suffer from biases such as the dust bias that prevents us from studying heavily dust obscured regions of star formation with optical instrumentation. Furthermore, all determinations of the cosmic star formation rate based on surveys for star forming galaxies (in the optical and at sub-mm wavelengths) rely on the extrapolation of number counts to flux-levels below the detection limit of the surveys. GRB-*selection* is independent of the total flux of a galaxy and hence allows the selection of a star forming galaxy across the complete luminosity function. Therefore, the study of the GRB host galaxies can tell us if the bulk of the star formation at high redshifts takes place in e.g. heavily dust-obscurred massive sources or in faint galaxies below the detection limits of current high-z galaxy surveys.

- **GRBs as beacons to the early universe and the epoch of re-ionization.** Since GRBs occur at cosmological distances they can be used as probes of cosmological lines-of-sight in a manner similar to that of bright quasars (Lamb & Reichart 2000). The advantage of quasars is that they are (and remain) very bright to allow very high signal-to-noise spectra to be collected in long exposure times. Therefore, quasars will remain important probes of the weak lines of the

Lyα forest at redshifts $2 < z < 5$. However, GRBs have a unique advantage over quasars in the study of the more rare high column density absorption systems such as MgII absorbers and the Damped Lyα absorbers. For these systems a central question is the relation to galaxies. The very bright quasars make it extremely difficult to search for the galaxy counterparts of the intervening absorbers. However, in GRBs the afterglow will disappear and the search for emission from the absorbing galaxy will only be affected by the light from the much fainter GRB host galaxy. More importantly, GRBs offer unique possibilities for the study of the very early universe, i.e. the epoch of the formation of the first stars and the reionization of the universe – the so called dark ages. There were no quasars at this epoch (per definition) – it takes several hundred million years to build up a supermassive black hole. The first stars, however, are expected to be supermassive (100 solar masses or more, e.g. Heger & Woosley 2002) and a fraction of these are expected to produce detectable GRBs. As has been shown in several papers in the literature, detection of the NIR spectra of the afterglow of such bursts at redshifts $7 < z < 10$ is feasible (due to time dilation) and will allow a measurement of the epoch of reionization (e.g. Madau & Rees 2000).

6.2.2 Instrument Requirements

The transient nature of gamma-ray bursts requires simultaneous observations across a maximal wavelength range to ensure a high quality study of the afterglow evolution. The isotropic distribution on the sky implies a random distribution of their positions (with the exception of positions near the Sun due to the sun-angle constraint of gamma-ray satellites.

The three crucial requirements that no existing VLT instruments meet are wide spectral coverage, resolution, and efficiency.

Wide spectral coverage

GRB redshifts have been measured directly via detection of absorption lines on the optical afterglows and indirectly through the optical and near-infrared emission line spectra of their identified host galaxies. **It is important to have a spectral coverage as wide as possible since the redshift is not known in advance**. The near UV is essential to cover the Lyα and strong interstellar metal absorption lines in the restframe UV which are redshifted into the near UV for redshifts $1 < z < 3$.

Fig. 6.4 shows as an example two spectra obtained at the Nordic Optical Telescope of the bright optical afterglows of GRB 000926 (about 20 hours after the burst when the afterglow was about R=19.0) and of GRB 021004 (about 11 hours after the burst when the afterglow was about R=18.3). Based on the strong Lyα and interstellar metal absorption lines seen in these spectra, redshifts of $z = 2.0378$ and $z = 2.3293$ were inferred for these two bursts. Note that the strongest lines are in near UV at these redshifts.

Obviously, the near-infrared from 1 μm to 1.9 μm is essential for the spectroscopy of very high redshift bursts. For $z > 7$ all the strong lines seen in Fig. 6.4 will fall in this spectral region and basically no emission will be emitted in the optical due to the Gunn–Peterson effect.

Resolution

A resolution high enough to resolve the sky-lines is essential for faint NIR objects. As an example, the redshift of GRB 020405, first measured by VLT+FORS1 ($z = 0.695$, Masetti et al. 2002), could be precisely measured and unambiguously confirmed only by Keck-ESI, due to its higher resolution and ability to remove the sky lines, which critically affected the optical spectrum (Price et al. 2002). The need for high resolution (R >5 000) is even more important in the near-IR in order not to be completely swamped by the bright OH night sky lines.

Higher resolution is also needed to identify metal systems along the line of sight, near the host galaxy redshift. For example, the afterglow of GRB 021004 has been observed at high resolution (R =42 000)

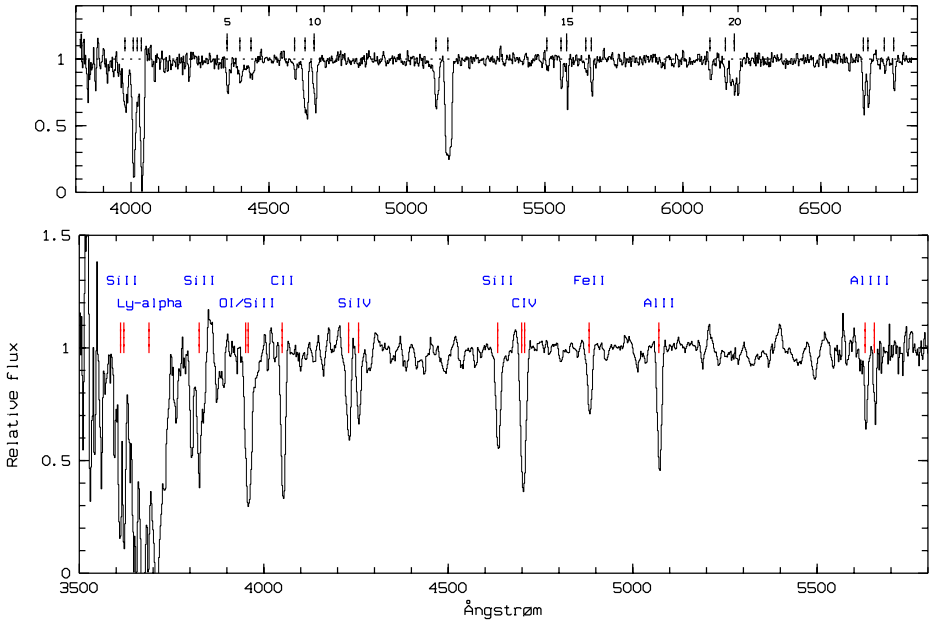

Figure 6.4 Nordic Optical Telescope low-resolution spectra of GRB 000926 and GRB 021004.

by UVES at VLT/Kueyen. At the time of the observations the afterglow magnitude was R∼18.6 and B∼19.0. Many absorption lines associated with several metal systems covering a velocity range of up to 3 000 km s^{-1} are detected in the UVES spectra (Savaglio et al. 2002; Fiore et al. 2003). Fig. 6.5 shows the UVES spectrum between 5090 and 5120 Å at full resolution (R=42 000, lower curve) and at 4 degraded resolutions: R=20 000, second curve from the bottom, R=10 000, third curve, R=5 000 forth curve and R=1 000, fifth curve). Strong C IV absorption systems are present in this wavelength range. Two main systems are present at $z = 2.2983$ (red labels in figure) and $z = 2.2959$ (black labels), respectively. Note that at the full UVES resolution each of these systems is resolved in at least 2 or 3 distinct components. Indeed one of the straightforward results of the UVES observations of GRB afterglows is that the GRB environment is complex and many components contribute to each main absorption system. This means that metal column densities estimated from low-resolution spectroscopy, i.e. without the capability to separate the components, are likely to be in excess to the real column densities. This complexity is completely lost at R=1 000. Resolutions of R=5 000 or higher are clearly needed to make full use of the powerful diagnostics that GRB observations offer to the study of the environment of GRBs and the ISM of their host galaxies.

Efficiency

The study of the immediate environment of GRBs can yield fundamental clues to reveal their origin. This is because the early fireball explosion erases all the direct signatures from the moment of the explosion. Afterglow continua generally decay in time following a power-law $t^{-\alpha}$ with $\alpha = 1.3$–1.6, and their average magnitude at 12 hours after the GRB is $V \sim 21$. Promptly activated time-resolved simultaneous optical and IR spectroscopy of the early counteparts of GRBs can yield information on the dust content of the medium. Most GRBs appear very little reddened. According to one hypothesis this is due to dust destruction. This idea can be tested by early time spectroscopy, when the destruction front is advancing in the medium, hence resulting in time dependent extinction.

Medium-high resolution optical-IR spectroscopy of the afterglow can be used as a powerful diagnostic of the medium on a scale larger than that probed by early-time X-ray spectroscopy (parsecs). Perna & Loeb (1998) showed that the time decrease of the EW of absorption lines (due to the gradual photoionization of the medium) is far more pronounced if the burst is located in a molecular cloud than

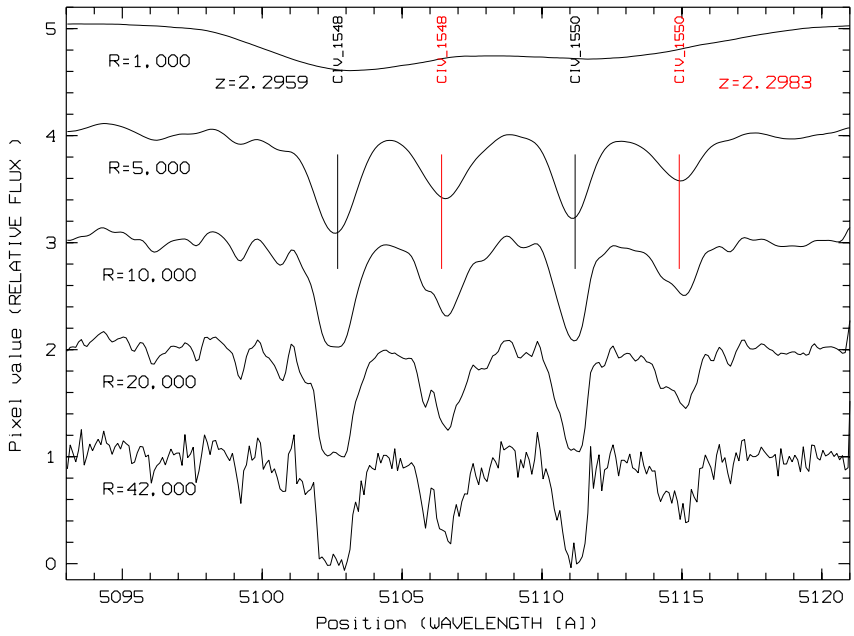

Figure 6.5 UVES observation of the gamma-ry burst GRB 021004.

if it is located in a diffuse, low-density medium. Therefore, time-resolved spectroscopy can be used to distinguish between competing scenarios for the GRB progenitor.

A spectroscopic facility of higher efficiency than those currently available allows a more intensive spectroscopic monitoring: for an early counterpart of magnitude between 15 and 18 (see GRB 990123, Akerlof et al. 1999; GRB 021004, Fox 2002), repeated integrations over increasing exposure times from few minutes to 10–20 minutes will allow us to reach a S/N better than 30 and detect absorption features of variable EW, if the FWHM is as small as 20–30 km s^{-1}.

6.2.3 Target Selection

GRB research will receive a boost in early 2004, following the lauch of the GRB-dedicated satellite Swift. Its actual duration will likely be longer than the nominal one of 2 years, allowing a significant overlap with the initial phase of X-shooter. Swift will deliver in real time about two accurate localizations of GRBs per week. This rate is at least an order of magnitude larger than afforded by any previous mission capable of delivering arcmin-sized error boxes. The Swift localizations will be immediately followed up by robotic optical and infrared telescopes around the world (e.g. ROTSE-III, REM, TAROT-2) and by the on-board optical monitor UVOT, for an efficient search of the bright optical flash or early afterglow. A wide-band, high throughput, efficient, medium-resolution spectrograph will be crucial in effectively following up these timely detections of the optical/infrared transients associated with GRBs and in addressing the fundamental questions of GRB science. The ESA satellite INTEGRAL will continue to be operational over the next decade, and other GRB-related missions will be been launched by 2007, e.g. AGILE, GLAST. These make the role of rapid, wide-range, medium-resolution spectroscopy of the identified lower energy afterglows essential.

6.2.4 X-shooter Performance

The current optical faint-object spectrographs at the VLT, FORS1 and FORS2, are multi-purpose and multi-object instruments and hence not optimized for getting a wide spectral-coverage, high signal-to-noise spectrum for a single source in the shortest possible time. This is exactly what the X-shooter is

optimized for.

Perhaps the ultimate science goal of the X-shooter is to get a spectrum of a GRB at a redshift beyond the reionization redshift. This is in fact quite feasible. In Fig. 6.6 we show the signal to noise ratio as a function of wavelength of a GRB observed at $z = 8.5$. Here we have assumed a re-ionization redshift of $z = 7$. To estimate the flux we have redshifted the afterglow of the $z = 2.3293$ GRB 021004 to $z = 8.5$ at an observer frame time of 7 hr post burst. The total integration time is 2 hr and as seen the red damping wing due to the foreground neutral hydrogen is detectable at high significance. The detailed shape of this red wing allows the measurement of the redshift of re-ionization.

For more frequent GRBs at redshifts $0.2 < z < 5$ the wide wavelength coverage and high efficiency will make the X-shooter the most powerful instrument available to determine redshifts and to study the environments of GRBs and the ISM of their hosts via the properties of absorption lines.

In addition, the majority, if not all, GRB host galaxies studied spectroscopically display strong emission lines. The high efficiency and spectral coverage of X-shooter will allow a systematic host spectroscopic survey. The X-shooter will cover almost the complete set of emission lines from Lyα to Hβ and [O III] and for a galaxy of $z \sim 1.5$–2.7 in a single exposure. A comprehensive host galaxy program can be conducted in the years following the guaranteed two years of operation of Swift.

The combination of wide spectral coverage, spectral resolution and scheduling efficiency of X-shooter makes it an unequalled and therefore very competitive instrument for GRB science, when compared with the spectroscopic performance of other instruments at VLT itself, Keck or Gemini in the present and near future. No current spectrograph has UV-to-NIR coverage, which is a fundamental advantage in the study of highly variable sources, like afterglows. While FORS has an echelle mode which may offer high resolution, this has a very low efficiency and little spectral coverage. With respect to ESI at Keck, X-shooter has better sensitivity in the blue part of the optical spectrum and covers the UV and NIR region. Moreover, it better exploits the synergy with the optical/infrared robotic La Silla telescope REM and TAROT-2. It is more efficient than the high resolution spectrographs UVES and CRIRES. With respect to ISAAC it provides a simultaneous coverage of the whole NIR band up to 1.9 μm, and is more sensitive. Its wide range and resolution have no counterparts in any spectrograph mounted at the Gemini units. Finally, X-shooter is an easier instrument to set-up than the other existing and planned spectrographs and faster to operate because of its fixed spectroscopic format.

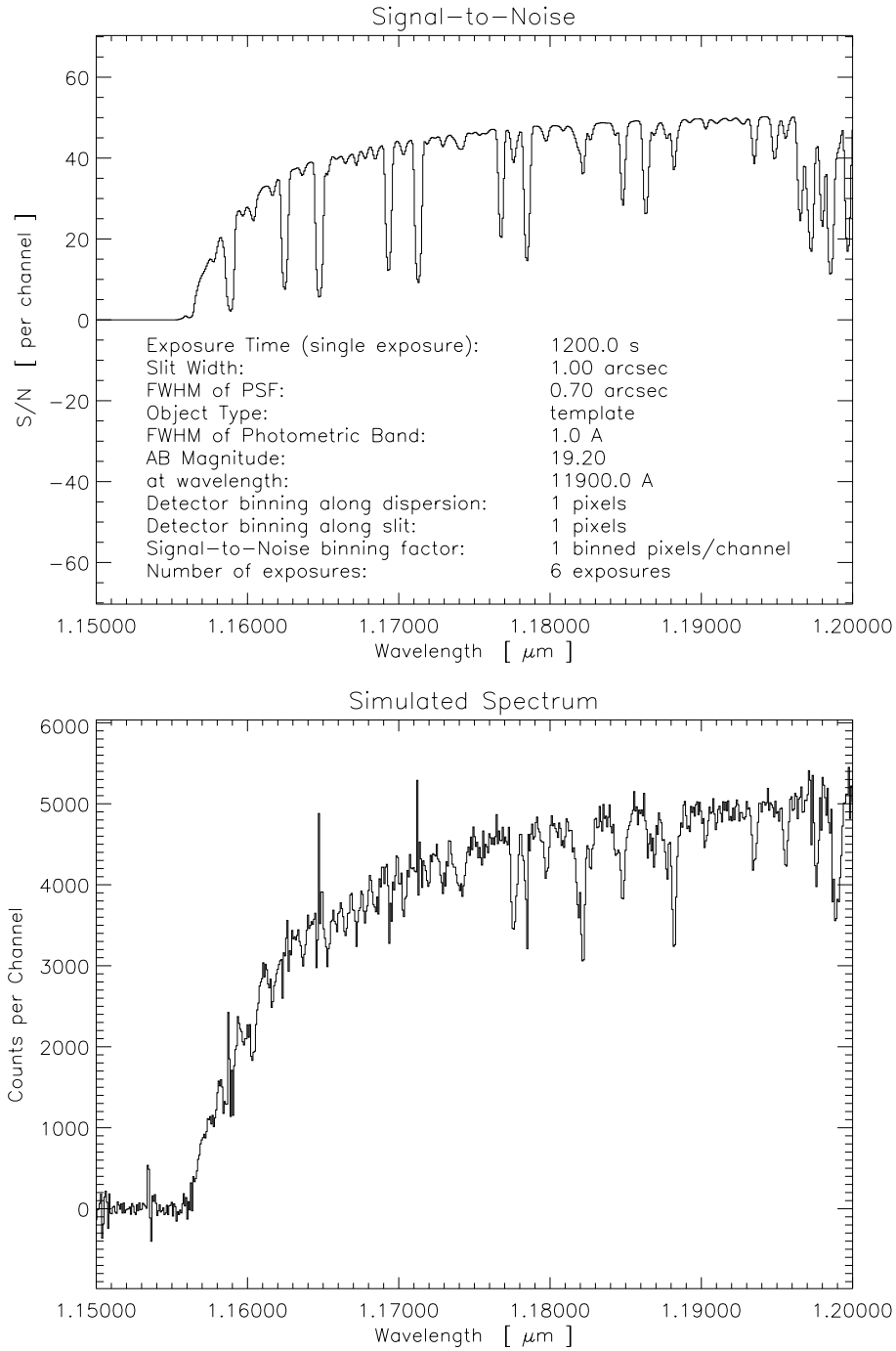

Figure 6.6 S/N as a function of wavelength for the spectrum of the GRB 021004 afterglow ($z = 2.3$) redshifted to $z = 8.5$.

CHAPTER 7

The High-Redshift Universe

SECTION 7.1

Faint Emission-Line Galaxies at $z = 1.6$–2.6

7.1.1 Astrophysical Importance

The 4000 Å jump and the H+K lines take a special place as the historically most important tools in the study of the local and low redshift universe. They have helped us identify and study galaxies out to redshifts close to 1. At redshifts 3 and above, the Lyman limit (912 Å) and Lyα (1215.6701 Å) have taken on a similar role as the most important tools for the mapping of the universe. Such studies have been undertaken during the past decade mostly in 'the optical' (here taken to mean 4000–9000 Å). Those tools give us access to the redshift ranges 3.4–9 (Lyman limit) and 2.3–6 (Lyα).

The HST Medium Deep Survey (and later studies) found that the galaxy types seen in the local universe are also found out to z approaching 1. Samples of Lyman break galaxies (LBGs; existing LBG samples go down to about $z = 2.6$) do not have similar morphologies. They tend to have compact or disturbed (multiple) appearences. Therefore the epoch of 'formation of the Hubble sequence' is hiding somewhere in the redshift range 1–2.6. This observational result is not understood, but one may find part of the explanation in the predictions of hierarchical structure formation models.

The space density of quasars increases rapidly from high redshifts towards a redshift around 2, after which it decreases. The quasars live inside the bulges of their host galaxies and are most easily understood as massive black holes fuelled by gas from their host galaxies. The correlation between black hole mass and bulge mass and the steep rise of the QSO space density towards a maximum at $z = 2$ signals that this is an important epoch in the formation history of the bulge population at large. Similarly, the transition towards the "dying out" phase of quasars at $z = 1$–2 suggests that the properties of bulges (or proto-bulges) are undergoing significant changes in this redshift range.

The redshift range 1–2.6 is thus of high astrophysical interest because it carries the key to the understanding of the formation of the Hubble Sequence and of the bulk of the bulge population. It is interesting to note that this currently 'hidden' part of the universe (redshifts 1–2.6) represents 3.5 Gyrs evolution, while for instance the redshift range 6–1000, which is currently being heavily pursued, represents only 0.9 Gyr.

In bright LBG galaxies at slightly higher redshifts it is known that the Lyα line is seen in absorption and emission with roughly equal probability, and it is one of the key features for redshift determination when the Lyman limit is not accessible. The fraction of galaxies seen with Lyα in emission becomes larger as one moves to the fainter end of the luminosity function.

7.1.2 Instrument Requirements

This important redshift range is largely inaccessible to the VLT due to the lack of high throughput, sky-noise limited instrumentation at wavelengths significantly below 4000 Å. UVES has too high resolution to fulfill the imperative condition of sky-noise dominance, the FORSes have dismal throughput below 4000 Å, and VIMOS is not designed for work in the UV either.

A high-throughput, sky limited UV/optical spectrograph in the wavelength range 3150–4400 Å would open up the redshift window 1.6–2.6 and allow the detection and study of the large population of faint Lyα emitting objects at an astrophysically very interesting, and until now virtually inaccessible, epoch of the evolution of the universe. The faint end of the luminosity function of high redshift galaxies is very steep. Therefore even a modest increase in sensitivity will result in a large increase in volume density of objects above the detection limit.

7.1.3 Target Selection

Two effects work together to make Lyα selection (as opposed to surveys based on continuum flux selection) particularly useful for high redshift surveys. (1) Because the line is predicted to have extremely large equivalent width (Valls-Gabaud 1993; Charlot & Fall 1993), it is possible to identify objects which are far below the detection limit of broad band surveys e.g. surveys based on the Lyman Break technique (Steidel & Hamilton 1992), and (2) as soon as a candidate Lyα emitter has been confirmed spectroscopically its redshift is known with very high accuracy.

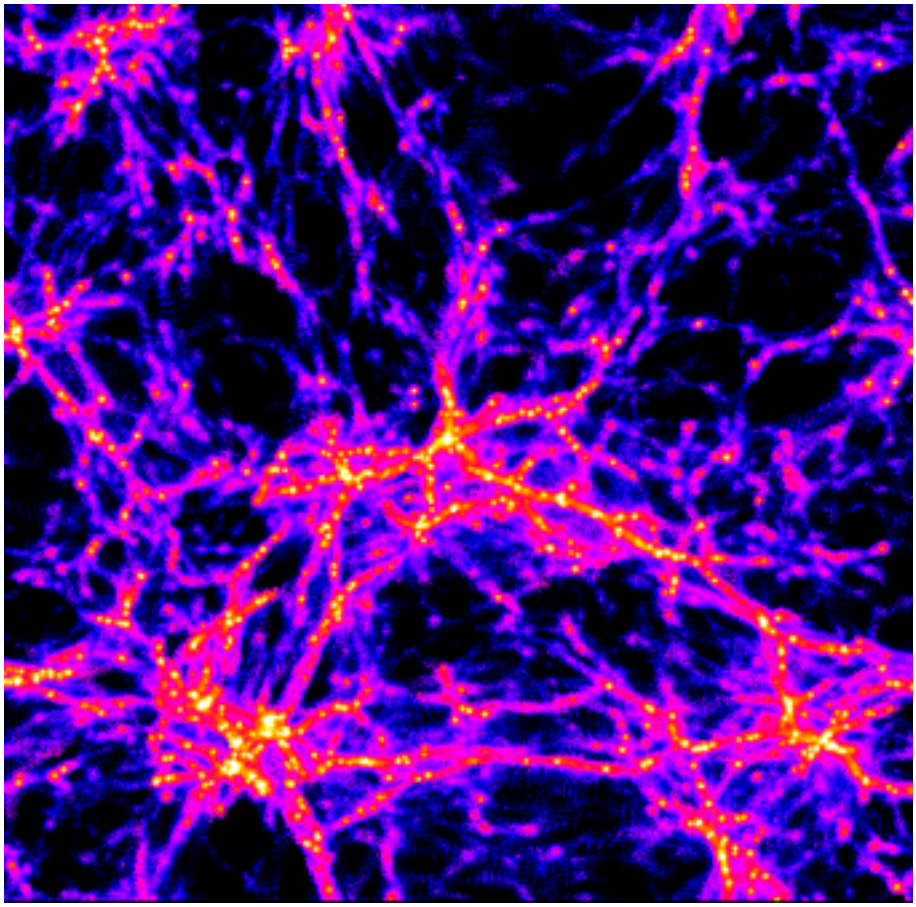

Figure 7.1 Simulation of structures at high redshift.

The volume density of faint Lyα galaxies is much higher than the volume density of the much brighter LBGs, and they can therefore very effectively be used to map out structures in the early

universe. Fig. 7.1 illustrates the current predictions for the structure formation at high redshifts. The filamentary structures seen is a generic prediction of all current simulations, and one would expect the numerous Lyα galaxies to clearly map out such structures. In one case this has already been seen: In Fig. 7.2 is shown the filament at $z = 3$ mapped by eight Lyα emitters and viewed from several different perspectives (Møller & Fynbo 2001).

The target galaxies can be selected in two ways:

- a "survey mode" where narrow band imaging of blank fields will provide large samples for spectroscopic followup. The candidate Lyα emitters will be selected from deep narrow-band (or tuneable filter) searches with blue-sensitive detectors (e.g. SUSI-2/NTT or future blue-sensitive cameras at ESO and other observatories). The blank fields can be selected in the HDFS, EIS and/or GOODS fields. This has two advantages: First the broad band images are already available so only observations taken with one additional narrow band filter is needed. Second, the wealth of additional information available for the confirmed Lyα emitters will provide both multiwavelength SEDs and morphological classifications.

- a "targeted single object" mode. Here the full potential of X-shooter will be truly realized as we will study single objects selected to be interesting in their own right, such as host galaxies of GRBs, AGN or SNe, or absorbers along the line of sight to GRBs or QSOs.

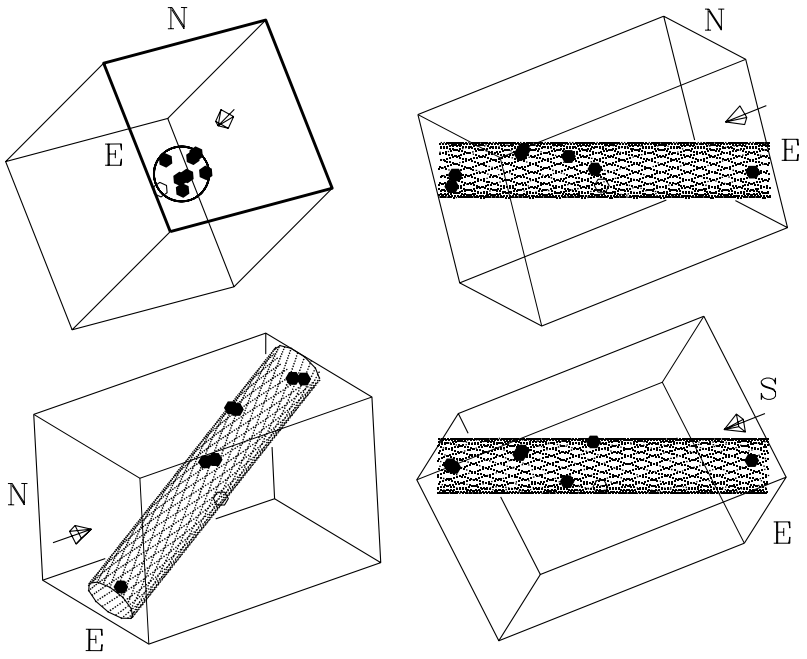

Figure 7.2 Filament at $z = 3$ mapped by Lyα emitters.

7.1.4 X-shooter Performance

The ultimate goal is to address the fundamental problems outlined in the introduction. What important events at $z \approx 2$ trigger the formation of bulges, the death of quasars, and the birth of the Hubble sequence.

- The large volume density and the precise redshifts of the Lyα emission lines, will allow the construction of detailed redshift-space maps of their distribution. Such maps will visualise directly

Table 7.1. Exposure Times for FORS1 and X-shooter

Wavelength	FORS1[a]	X-shooter
3200 Å	not feasible	23.0 min
3500 Å	8.5 hours	12.5 min
3800 Å	1.9 hours	11.5 min

[a]grism 600B used in the estimates

the large scale structures (voids, walls, filaments) predicted to have been formed at $z = 2$. Such maps will provide both a critical test of the current ΛCDM structure formation paradigm, and information on local (environment dependent) biasing of the star formation rates. Moreover, since similar projects are currently underway at redshifts from 3 to 5, the evolution of structure will become directly observable.

- With a large sample of confirmed Lyα emitters one shall be able to fully characterise this class of objects at $z = 2$: volume density, luminosity function, Lyα equivalent width distribution. In addition, the wide spectral coverage of the X-shooter will provide several other emission lines adding information on the dynamical state of the galaxies, and on the ionization state and metallicity of its gas. Again comparison to similar samples at higher redshifts will provide information on the global evolution of the galaxy population.

- The typical Lyα selected high redshift object is much fainter, smaller, and less massive than today's fully formed galaxies (Fynbo et al. 2001). In numerical simulations of the early universe such low mass clumps are seen to attract each other, to collide, and finally to merge to build up larger and larger galaxies. Typical high redshift Lyα emitters can therefore be seen as the elemental "galaxy building blocks".

For a galaxy with a Lyα luminosity typical of those found at $z \approx 3$ (e.g. Møller & Fynbo 2001) the required exposure times for a 5σ detection of the Lyα line are shown in Table 7.1 at redshifts of $z = 1.63$, $z = 1.88$ $z = 2.13$ (Lyα located at 3200 Å, 3500 Å, and 3800 Å, respectively). Even if the multiplexing capability of FORS1 is taken into account (typically 6–8 Lyα emitters can be observed) X-shooter will be more efficient below 4000 Å for objects at the assumed flux level.

MUSE, the proposed 2nd generation VLT instrument dedicated to deep area spectroscopy, is not expected to operate in the U and B bands and thus cannot be used for this type of observations.

7.2.1 Astrophysical Importance

A leading component in the scientific case for the JWST multi-object spectrograph is the proposal to study the familiar restframe optical nebular spectrum in large numbers of star-forming galaxies at early epochs. Beyond $z \sim 2.7$, where the Hα line moves out of the K-band, this project will be essentially the sole preserve of JWST. The forbidden lines of interest range from [O II] 3727 to [S II] 6725 and, at low redshift, their analysis is a familiar stamping ground for spectroscopists using groundbased telescopes (Kennicutt 1998). The principal goals of such a study are to trace the early chemical evolution of galaxies and, if sufficiently high spectral resolution is available, the kinematic masses of the systems.

HII regions and star-forming dwarf galaxies at the current epoch have rather weak ultraviolet emission line spectra, a fact that follows from the moderate temperatures of their ionizing stars and the efficient radiative cooling resulting from the approximately solar metallicity of the nebular gas. In low metallicity and Population III star-forming regions however, we anticipate an IMF extending to higher stellar masses producing hotter ionizing spectra and warmer, low metallicity and more highly ionized nebulosity (Bromm et al. 2001; Schaerer 2002). From their observational and modelling analysis of low redshift HII regions, Dopita & Evans (1986) showed the strong inverse coupling between the mean ionization parameter U and the metallicity Z. The expectation that early, very low metallicity star-formation produces compact, high ionization HII regions opens the exciting possibility of being able to make a profitable study of their restframe UV emission line spectra at high redshifts. Using an analytic procedure based on measurements of strong intercombination lines of C, N, O and Si in the UV, it will be possible to commence, from the ground, the process of mapping the early chemical evolution of the universe in gas associated directly with the assembly of galaxies.

These expecations have recently been put to the test by what was, in essence, the serendipitious discovery of a very low metallicity HII galaxy at $z = 3.4$ which has been amplified by a factor of order 10 by an intervening cluster lens (Holden et al. 2001; Fosbury et al. 2002; Fosbury et al. 2003, in prep.). This object is sufficiently bright that high quality, intermediate dispersion spectroscopy has been possible most of the way from Lyα at 5300 Å to the nebular [O III] lines in the K-band. The broadband photometry is dominated by the strong emission lines and the arc is notable for its brightness at K: Johnson K ~ 18 and red colour; R$-$K ~ 4 (Stern et al. 2002). Fig. 7.3 shows an HST WFPC2 image of this arc in Lynx.

Emission line objects with weak continua are difficult to find using broad-band imaging techniques. This has stimulated spectroscopic searches from the ground, notably ones using clusters as magnifying lenses (Ellis et al. 2001). Holden et al. (2001) have reported the serendipitous discovery of a bright emission line arc in the southern, slightly lower redshift ($z = 0.543$) part of the cluster RX J0848+4456. This shows narrow emission lines of Lyα; N IV] 1486; C IV 1550; He II 1640; O III] 1664 and C III] 1909 at a redshift of 3.357. The spectrum suggests that this is a giant HII region-like object with ionizing stars with an effective temperature of at least 70 000 K. Such stellar temperatures and low gas metallicities are approaching the extreme values expected for a primordial HII region ionized by the first generation stars (see eg. Bromm et al. 2001; Shaerer et al. 2002). Subsequent H and K-band spectroscopy allowed the measurement of the rest-frame optical lines of Hβ, [Ne III] and [O III] (see Fig. 7.4).

A high ($R \simeq 4000$) resolution one hour exposure optical spectrum has been obtained with the Keck ESI spectrograph. This allows the measurement line profiles and the detection of some additional weak lines. Gaussian fits to Lyα and C IV emission and wind absorption are shown in Fig. 7.5.

An analysis of the broad-band photometric and the spectrophotometric data (Fig. 7.6) shows that the only detected continuum in the UV-optical spectrum is the nebular emission from the HII region (mostly the hydrogen 2-photon emission longward of Lyα). This indication that the stellar continuum must only dominate at shorter wavelengths provides important constraints on the cluster IMF and on the mass-to-light ratio.

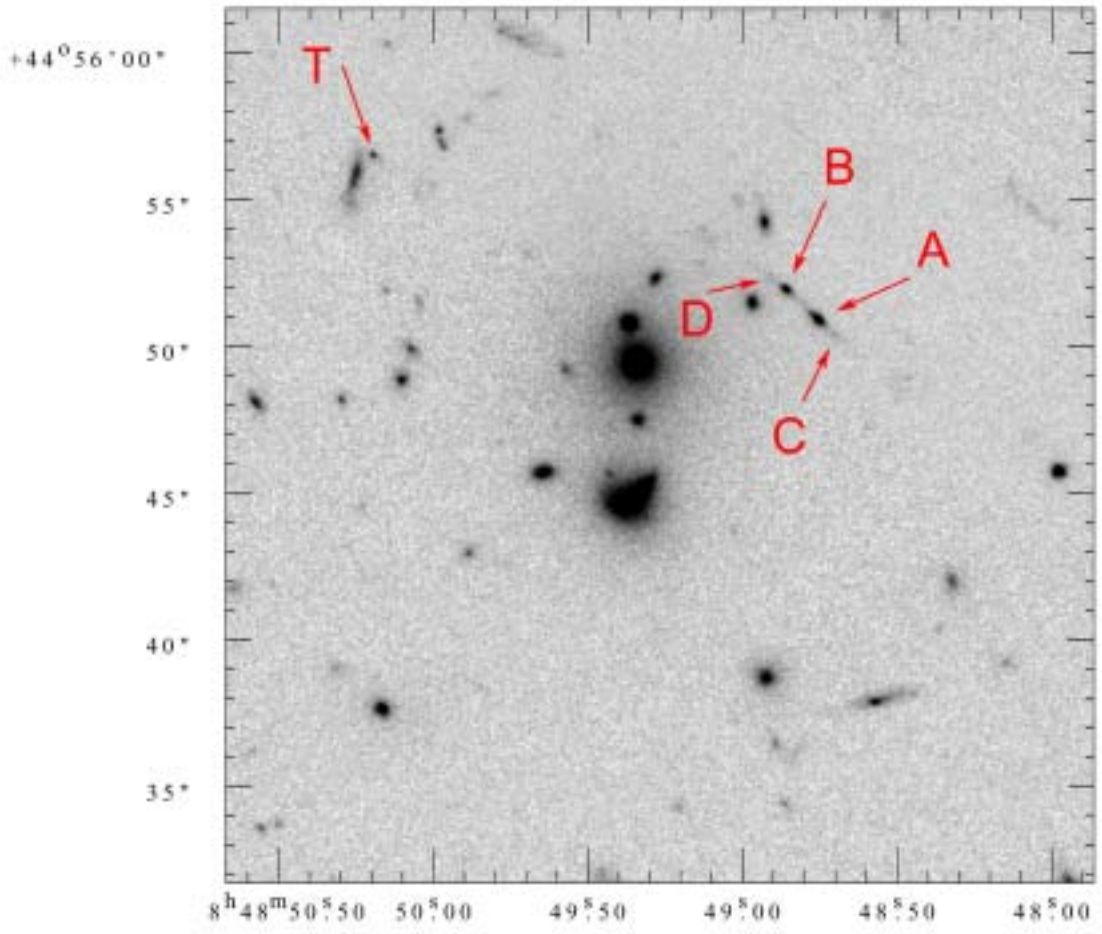

Figure 7.3 The F702W image of the Lynx arc from the HST WFPC 2 camera. The lensed arc is labelled with its two bright components A and B. A thin arc extends over about $9''$ with two very faint components, C and D, lying along it. A candidate third image, T, has similar colours.

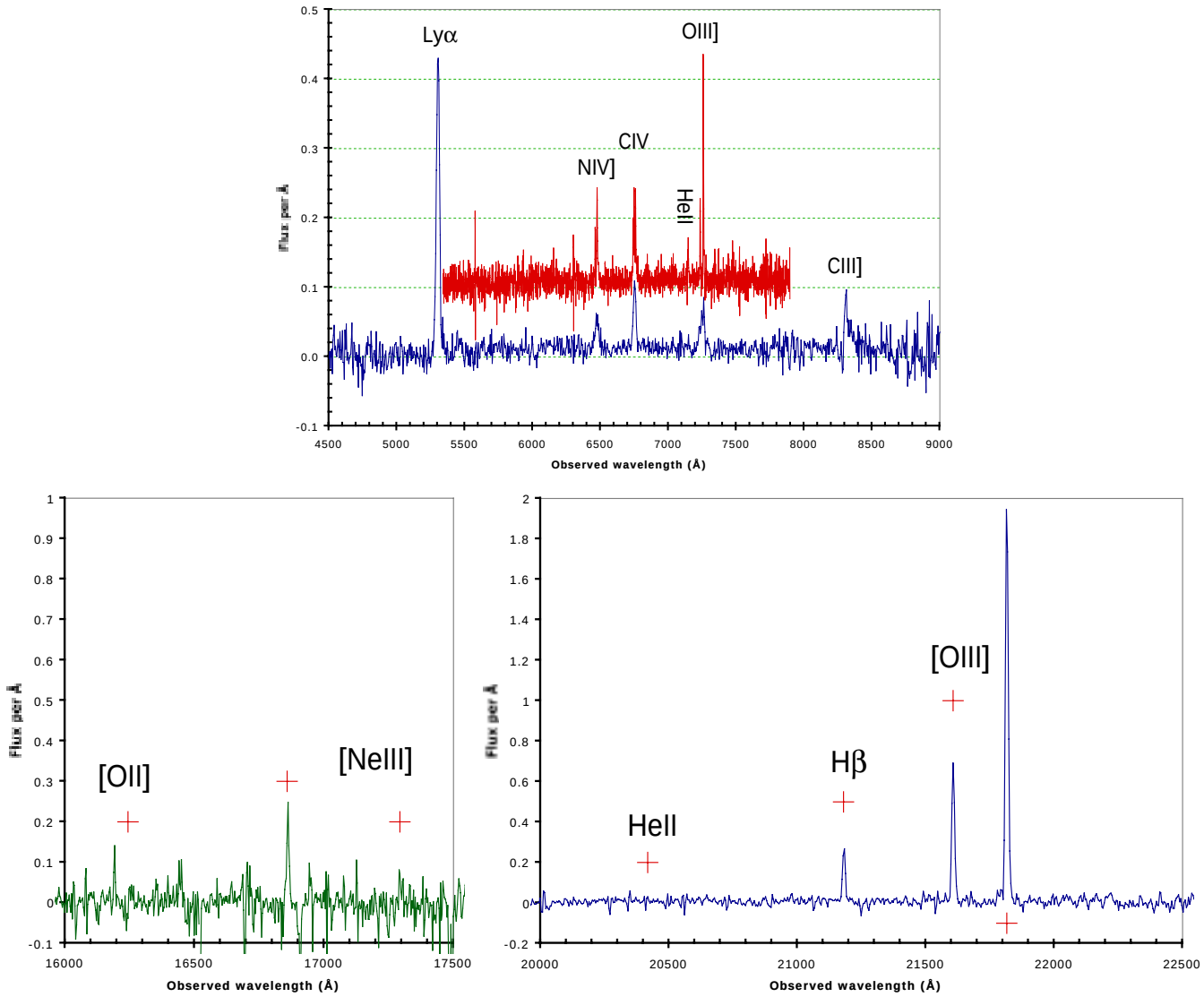

Figure 7.4 Keck LRIS and NIRSPEC spectra of the Lynx arc showing emission lines from Lyα to [O III] 5007 Å. Note the very strong nebular lines and the strength of [Ne III] relative to the undetected [O II] 3727 Å.

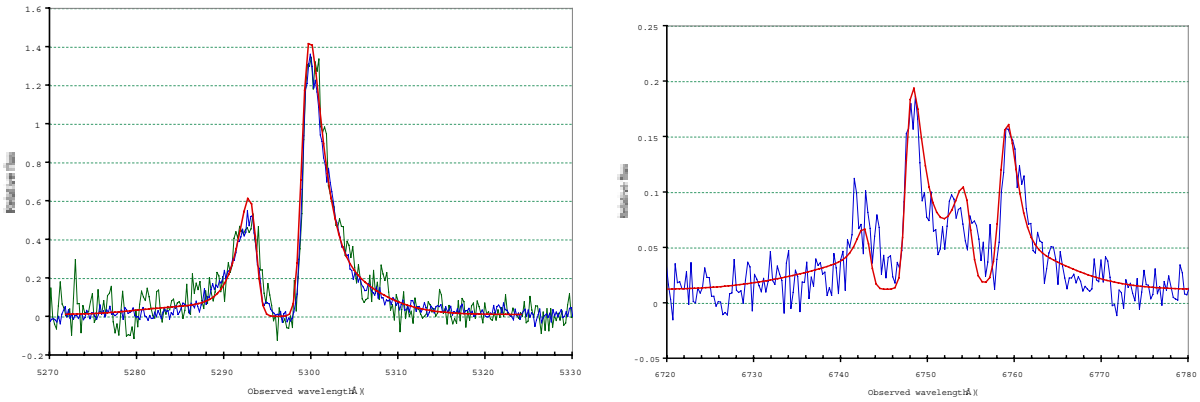

Figure 7.5 Multiple gaussian fits to the Lyα and C IV lines in the Keck ESI spectrum of the Lynx arc. The absorption components in these resonance lines indicate the presence of a highly ionized wind with a column density of about 10^{15} cm^{-2} in each ion.

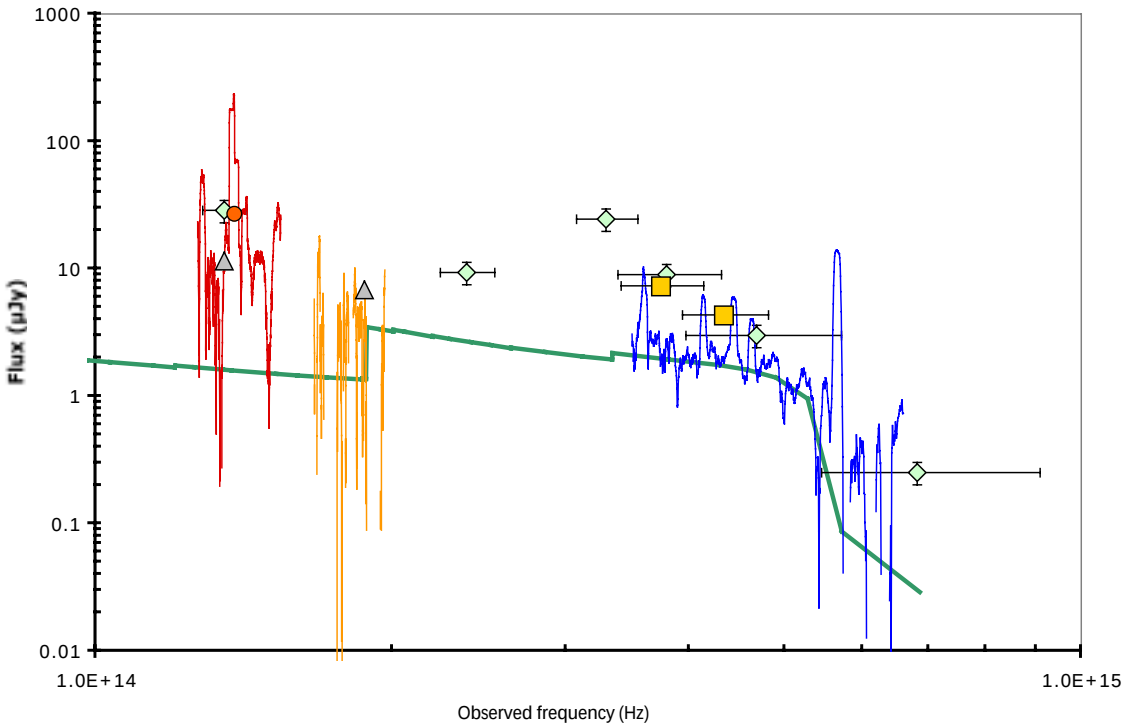

Figure 7.6 A collection of groundbased and HST broadband photometry of the Lynx arc overplotted on the LRIS and NIRSPEC spectrophotometry. The thick continuous line represents the hydrogen and helium bound-free and the hydrogen 2-photon continuum scaled to the observed strength of Hβ with no reddening correction. There is no evidence of any stellar continuum in this region of the spectrum: further evidence for very hot ionizing stars.

An analysis of these data (Fosbury et al. 2003, in prep.) has given an extraordinarily detailed insight into a star formation event that may contain in excess of 10^6 massive, high temperature stars of very low metallicity at a time when the universe was only 2 Gyr old. The combination of classical nebular astrophysical analysis and sufficient spectral resolution to measure kinematic properties and so to make mass and mass-to-light ratio estimates means that such sources may be used, via the $L_{H\beta} - \sigma_v$ relation for HII regions (Melnick, Terlevich & Terlevich 1999), as cosmological 'standard candles'.

This example observation demonstrates the possibility of obtaining high quality spectra of young, actively starforming regions at early epochs in regions where there has been little or no chemical enrichment since the Big Bang. Such emission line studies are complimentary to absorption line studies along sightlines towards distant quasars since they sample such differently selected environments.

7.2.2 Instrument Requirements

The instrumental requirement for this kind of spectroscopy is basically the need for high throughput with a resolution matched to narrow emission lines (velocity dispersion 30-50 km s^{-1}) and covering as large a wavelength range as possible. For high redshift sources ($z \gtrsim 2$), some additional information (Hα, [S II]) would be obtained by securing K-band spectra. For $z \lesssim 2.8$ however, the [O III] lines would appear in H or shorter wavelength bands. The main requirements are therefore:

- Wavelength coverage: maximise number of emission lines measured.
- Spectral resolution: need to measure velocity dispersions typical of giant HII regions ($\sigma \sim 30$ km s^{-1}).
- Good sky subtraction implying a long enough slit.
- Calibration accuracy: relative flux measurements over wide wavelength range; good internal wavelength precision for confident line identifications and internal kinematics for different ionization states.
- Precision target acquisition for sources that are very faint in continuum bands (large line equivalent widths).

7.2.3 Target Selection

The successful design of a research programme to investigate the properties of early star formation and chemical enrichment requires an efficient survey strategy to find candidate sources. The possibility of exploiting gravitational lensing amplification to shift intrinsically rather faint sources into a spectroscopically observable magnitude range suggests restricting the search to the regions surrounding known massive galaxy clusters.

Although broadband imaging is not particularly sensitive to faint sources with large emission line equivalent widths, deep broadband multicolour cluster imaging is a way of selecting those sources that are bright enough for detailed spectroscopic study. The HST ACS is currently being used to survey a sample of clusters as part of the GTO programme and its sensitivity and high resolution are ideally suited to this task. Searching these images for background sources with colours that suggest the presence of strong emission lines would provide the first candidate list.

With the advent of high multiplex integral field spectrographs such as VIMOS, effective searches can be made in the vicinity of clusters to search directly for emission line signatures of young starforming regions. Even simple long-slit searches are capable of sampling areas of a few hundred square arcseconds in a reasonable time (R. S. Ellis has used LRIS at Keck to find several Lyα candidates at $z > 5$ using this technique – private communication).

Candidate sources can be selected from the multi-band object catalogues derived from such deep imaging surveys. For all but the very faintest candiates, a refining selection process – essentially a search

for emission lines – can be carried out as a by-product of the $R \sim 1000$ multi-object spectroscopy which is carried out to confirm cluster membership and measure velocity dispersions. For very faint candidates, the sensitivity of the X-shooter to narrow emission lines over a very wide baseline in wavelength would offer the most efficient source classification as well as the tool for detailed study.

We envisage a research programme starting with a colour- and morphology-based source selection from deep HST and groundbased optical/NIR imaging aiming to obtain high quality near-UV to H-band spectroscopy of a few sources per cluster for up to 10 clusters. The initial aim of the programme will be to sample young star cluster metallicity at $z \gtrsim 2$, using either Lyα or [O III] as the lines on which to search.

7.2.4 X-shooter Performance

For very faint candidates, the sensitivity of the X-shooter to narrow emission lines over a very wide baseline in wavelength would offer the most efficient source classification as well as the tool for detailed study.

- Sensitivity. The nebular continuum in the Lynx arc is shown in Fig. 7.6. The detected emission lines range from $0.2 - 27 \times 10^{-16}$ erg cm^{-2} s^{-1}.
- Wavelength coverage. The analysis depends on maximising the number of measured emission lines spread between redshifted Lyα and Hα. Using two or three different spectrographs to achieve this is very inefficient.
- Resolution. Sensitivity is maximised when the resolving power is matched to the linewidth. It is also necessary to measure the emission line velocity dispersions if these objects are to be used as 'standard candles'
- Sky subtraction. For observations of the faintest sources, several magnitudes below the sky, integrations must be obtained as individual sky limited exposures at different positions along the $12''$ slit, in order to optimize sky subtraction. This is also foreseen in the operational capabilities of X-shooter (see Sec. 5.3 of part B).
- Target acquisition. For faint objects, target acquisition will rely on blind offsetting relative to one or more reference objects (see Sec 5.3 of part B).

X-shooter ETC calculations for the visual and NIR arm show that the continuum of the Lynx arc will be detected at S/N$\sim$5–10 for exposure times of 4–6 hours at a post-observation binned resolution of 10 Å. The emission lines will of course be detected at much higher significance and spectral resolution.

7.3.1 Astrophysical Importance

One of the "evergreen" questions of galaxy evolution remains how and when the present-day massive galaxies ($M > 10^{11}$ M$_\odot$) formed. In the current most popular ΛCDM scenario, massive galaxies are the product of rather recent hierarchical merging of pre-existing disk galaxies taking place largely at $z < 1.5$ and with moderate star formation rates (e.g. Kauffmann et al. 1993; Cole et al. 2000; Somerville et al. 2001). In such a scenario fully assembled massive galaxies with $M > 10^{11}$ M$_\odot$ at $z > 1$ are very rare. An alternative possibility is that massive systems formed at much higher redshifts (e.g. $z > 2$–3), through a short and intense epoch of star formation, followed by a passive evolution (or pure luminosity evolution) of the stellar population. Such a possibility is supported by the properties of local and intermediate redshift spheroidals (see e.g. Renzini 1999; Renzini & Cimatti 1999; Peebles 2001, for recent reviews), and by the existence of a substantial population of old and passive galaxies at $z \sim 1$ that are strongly underpredicted by hierarchical merging models (e.g. Cimatti et al. 2002).

Particularly relevant will be the next surveys in the mid- and far-IR (e.g. SIRTF, Herschel) and submm-mm continuum (APEX, ALMA) because they will search directly for the candidate *progenitors* of the present-day massive spheroids assuming that they formed through a starburst episode obscured by dust. In this case, we expect such primordial massive galaxies to be starburst systems in dusty environments, with large masses of gas available to be converted into stars and strong star formation rates of the order of several hundreds solar masses per year. Recent surveys done with JCMT + SCUBA and IRAM 30m + MAMBO have shown the existence of a population of dusty and infrared luminous galaxies at high z. The aim of the future observations will be to find large numbers of submm-selected galaxies with the forthcoming facilities (e.g. APEX, ALMA) and to follow them up with deep optical/near-IR observations in order to unveil their nature and verify if they represent the progenitors of the present-day massive spheroids.

As a target example we consider the $z = 2.8$ galaxy SMM 02399−0136, selected during a SCUBA survey at 850 μm of lensing clusters of galaxies (Ivison et al. 1998). It is one of the few high-z submm sources with unambiguous optical identification and redshift. The inferred unlensed far-IR luminosity is about 10^{13} L$_\odot$, placing it in the class of "hyperluminous" infrared galaxies, i.e. with SFR compatible with > 1000 M$_\odot$ yr^{-1}. CO emission observations indicated the presence of M$_{H_2} \sim 10^{11}$M$_\odot$ (Frayer et al. 1998). The high redshift, the extreme SFR and the large gas reservoir makes this galaxy a primordial system likely to evolve into a present-day massive elliptical. HST imaging shows a compact object with a fainter companion (at the same redshift) 3 arcsec away, thus suggesting the presence of a merging episode. The optical spectrum shows a wide range of high-ionization narrow emission lines typical of both AGN and starburst galaxies (Lyα, NVλ1240, CIVλ1550, ...). [OIII]$\lambda\lambda$ 4959+5007 and Hα were detected in the K band with UKIRT with near-IR spectroscopy. Subsequent VLT low-resolution (R$\sim$500) spectropolarimetry (see Figs. 7.7 and 7.8) revealed significant polarization and a very complex optical (rest-frame UV) spectrum characterized by high ionization absorption troughs, broad low-ionization absorption lines, presence of large scale ordered kinematical field compatible with rotation and possible dynamical mass of the system $> 10^{11}$M$_\odot$ (Vernet & Cimatti 2001). SMM 02399−0136 shows that the following scientific aims can only be reached through deep spectroscopy:

- Dynamical masses can be derived through the analysis of the velocity fields using different kinematical tracers. Independent estimates can serve as verification of the reliability of the lines used as kinematic probes (e.g. Courteau & Sohn 2002). Such kinematical studies will be of fundamental importance to measure the masses of high-z galaxies selected in the far-IR and submm and to verify the hypothesis that they are the progenitors of the most massive present-day systems. Detailed kinematics in the optical and near-IR can be compared with the kinematics of the molecular gas as traced by the CO emission observed by ALMA at comparable resolution.

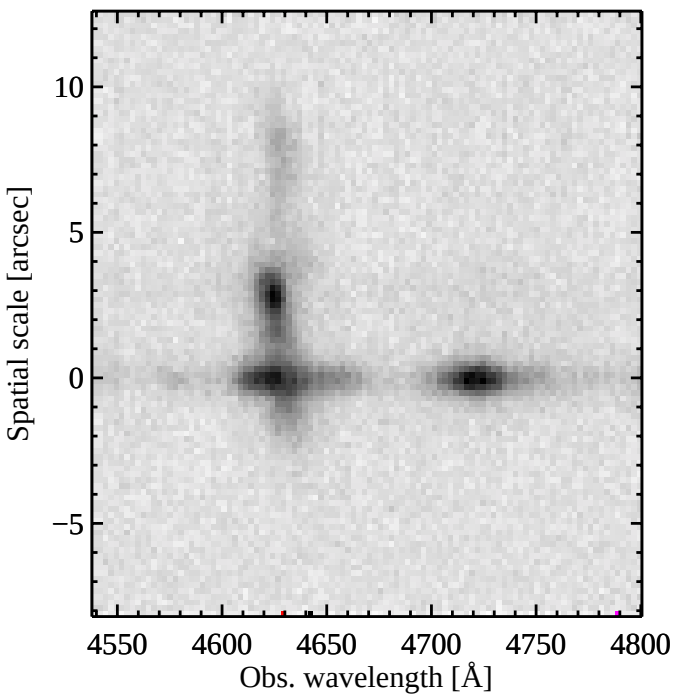

Figure 7.7 2D VLT+FORS1 low resolution (R=500) Lyα spectrum of SMM 02399−0136 (Vernet & Cimatti 2001). This 2D spectrum taken at low resolution shows the wealth of information that can be derived from multi-component objects with spatially extended emission lines.

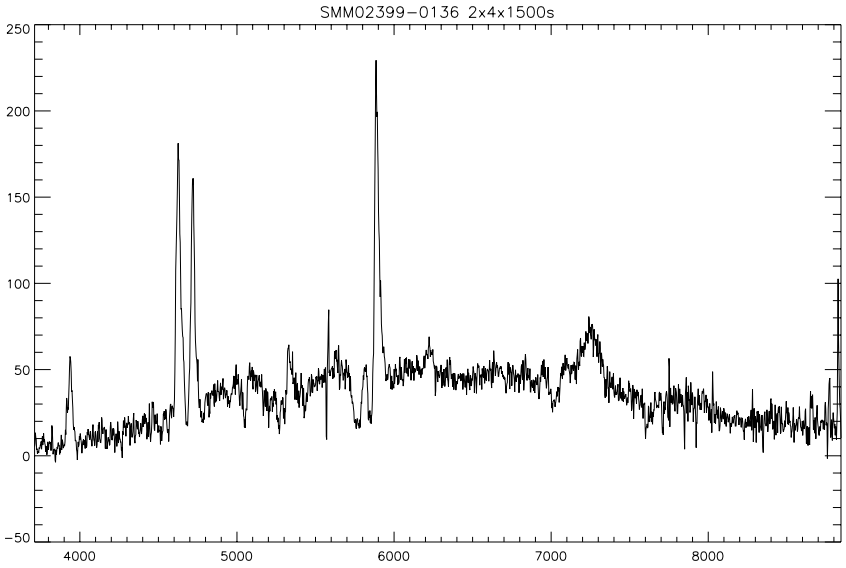

Figure 7.8 1D extracted spectrum of the component with Y-coordinate=0 in Fig. 7.8. The spectrum shows several features: emission lines, absorption interstellar lines, broad absorptions similar to those observed in BAL quasars and highly structured continuum. X-axis is the observed wavelength, Y-axis is F_λ in arbitrary units.

- The profiles of emission/absorption line profiles (see e.g. SMM 02399−0136) can be used to probe the outflow/inflows kinematics of the gas and to unveil the structure of such primordial galaxies.
- Spectrophotometry of the continuum over a wide spectral range can be used to model the rest-frame UV–optical spectra with spectral synthesis models and to estimate the age of the stellar population(s). The modeling of the spectra can be used to uncover the different contributions from stars and AGN in galaxies with composite spectra.
- Emission line ratios can be used to investigate the photoionization mechanisms (e.g. AGN vs. starburst). Broad line components in the emission lines would be indicative of hidden QSO activity.
- Star formation rates can be estimated through different estimators (e.g. emission line and UV continuum luminosities).
- An estimate of dust reddening can be obtained from the Balmer decrement (e.g. Hα/Hβ ratio), at $z \sim 1$ with optical+J-band and at $z \sim 1.5$ with $J + H$ bands), as well as the spatial distribution of dust reddening from extended emission line regions using spatially resolved Balmer line ratios.
- The gas metal abundance can be derived from emission line ratios, for which it is required to observe [OII]λ3727, [OIII]λ5007, Hβ, supplemented by Hα, [NII]λ6584 and [SII]$\lambda\lambda$6717,6731 to derive the reddening, the isolation of an AGN, and the breaking of the R_{23}-degeneracy with metallicity (Kobulnicky et al. 1999; Teplitz et al. 2000; Carollo & Lilly 2001).

7.3.2 Instrument Requirements

To constrain models of galaxy formation and to probe the genesis of massive systems through their complex physical, dynamical and evolutionary properties requires deep and detailed spectroscopic observations.

Distant submm detected galaxies may be very faint. Hence it is important to optimize the sensitivity and efficiency of the instrument. The typical velocity field amplitudes observed in high-z galaxies are in the range of 100–300 km s^{-1} (e.g. Moorwood et al. 2000; Pettini et al. 2001; Vernet & Cimatti 2001) and the velocity widths of the emission lines are around $\sigma \sim$ 70–80 km s^{-1}, thus demonstrating the need for medium resolution spectroscopy. Galaxies like SMM 02399−0136 must be observed over a wide range of emission line suitable for several diagnostics. For instance, for systems up to $z \sim 1.7$ it will be possible to observe Hα in the near-IR, [OII]λ3727 in the far-red and [OIII]$\lambda\lambda$4959+5007 in the J band. For systems at $z > 2$ it will be possible to observe Lyα in the blue, [OII] λ3727 in the J band and [OIII]$\lambda\lambda$4959+5007 in the H band. With a fairly long slit length (10–20 arcsec) it would be possible to explore regions of spatially extended galaxies at distances of tens of kiloparsec from the nucleus, or, in the case of mergers, to perform detailed observations of their spatially resolved kinematics, provided that the angular distance between the mergers is less than the slit length.

7.3.3 Target Selection

Future submm surveys are expected to find several cases like this over a wide range of redshifts at $z > 1$ (Blain et al. 2002), both in the "field" and through gravitational amplification using galaxy clusters. The ESO/MPIfR/Swedish APEX telescope (2004+) will perform surveys at 850μm and will play an important role in selecting samples of submm galaxies in the southern emisphere. The optical/near-IR counterparts of such galaxies will be ideal targets for follow-up VLT spectroscopy with the X-shooter. Additional samples of infrared luminous galaxies at cosmological distances will also come from surveys performed in the mid- and far-IR with SIRTF (2003+), ASTRO-F (2004+) and Herschel (2007+).

7.3.4 X-shooter Performance

The X-shooter will allow a large variety of studies of such high-z systems, ranging from the kinematics to their physical and evolutionary state. Some of the obvious advantages are

- The X-shooter spectral resolution of R$\sim$4000–7000 is ideally suited to probe the velocity fields and the dynamics of high-z galaxies. This resolution is also essential for an accurate subtraction of the strong OH lines present in the optical-red and in the near-IR in order to reach the faintest fluxes and not to "contaminate" the shape and profiles of galaxy spectral lines.
- The high sensitivity as well as the simultaneous coverage of the 0.3–1.9 μm spectral range results in a drastic reduction of observing time per target enabling us to observe more targets so as to build up a representative sample or to perform ultra-deep observations of faint galaxies.
- Derivation of accurate and homogeneous spectrophotometry and emission line ratios would be very difficult to obtain with independent optical and near-IR spectrographs because of slit losses and seeing/transparency variations.

Sensitivity and feasibility

The optical magnitudes and main emission line fluxes of SMM 02399−0136 (corrected for the gravitational lensing, factor of 2.5) are $R = 23.6$, $I = 22.9$, $\geq 1 \times 10^{-16}$ erg s^{-1} cm^{-2}, i.e. well within the expected sensitivity of X-shooter (superior to ESI in the blue and in the far-red, ISAAC-like in the near-IR, albeit using a detector with much lower dark current).

The X-shooter Exposure Time Calculator (ETC) shows that for a galaxy with the same spectrum as SMM 02399−0136 and a typical magnitude of I_{AB}=23.0, observed in 0.8$''$ seeing with a 1$''$ slit, a S/N ratio of $\sim$4 per channel (with post-observation 3-pixel binning along the dispersion) on the continuum spectrum can be reached in the optical channel(s) with only 2 hours of integration time. With these parameters, the S/N ratio would be $\sim$10 for the main emission lines in the optical channel. For I_{AB}=23.0, the expected typical near-IR magnitudes are $H_{AB} \sim 22.5$ and $J_{AB} \sim 23$. For these magnitudes (and with the same parameters as for the visual arm) the ETC shows that a S/N ratio of $\sim$4–5 per channel can be reached on the continuum between the OH sky lines, thus allowing to derive accurate spectrophotometry of the continuum SED. With such parameters, and without the need of binning, it will be also possible to detect the main emission lines redshifted in the near-IR channel.

A direct demonstration of the feasibility of emission line studies and kinematics in the near-IR comes empirically also from the results obtained so far with ISAAC at the VLT. Spectroscopy at a resolution of R$\sim$3000–5000 showed that spatially resolved kinematics and the analysis of the line profiles and widths can be done for emission lines with fluxes around 10^{-16} erg s^{-1} cm^{-2} with slit width of 1 arcsec, seeing of 0.5–1.0 arcsec, integration times of 2–3 hours (e.g. Moorwood et al. 2000; Pettini et al. 2001). In the case of X-shooter, better performances is expected, with the advantage to cover the $J + H$ (and the optical) spectral region simultaneously.

For a sample of sub-mm selected galaxies 5 min will be needed to detect emission lines at $S/N \geq 5$ in the optical and near-IR with integrated fluxes of $\sim 10^{-17}$ erg s^{-1} cm^{-2} if they are located between the night-sky emission lines. A few hours will be needed to follow their spatially resolved velocity fields along the slit. With integration times of the order of 3 hours, it will be possible for instance to reach on the continuum $S/N \sim 4$ per pixel along the dispersion for $H_{AB} \sim 22.5$, thus increasing to $S/N \sim 9$ with a binning of 5 pixels along the dispersion. Assuming a sample of ten high-z infrared luminous dusty galaxies with typical magnitudes of $I_{AB} \sim 23$, about 30 hours are needed totally if we adopt an average integration time of 3 hours per target.

7.4.1 Astrophysical Importance

The line of sight from a distant, luminous QSO may intersect a wide variety of structures on its long passage to Earth. Any intervening structure with a significant gas content will imprint its signature onto the QSO's spectrum, ranging from the low density intergalactic medium (IGM) to the most massive galaxies of that epoch. The study of QSO absorption lines (QALs) permits the detailed study of metal abundances in high redshift galaxies and the IGM, providing a unique insight into the processes of nucleosynthesis, dust and molecule formation and dispersion. Important results that have come from QAL studies in recent years are numerous, here we mention a few of the highlights:

- Measurements of deuterium abundances which can be used to constrain the baryon density Ω_b (e.g. D'Odorico, Dessauges-Zavadsky & Molaro 2001)
- Determination of the H_2 molecular fraction in early galaxies (e.g. Petitjean, Srianand & Ledoux 2002).
- Abundances in DLAs to unprecedented high redshifts (e.g. Dessauges-Zavadsky et al. 2001) and of new elements (Ellison, Ryan & Prochaska 2001a).
- Chronicling the chemical enrichment history of galaxies from $z = 4$ to the present day (Prochaska, Gawiser & Wolfe 2001a; Pettini et al. 1999).
- Measuring the metal pollution of the Lyα forest and investigating its enrichment processes (e.g. Ellison et al. 2000)

Despite this significant progress, thanks in large part to echelle spectrographs on 8-m class telescopes such as UVES on the VLT, there remain many pressing questions about the chemical history of the early universe. For example, although much progress has been made in establishing sizeable abundance databases for studying nucleosynthesis histories of DLAs (Prochaska et al. 2001b), the time consuming nature of this work means that conclusions are still limited by small number statistics. Moreover, pushing QAL studies to the highest redshifts of QSOs now routinely found by surveys such as SDSS (Fan et al. 2001) requires extension into the infra-red domain.

7.4.2 Instrument Requirements

Simultaneous wavelength coverage from the blue atmospheric cut-off out to the H-band at medium-high spectral resolution would permit one-shot abundances for many elements in a large number of faint quasars. A dramatic improvement in sensitivity over UVES and large wavelength coverage would represent a huge boon for the field of early metal production by the first generations of stars and subsequent galactic chemical evolution. This is precisely the niche that X-shooter will exploit.

For example, exploration of new elemental abundances in QALs is an excellent complement to the study of Galactic metal poor stars. Pushing QAL surveys to fainter magnitudes will contribute to the quantification of dust production in early galaxies, an important factor in many fields of cosmology ranging from biasing in magnitude limited QSO surveys, the reddening mechanism of QSOs to calibrating the supernova distance scale. Here, we explore in more detail a few of the potential fields where X-shooter will contribute.

7.4.3 Target Selection

Several large QSOs surveys that will provide extensive fodder for future QAL studies are already reaching maturity. The 2dF QSO survey is now almost complete and contains 25,000 southern targets, mostly at

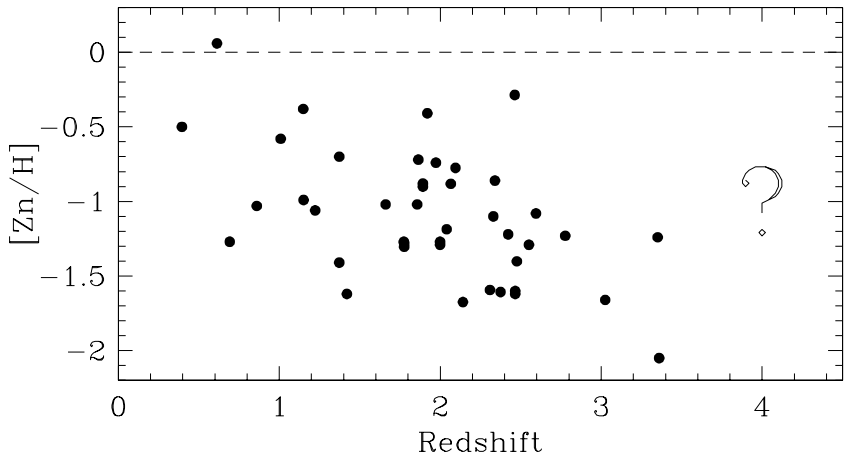

Figure 7.9 Redshift distribution of DLA metallicities from 43 literature measurements; there is little evolution between $1 < z < 3$. Exploring evolution at the high end of this redshift range by measuring [Zn/H] at $z > 3.5$ will be an important contribution from X-shooter.

$z < 2$. Pushing to higher redshifts is the Sloan Digital Sky Survey (SDSS) which will soon be announcing the first data release of a further 25,000 QSOs, a large fraction of which will be at $z > 2$. When complete, this number will increase to 100,000 QSOs, and all data will be available to the community by 2006. Extensive coverage of equatorial latitudes will provide a large database of high redshift QSOs that can be observed with ESO telescopes. Further on the horizon will be the ESO-run surveys associated with VISTA and VST which will be multi-wavelength programs on with some of the largest CCD mosaics available.

7.4.4 High Redshift Galaxy Abundances with DLAs

Damped Lyman Alpha systems (DLAs) represent the heavy-weight end of the H I column density distribution and are defined as those systems with neutral hydrogren column density N(H I) $> 2 \times 10^{20}$ atoms cm^{-2}. As the main reservoirs of neutral gas at high redshift, they have been logically associated with proto-galaxies. Echelle spectrographs, such as UVES, have played a critical role in advancing DLA abundance studies in specific areas where high resolution and S/N are essential, such as determining the primordial deuterium abundance (D'Odorico, Dessauges-Zavadsky & Molaro 2001; Pettini & Bowen 2001), investigating N/O ratios (Pettini et al. 2002) and molecular fractions (e.g. Petitjean, Srianand & Ledoux 2002). Through these and other similar studies we can piece together the history of star formation in galaxies at very early epochs. However, there are many cases when it is not necessary to resolve the absorption lines and this is where X-shooter can be best exploited.

DLA Metallicity as measured by [Zn/H]

The abundance of Zn is one of our most faithful indicators of DLA metallicity and is therefore a very promising tracer of chemical evolution through time (e.g. Pettini et al. 1994). Figure 7.9 illustrates the current knowledge of metallicity evolution in DLAs; it shows a spread of [Zn/H] at a given redshift and little change between $1.0 < z < 3.0$. There is a hint that the metallicity at $z > 3$ may drop significantly, but there are too few data points in this region to reach any firm conclusions. Given the combination of apertures, resolution and wavelength coverage of various telescope and instrument combinations, it is currently very challenging to obtain [Zn/H] for DLAs at $z_{abs} \gtrsim 3.5$ or towards QSOs with $V > 19$. Therefore, X-shooter will be required in order to exploit the large target lists from the latest generation

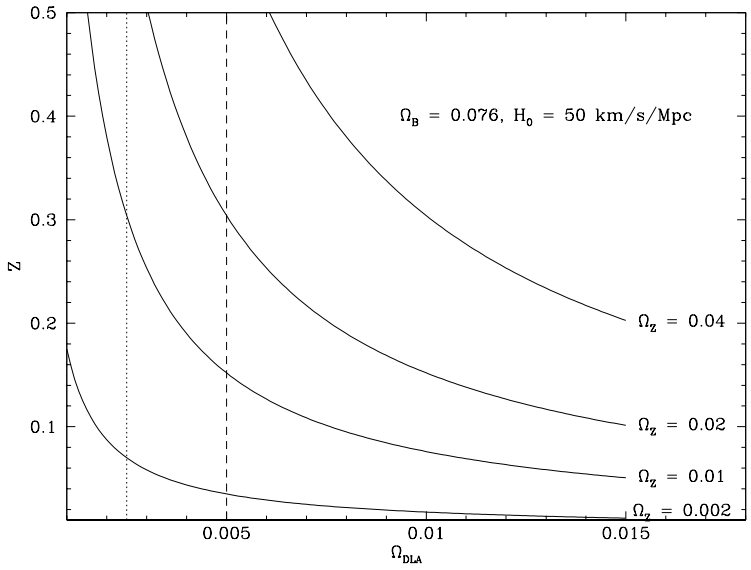

Figure 7.10 The combination of Ω_{DLA} and typical DLA metallicity can be used to calculate the mass density of metals in DLAs, Ω_Z. From the cosmic star formation rate, it can be shown that the total Ω_Z can reach 0.04 (1/25 solar metallicity) by $z \sim 2.5$. From this figure, it can be seen that combining the Ω_{DLA} derived from bright galaxies (dotted line) with the corresponding metallicity, $Z \sim 0.07$, only yields $\Omega_Z \sim 0.002$. If Ω_{DLA} is actually twice as large (e.g. the CORALS survey, Ellison et al. 2001b) as shown by the dashed line, and metallicity similarly underestimated, DLAs could account for at least 25% of the cosmic metal content.

of deep, wide and multiwavelength QSO surveys such as SDSS, 2dF and ChaMP (Chandra), which often comprise faint, high redshift targets. It is important to realise that since the Zn II lines are unsaturated, [Zn/H] can be derived from a simple equivalent width conversion of unresolved transitions and therefore moderate resolution spectrographs with broad wavelength coverage on large telescopes can make a significant impact on this problem, a possibility which we illustrate with two simple examples.

Example 1: Is the lack of evolution of DLA metallicity due to dust bias in current samples whereby metal-rich, dusty absorbers have hidden background QSOs from view (e.g. Fall & Pei 1993)? That is, are DLAs towards *bright* QSOs a fair representation of galaxies at a given epoch? Although calculations have shown that there has been sufficient star formation by $z \sim 2.5$ to enrich the entire baryonic content of the universe to 1/25 $Z_\odot$ (e.g. Pettini 1999), a census of metals in the early universe can so far only account for a small fraction of this. Observations of DLAs towards fainter QSOs, such as those in complete and unbiased surveys (e.g. CORALS, Ellison et al. 2001b) could determine if a significant fraction of these metals could be at large in chemically mature, dusty absorption systems (see Fig. 7.10). Such observations are not feasible with UVES due to the faintness of the majority of QSOs in optically complete samples, but would be readily addressed by X-shooter. For example, for a typical $z = 2.5$ DLA with log N(H I) = 20.6, a 3 σ limit of 1/15 $Z_\odot$ at $R \sim 7000$ requires S/N ~ 45. With X-shooter, this could be achieved for a B=20 QSO in approximately 2 hours. **Using the example of CORALS (Ellison et al. 2001b), the first survey of DLAs in an optically complete QSO sample, abundances for the entire DLA sample could be completed in approximately 5 nights using X-shooter.** This would be the first unbiased census of DLA metallicity.

Question 2: It is feasible to suppose that 'pristine' galaxies must have existed at some early epoch. By pushing to higher redshifts can we identify super-metal poor DLAs? If so, these would be extremely important laboratories for early chemical evolution studies, similar to very metal poor stars and galaxies, like IZw18. Alternatively, are there mechanisms that pre-enrich galactic interstellar media (e.g. Ellison et al. 2000)? A simple search of the SDSS EDR reveals 101 $z > 3.5$ QSOs (many of which are in the Sloan equatorial band) and this number will increase by at least a factor of 20 by the end of the survey.

This will be one of the most important sources for the identification of very high redshift DLAs. In order to study the abundances of the same elements typically targeted in $z \sim 2.5$ DLAs, observers will have to extend into the near-IR regime, in particular, to trace the metallicity evolution of DLAs via the Zn II transitions at $\lambda \sim 2000$ Å. Although [Fe/H] has been tracked out to $z \sim 4$ (Prochaska, Gawiser & Wolfe 2001a), there is the perennial concern that dust will affect the abundance measurement of iron. With wavelength coverage extending to the H-band, X-shooter could cover Zn II transitions out to an arbitrarily high redshift. At $z > 4$, the Zn II transitions fall in the J band. For a log N(HI)=20.8 DLA at $z = 4.5$ towards a J=17 QSO (typically, QSOs have $B - J > 1.5$) a S/N=70 would be required to achieve a 1/50 $Z_\odot$ 3σ ([Zn/H]= -1.7) detection limit, achievable with an exposure time of approximately 3 hours on X-shooter. **A sample of the order of 10 $z > 4$ DLAs would already yield meaningful limits on the evolution of Zn at high redshifts. This science goal could be achieved with 4–5 nights of time on the X-shooter.**

Access to New Elements

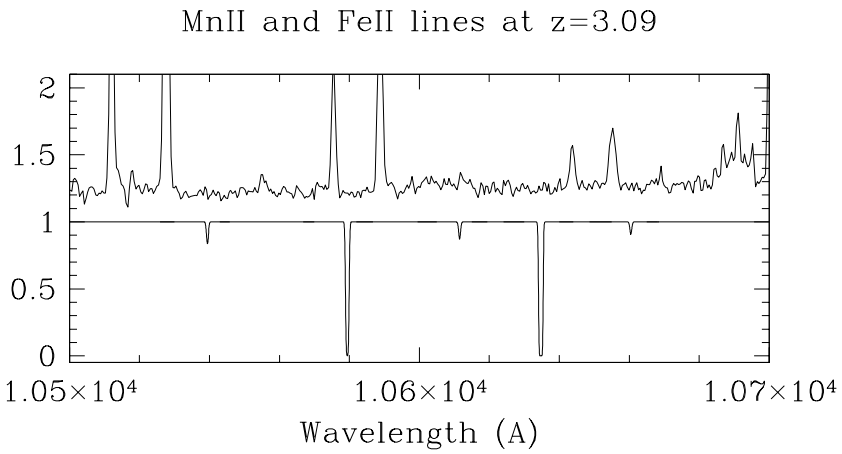

Figure 7.11 An example of a synthetic absorption spectrum convolved with the resolution of X-shooter for a single component system at $z = 3.09$, log N(HI)=20.5, $Z = 1/30 Z_\odot$, $b = 10.0$ km/s. The Mn II λ2576, 2594, 2606 triplet is shown, as well as Fe II λ2586 and Fe II λ2600. Overplotted (and shifted vertically for clarity) is a spectrum of the night sky – careful selection will place absorption lines between the bright night sky lines.

With the extension to new wavelength ranges, so comes the possibility of covering new elements with rest frame optical transitions *simultaneously with rest frame UV transitions*. Extending to the IR, for carefully selected regions with few sky lines, allows us to study the same elements for high redshift DLAs as have previously been targetted for more nearby galaxies, such as Ca and Na. Although these particular lines are generally strong and therefore maybe saturated, they may be useful for pre-selection of very low redshift DLA candidates, in the same way that Mg II absorbers are currently used to select $0.4 < z < 1.5$ DLA candidates. Ca or Na lines could be used to extend this idea to even lower redshifts where the gas properties of DLAs are poorly constrained, but calibration with known (i.e. higher z) DLAs is first needed. Moreover, Na and Ca could be used to further probe the dust properties of DLAs, since Ca is extremely prone to depletion, and in the Milky Way Na I correlates with optical extinction. There are also certain key elements that may provide further insight into the dust/nucleosynthesis degeneracy, such as Ti and Mn. These elements have so far posed problems for instruments like UVES due to their red rest wavelengths which can only be studied at relatively low redshifts. Mn and Ti can be used to investigate α/Fe-peak and odd-even trends, even in the presence of dust depletion (Dessauges-Zavadsky, Prochaska & D'Odorico 2002). By carefully selecting systems where important transitions fall between night sky lines, X-shooter will be able to determine abundances for many more DLAs,

including those at high z (e.g. Fig. 7.11). Finally, the one shot wavelength coverage from the UV to H-band of X-shooter will permit the chemical profiling of individual DLAs for many (> 10) elements at once. This will allow us to establish a uniform abundance database of many elements covering the same metals for each DLA (again possible due to the broad wavelength coverage).

7.4.5 Abundances in the Intergalactic Medium

In addition to large galactic structures, QSO absorption lines can also be used to probe the IGM via the Lyα forest. High quality echelle spectra have permitted detailed studies of the $z \sim 3$ IGM, which conclude that metal enrichment is already well-advanced and wide-spread at these early epochs (e.g. Ellison et al. 2000). As QSOs are found at ever increasing redshifts, and in significant numbers, thanks to surveys such as SDSS, so can our investigation of the IGM be extended backwards in time. Songaila (2001) has already pushed the limits out to $z \sim 5$, and although the statistics are still low for the highest redshifts, it appears that the bulk of Lyα forest enrichment occured prior to this epoch (see Fig. 7.12). **X-shooter's main design properties make it the ideal instrument for pushing the detection of intergalactic C IV to even higher redshifts: its red wavelength capability is essential for detection of CIV at $z > 5$, but its wide coverage will also cover much lower redshifts in one shot.** At these redshifts, the C IV doublet could be routinely detected down to column densities of log N(C IV)=13.3 with a S/N of only 30 (the exact limit is sensitive to contamination by sky lines). For a S/N of 70, achievable in 3 hours for J=17, column densities of N(C IV)=12.8 could be obtained, an order of magnitude deeper than the current limits of Songaila (2001).

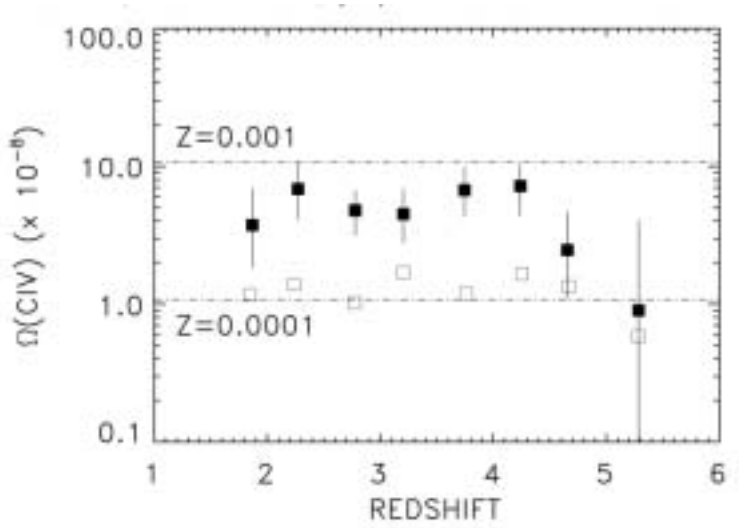

Figure 7.12 Redshift evolution of Ω(CIV), the mass density of CIV, for $12 < \log \mathrm{N(CIV)} < 15$ (filled points) and $13 < \log \mathrm{N(CIV)} < 14$ (open points). Taken from Songaila (2001).

In summary, X-shooter's moderate resolution and high efficiency are ideally suited to the determination of abundances at high z. Compared with current instruments, it offers the possibility of reaching targets several magnitudes fainter. Combined with the simultaneous optical and IR coverage, this permits exploitation of fainter QSOs (many at very high redshift) that are being uncovered in large numbers by new surveys.

7.5.1 Astrophysical Importance

The Intergalactic Medium as a Cosmological Probe

Our understanding of the Lyα forest has dramatically improved in the recent decade, both on the theoretical and the observational side. For redshifts accessible to ground observations, Lyα clouds outnumber any other known object and constitute an invaluable probe of the matter distribution in the universe. Most of the absorption arises in low density un-shocked gas, characterized by moderate over-densities and in ionization equilibrium with the metagalactic UV background. The interplay between the evolution of this medium and the galaxies is close: at $z > 1$ most of the baryons reside in the Lyman forest, acting as a reservoir for galaxy formation, while star formation influences the physical state of the IGM through metal enrichment and emission of ionizing radiation. It is therefore of fundamental cosmological interest to compare the spatial distribution of the intergalactic gas with that of galaxies (Pichon et al. 2001). Hydrodynamic cosmological simulations have been remarkably successful in reproducing the observed characteristics of the Lyman forest: from the column density and Doppler parameter distribution to the number density and effective opacity evolution (e.g. Davé et al. 1999; Bryan & Machacek 2000). Relatively simple physical processes govern the thermal state of the gas, which effectively traces the underlying distribution of dark matter. This allows to recover the mass power spectrum from the inversion of the observed Lyα forest spectra (e.g. Zaldarriaga et al. 2001; Nusser & Haehnelt 2000) and derive cosmological constraints that complement the observations of the CMB, SNIa and the large scale distribution of galaxies at low redshift. The Lyα forest is particularly valuable since it probes intermediate epochs and responds differently to variations of the cosmological parameters.

Simulations have shown that Lyα "clouds" are associated with filaments or large flattened structures (Miralda-Escudé et al. 1996; Davé et al. 1999) with typical mean scale of few comoving Mpc Observationally the sizes and spatial distribution of Lyα clouds can be probed in the velocity space by measuring their clustering along isolated lines of sight (LOS) or in the real space with multiple lines of sight across the sky. (see Fig. 7.14). Correlations in the Lyα forest have been detected with a $4-5\sigma$ confidence by various authors at typical scales $\Delta v \leq 350$ km s^{-1} observing at high resolution individual LOS (Kim, Cristiani & D'Odorico 2001 and references therein). This velocity range corresponds to scales $\lesssim 2.5 h_{70}^{-1}$ Mpc. Structures on larger scales (tens of Mpc) have been identified in the form of over-densities (Pando & Fang 1998) or under-densities/voids (Cristiani et al. 1997; Kim et al. 2001). In this observational approach, however, the 3-D information is convoluted with distortions in the redshift space, due to peculiar motions and thermal broadening.

Multiple LOS observations offer an invaluable alternative. Common absorption features in the spectra of multiply lensed quasars (Smette et al. 1992; 1995) indicate that the absorptions are produced in structures exceeding a few tens of kpc. Studies of close quasar pairs provide evidence for dimensions of a few hundred kpc (e.g. D'Odorico et al. 1998; Aracil et al. 2002). The analysis of the two point correlation function of the absorbers in a sample of 10 QSOs concentrated in a 1° diameter field suggests that a significant fraction of the Lyα forest arises in structures with a correlation scale of about 6–10 Mpc at $z \sim 2.6$ (Williger et al. 2000; Liske et al. 2000). Furthermore, the cross-correlation of spectra of QSO groups suffers much less than the auto-correlation from errors uncorrelated in different lines-of-sight, like those introduced by continuum fitting. These errors basically prevent any attempt of recovering the correct dark matter power spectrum on scales larger than $10-15h^{-1}$ Mpc from single line-of-sight observations (Viel et al. 2002).

The scale of physical interest is the Jeans length, $\lambda_c \sim (5\pi RT\Omega_b/3G\rho_{gas})^{0.5}$, which is of the order of 0.7 to 2 Mpc (comoving) for over-densities $\rho/\rho_o = 1$–5, characteristic of the N(HI) $\sim 10^{13}$ cm^{-2} absorption features in the Lyα forest. The corresponding angular separation on the sky scales from ~ 1

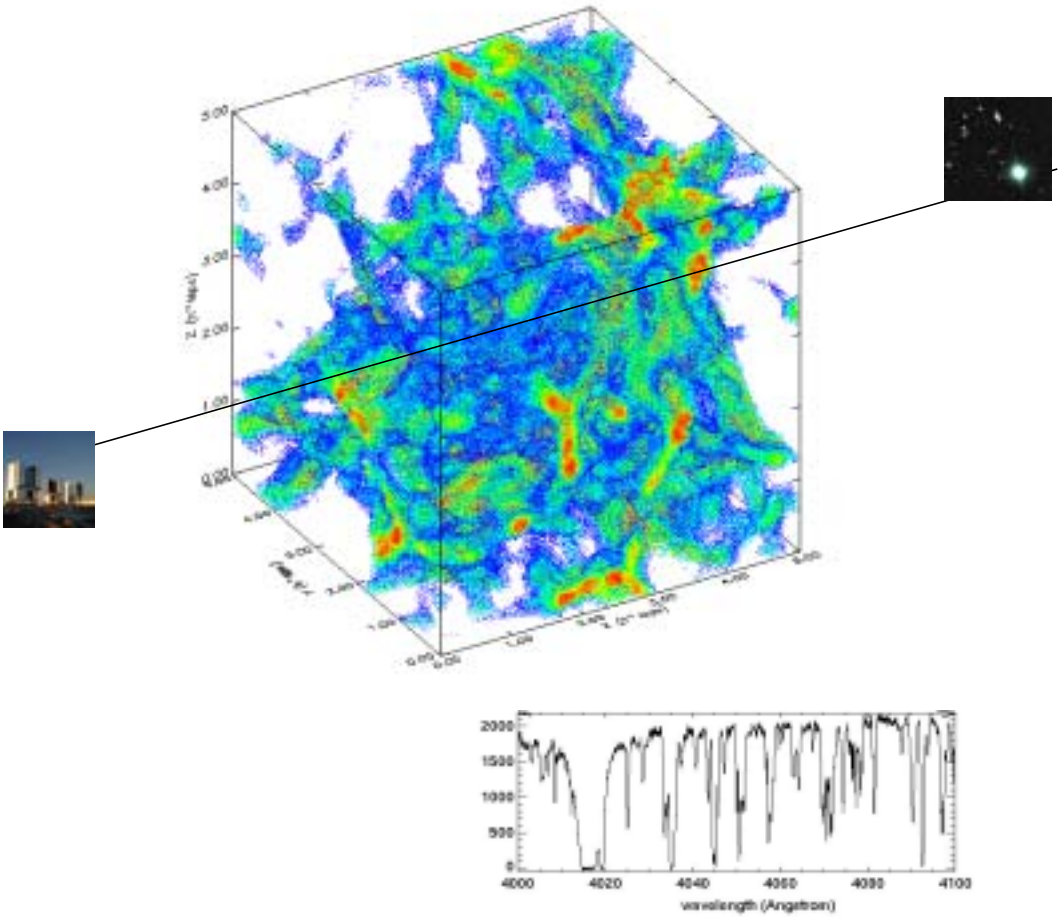

Figure 7.13 Dark matter distribution in a CDM simulation, at $z \sim 2$. Lighter regions are denser (logarithmic scale). A line of sight through the box is defined along the direction shown by the arrow (courtesy of M. Viel).

to a few arcmin. At this scale there should be a transition from smooth gas distribution which produces nearly identical absorption features in neighboring LOS to a correlated density distribution where the correlation strength decreases with increasing separation of the LOS.

Up to now the full exploitation of the potential offered by multiple QSO LOS has been limited by the dearth of groups of QSOs bright enough to make high resolution spectroscopy possible.

7.5.2 Target Selection

Recent QSO surveys (2dFQRS, SDSS) have provided large and dense samples of QSOs at high redshifts. However, when looking for small angular separations the quasar magnitudes often exceed the B or V $\simeq 20.5$ which are the approximate limits for high spectral resolution observations at an 8-10 m telescope. To measure the correlation of the Lyα absorptions typical statistical tools are the two-point correlation function and the step optical depth correlation function (Miralda-Escudé et al. 1996; Kim et al. 2001).

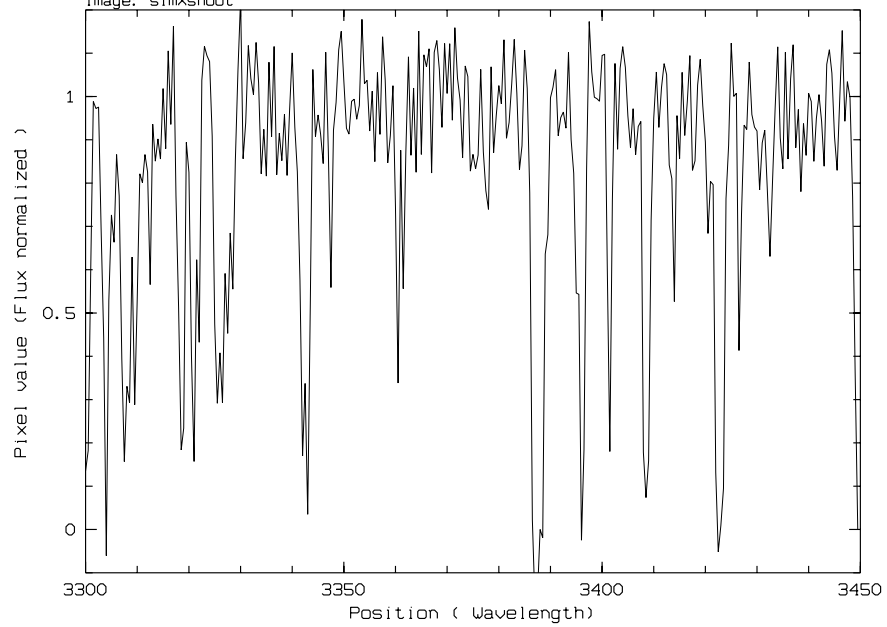

Figure 7.14 A typical spectrum of the Lyman forest of a $z \sim 2$ QSO at $R \sim 4000$ at a S/N $\simeq 7$ per resolution element. This is a small fraction of a 1 hr exposure of a $B \simeq 21.5$ QSO that could be obtained with X-shooter.

7.5.3 Instrument Requirements

A relatively high resolution is necessary to clearly define the line-free continuum, which is essential for measurements of optical depth. Spectral resolution and complete wavelength coverage including regions longward of the Lyα emission are also important to identify and remove metal lines falling in the Lyα forest, as well as to study the physical properties of the gas.

To extract the close groups from inhomogeneous catalogs (e.g. Véron-Cetty, and Véron, 2001) and from the new 2dFQRS and SDSS surveys it is necessary to reach magnitudes around $B \simeq 21.5$. In order to apply the standard methodology a S/N$\simeq 7$ per resolution element and a resolution $R \gtrsim 5000$ have to be reached. In this respect the UV sensitivity is important since it provides access to a lower redshift domain in which brighter and/or denser targets are easier to find.

At present, the ESO instrumentation shows a gap in this area of the parameter space: UVES is not sensitive enough and FORS resolution is too low (and, with the higher resolution grisms, the spectral range is too limited), FLAMES/GIRAFFE would provide the desired resolution but the limited spectral coverage in the individual exposures and the lack of UV-blue sensitivity are major drawbacks (as it is also the case of FORS). **All this demonstrates the necessity of a highly efficient and intermediate resolution ($R \gtrsim 5000$) spectrograph with a large spectral coverage extending into the UV.** At the moment, the only instrument with similar capabilities in the world is ESI at Keck. Its UV efficiency is however very poor and this makes it impossible to carry out a systematic study of QSO pairs in the $z = 2$–2.5 range.

7.5.4 X-shooter Performance

The proposed observations of the 3-D large scale structure represent an important verification of the results obtained along individual LOS (and of the corresponding assumptions) which presently favor a universe with $\Omega_m \simeq 0.4$ and $\Omega_\Lambda \simeq 0.6$ (Croft et al. 2002), close to the predictions of leading cosmological models, but different enough to create slight tensions on the parameter values when combined with other constraints.

The long-term goal is to carry out the Alcock-Paczyǹski test that bases the measurement of the geometry of the universe (with particular sensitivity to Ω_Λ) on the comparison between the 3-D correlation of neighboring QSO spectra and the clustering along the individual LOS. Rollinde et al. (2003)

have recently shown that the observations of at least 30 pairs at 2 arcmin separation, and 30 pairs at about 4–8 arcmin separation are needed to apply the Alcock-Paczyǹski test and determine the value of Ω_Λ with an accuracy of 15 %.

The time allocation to obtain the spectra of about 120 faint quasars with X-shooter would be of the order of 140 hr (see Fig. 7.14 and estimates from the ETC). X-shooter does provide the suitable trade-off between resolution, sensitivity and spectral range to carry out these observations in a reasonable amount of time, and would thus give the chance to get a unique cosmological result.

Bibliography

Akerlof, C. et al. 1999, Nature, 398, 400

Aracil, B. et al. 2002, A&A, 391, 1

Balbus, S. A. & Hawley, J. F. 2002, ApJ, 573, 749

Belczynski, K., Bulik, T. & Rudak, B. 2002, ApJ, 571, 394

Benetti, S. et al. 1994, A&A, 285, L13

Bergeron, P & Leggett S. K. 2002, ApJ, 580, 1070

Bloom, J. S., Kulkarni, S. R. & Djorgovski, S. G. 2002, AJ, 123, 1111

Bromm, V. et al. 2001, ApJ, 552, 464

Bryan, G. L. & Machacek, M. E. 2000, ApJ, 534, 57

Carollo, C. C. & Lilly, S. J. 2001, ApJ, 548, L153

Castro, S. et al. 2003, ApJ, 586, 128

Charlot, S. & Fall, M. S. 1993, ApJ, 415, 580

Cimatti, A. et al. 2002, A&A, 381, L68

Cole, S. et al. 2000, MNRAS, 319, 168

Courteau, S. & Sohn, Y.-J. 2002, in "The Mass of Galaxies at Low and High Redshift", ESO/USM Workshop, Venice, Oct. 2002, eds. Bender. R. & Renzini, A., Springer (astro-ph/0202267)

Cristiani, S. et al. 1997, MNRAS, 285, 209

Croft, R. A. C. et al. 2002, ApJ, 581, 20

Davé, R. et al. 1999, ApJ, 511, 521

Dessauges-Zavadsky, M. et al. 2001, A&A, 370, 426

Dessauges-Zavadsky, M., Prochaska, J. & D'Odorico, S. 2002, A&A, 391, 801

Djorgovski, S. G. et al. 2003, Proc. SPIE, vol. 4834, Ed. P. Guhathakurta, in press (astro-ph/0301342)

D'Odorico, S., Dessauges-Zavadsky, M. & Molaro, P. 2001, A&A, 368, L21

D'Odorico, V. et al. 1998, A&A, 339, 678

Dopita, M. A. & Evans, I. N. 1986, ApJ, 307, 431

Ellis, R. et al. 2001, ApJ, 560, L119

Ellison, S. et al. 2000, AJ, 120, 1175

Ellison, S., Ryan, S. & Prochaska, P. 2001a, MNRAS, 326, 628

Ellison, S. et al. 2001b, A&A, 379, 393

Fall, M. & Pei, Y. 1993, ApJ, 402, 479

Fan, X. et al. 2001, AJ, 122, 2833

Fernández, M. & Comerón, F. 2001, A&A, 380, 264

Fiore, F. et al. 2003, ApJ, submitted

Fosbury et al. 2002, in "The Mass of Galaxies at Low and High Redshift", ESO/USM Workshop, Venice, Oct. 2002, Bender, R. & Renzini, A. (Eds), Springer

Fox, D. W. 2002, GCN Circ., 1564

Fransson, C. & Kozma, C. 2002, New AR, 46, 487

Fruchter, A. et al. 1999, ApJ, 516, 683

Fynbo, J. et al. 2001, A&A, 374, 443

Galloway, D. K. et al. 2002, ApJ, 576, L137

Geballe, T. R. et al. 2002, ApJ, 564, 466

Gorosabel, J. et al. 2003, A&A, 400, 127

Groot, P. J., Rutten, R. G. M. & Van Paradijs, J. 2001, A&A, 368, 183

Hamuy, M. et al. 2002, AJ, 124, 417

Hansen, B. 1999, ApJ, 520, 680

Harris, H. et al. 1999, ApJ, 524, 1000

Harris, H. et al. 2001, ApJ, 549, L109

Heger, A. & Woosley, S.E. 2002, ApJ, 567, 532

Holden, B. P. et al. 2001, AJ, 122, 629

Horne, K. 1986, PASP, 98, 609

Israel, G. L. et al. 2002, A&A, 386, L13

Israelian, G. et al. 1999, Nature, 401, 142

Jonker, P. G. & Van der Klis, M. 2001, ApJ, 553, L43

Jonker, P. G. Van der Klis, M. & Groot, P. J. 2003, MNRAS, 339, 663

Kahabka, P., Pietsch, W. & Hasinger, G. 1994, A&A, 288, 538

Kauffmann, G., White, S. D. M. & Guiderdoni, B. 1993, MNRAS, 264, 201

Kennicutt, R. 1998, ESA–SP429, p. 81

Kim, T.-S., Cristiani, S. & D'Odorico, S. 2001, A&A, 373, 757

Lamb, D. Q. & Reichart, D. E. 2000, ApJ, 536, L1

Liske, J. et al. 2000, MNRAS, 311, 657

Livio, M. 2000, in *Type Ia Supernovae, Theory and Cosmology*, eds. Niemeyer, J. C & Truran, W. (Cambridge U. Press), p. 33

Lucy, L. B et al. 1991, in "The Tenth Santa Cruz Workshop", ed. Woosley, S. E., p. 82

Madau, P. & Rees, M. 2000, ApJL, 542, L69

Markwardt, C. B. et al. 2002, ApJ, 575, L21

Marsh, T. R. & Horne, K. 1988, MNRAS, 235, 269

Masetti, N. et al. 2003, GCN Circ., 1330

Matthews, K. et al. 1996, AJ, 112, 1678

Meikle, W. P. S. 2000, MNRAS, 314, 782

Melnick, J., Terlevich, R. & Terlevich, E. 1999, MNRAS, 311, 629

Menou, K., Perna, R. & Hernquist, L. 2002, ApJ, 564, L81

Miralda-Escudé, J. et al. 1996, ApJ, 471, 582

Moorwood, A. F. M. et al. 2000, A&A, 362, 9

Møller, P. & Fynbo, J. 2001, A&A, 372, L57

Nusser, A. & Haehnelt, M. 2000, MNRAS, 313, 364

Oppenheimer, B. R. et al. 2001, Science, 292, 698

Orosz, J. A. 2002, in *A Massive Star Odyssey, from Main Sequence to Supernova*, eds. van der Hucht, K. A., Herraro, A. & Esteban, C. (astro-ph/0209041)

Pando, J. & Fang, L.-Z. 1998, A&A, 340, 335

Peebles, P. J. E. 2001, astro-ph/0201015

Perna, R. & Loeb, A. 1998, ApJ, 503, L135

Petitjean, P., Srianand, R. & Ledoux, C. 2002, MNRAS, 332, 383

Pettini, M. et al. 1994, ApJ, 426, 79

Pettini, M. et al. 1997, ApJ, 486, 665

Pettini, M. 1999, in "Chemical Evolution from Zero to High Redshift", Proceedings of the ESO Workshop, p. 233

Pettini, M. et al. 1999, ApJ, 510, 576

Pettini, M. et al. 2001, ApJ, 554, 981

Pettini, M. & Bowen, D. 2001, ApJ, 560, 41

Pettini, M. et al. 2002, A&A, 391, 21

Pichon, C. et al. 2001, MNRAS, 326, 597

Price, P. et al. 2002, GCN Circ., 1340

Prochaska, J., Gawiser, E. & Wolfe, A. 2001a, ApJ, 552, 99

Prochaska, J. et al. 2001b, ApJS, 137, 21

Renzini, A. 1999, astro-ph/9902108

Renzini, A. & Cimatti, A. 1999, astro-ph/9910162

Riess, A. G. et al. 1998, AJ, 116, 1009

Riess, A. G. et al. 1999, AJ, 118, 2675

Rigopolou, D. et al. 2002, ApJ, 580, 789

Rollinde, E. et al. 2003, MNRAS, in press (astro-ph/0302145)

Rousselot, P. et al. 2000, A&A 354, 1134

Ruiz, M. T., Leggett, S. K. & Allard, F. 1997, ApJ, 491, L107

Savaglio, S. et al. 2002, GCN Circ., 1633

Savaglio, S., Fall, S. M. & Fiore, F. 2003, ApJ, 585, 638

Schaerer, D. 2002, A&A, 382, 28

Smette, A. et al. 1992, ApJ, 389, 39; 1995, A&AS, 113, 199

Somerville, R. S., Primack, J. R. & Faber, S. M. 2001, MNRAS, 320, 504

Songaila, A. 2001, ApJ, 561, 153L

Steidel, C. C. & Hamilton, D. 1992, AJ, 104, 941

Stern, D. et al. 2002, AJ 123, 2223

Teplitz, H. I. et al. 2000, ApJ, 533, L65

Thorsett, S. E. & Chakrabarty, D. 1999, ApJ, 512, 288

Valls-Gabaud, D. 1993, ApJ, 419, 7

Vernet, J. & Cimatti, A. 2001, A&A, 380, 409

Véron-Cetty, M. P. & Véron, P. 2001, A&A, 374, 92

Viel, M. et al. 2002, MNRAS, 329, 848

Vietri, M. & Stella, L. 1998, ApJ, 507, L45

Vreeswijk, P. M. et al. 2001, A&A, 380, L21

Warner, B. & Woudt, P. A. 2002, PASP, 114, 129

Wheeler, J. C. & Benetti, S. 2000, 18^{th} Chapter of *Allen's Astrophysical Quantities*, IVth edition, ed. Cox, A. N., AIP Press, p. 451

Wijnands, R. A. D. & Van der Klis, M. 1998, Nature, 394, 344

Williger, G. M. et al. 2000, ApJ, 532, 77

Zaldarriaga, M., Hui, L. & Tegmark, M. 2001, ApJ, 557, 519

Zhang, W., Woosley, S. E. & MacFadyen, A. I. 2003, ApJ, 586, 356

CHAPTER A

Exposure Time Calculator for X-shooter

SECTION A.1

Purpose

The Consortium has developed an ETC for the X-shooter as a tool to simulate the performance of the instrument on a variety of targets and observing parameters. The ETC produces a plot of the signal-to-noise (S/N) and the simulated spectrum per spectral channel for a user-selected or provided input spectrum over a given wavelength interval. The spectral channel in the dispersion direction is the size of the physical pixel for the IR detector, and a binned pixel for the two optical CCD detectors. The signal is the integrated flux over the source profile perpendicular to the dispersion direction, as obtained by fitting the sum of a constant background and a scaled seeing profile using a least-squares technique. The noise is the standard deviation of this amplitude. Optionally, the software has can also give the S/N for any odd number of summed channels.

SECTION A.2

Technique

The signal is assumed to be obtained by fitting the model $E\{N(x)\} = fP(x) + s + d$ to the number of electrons in each of the possibly binned pixels in a column along the full length of the slit. s is the mean number of electrons per pixel from night sky emission, d is the mean number of electrons per pixel from dark current, and $fP(x)$ is the mean number of signal electrons from the point source at the pixel location x along the slit. $P(x)$ is the normalized seeing profile as transmitted by the slit. f is thus the total number of signal photons transmitted by the slit. The variance of $N(x)$ is $Var\{N(x)\} = fP(x)+b$, where $b = s+d+r^2+(gs)^2$. r is the r.m.s. read noise in electrons and g is the fractional flat-field error. The weight per pixel used in the least-squares fitting is $W(x) = 1/Var\{N(x)\}$. It is convenient to introduce $P_0 = [WP]/[W]$, where $[\cdot]$ indicates a summation over all pixels along the slit, and $Q(x) \equiv P(x) - P_0$. The least-squares solution is then simply $a = [WQN]/[WQ^2]$. Furthermore, it can be shown that $E\{a\} = f$ and $Var\{a\} = 1/[WQ^2]$. By definition the S/N is then given by $S/N \equiv E\{a\}/\sigma\{a\} = f[WQ^2]^{\frac{1}{2}}$.

The OH emission lines in the IR arm are given as a table of wavelengths and relative photon fluxes, so it is most useful to assume a Gaussian Line Spread Function in the dispersion direction, instead of a strict top-hat function with sharp edges. The equivalent width of the Gaussian must be equal to the width of the slit, implying that the Gaussian $\sigma = S/\sqrt{2\pi}$, where S is the slit width. In order to relate the angular scale to the wavelength scale we need to know the spectral dispersion as a function of wavelength. We assume that $d\theta/d\lambda = RS/\lambda$, where $R = 4600$, 7000, and 4500 for the UVB, VIS, and IR arms, respectively. We do not use the exact DQE along each order, as it is not yet known. Instead we use 80% of the DQE at the blaze wavelength for each order. The transmissions of the dichroic beam

splitters have been included.

SECTION A.3

Fixed Input

The slit is assumed to be 12.0 arcsec long. The telescope has an aperture of 49.21 m^2. The physical size of the CCD pixels in the UVB and VIS arms is 0.14 arcsec. The two CCDs are assumed to have a read noise of 2.5 electrons r.m.s and a dark current of 0.001 e/s per pixel. The pixel size of the IR detector is 0.31 arcsec. The read noise is assumed to be 10 electrons r.m.s. and the dark current is set to 0.01 e/s per pixel. In addition we have assumed a flat-field error of 0.1 % for both detector types.

The night-sky surface-brightness was kindly supplied by Reinhard Hanuschik (private communication) in the form of calibrated UVES spectra. They cover the range 3140 Å – 10376 Å with two gaps at 5770 Å – 5850 Å and 8540 Å – 8614 Å respectively. The night-sky surface-brightness for the IR arm is more uncertain. Relative photon fluxes from OH emission lines were taken from Rousselot et al. (2000, A&A 354, 1134). The absolute specific photon fluxes from the continuum at 1.25 μm and 1.67 μm were taken from a report, *Enabling a Giant Segmented Mirror Telescope for the Astronomical Community*, prepared for the New Initiatives Office (2001). In the lack of better data the continuum emission was assumed to be a power law defined by these two points. The OH emission lines were scaled in order to approximately reproduce the counts given by the ISAAC ETC for the J and H bands. In addition, a thermal continuum with a temperature of 288 K and en emissivity of 0.25 was added. This is, however, only important for wavelengths longer than about 1.8 μm. It should be noted that the count rate from the sky continuum at J is only 0.1 e/s per pixel for a slit width of 1 arcsec. This is larger than the dark current, but not by a large factor.

The atmospheric extinction coefficients from 3000 Å to 8200 Å at 200 Å intervals, and the atmospheric transmissions from 8146 Å to 20000 Å at 0.7/1.5 Å intervals were kindly made available by P. Ballester (private communication). An average airmass of 1.2 is assumed.

SECTION A.4

User Input

The user must submit the following input parameters: (1) *exposure time* for a single sub-exposure, t_{exp}, (2) *type* of source spectrum (power-law, black-body, or user supplied template) and a *numerical* value (spectral index, temperature, width of band-pass used to normalize the template), (3) the *AB magnitude*, m_{AB}, of the source, (4) the *wavelength*, λ_{AB}, where m_{AB} is defined, (5) *lower limit* of the plotted wavelength range, λ_{min}, (6) *upper limit* of the plotted wavelength range, λ_{max}, (7) *slit width*, (8) the *FWHM* of the Gaussian seeing profile, (9) on-chip binning in the *dispersion direction*, (10) on-chip binning in the *spatial direction*, (11) a *post-detector binning* of the S/N, and finally (12) the *number* of sub-exposures, N.

The source spectrum is specified by giving the spectral index as *Pn.nn* for a power-law, the temperature as *Bnnnn* for a black-body spectrum, or the FWHM of a photometric band-pass as *Tnn.n* for a spectral template. The spectral index is defined as $-dlogf_\nu/dlog\nu$. A band-pass of the form $exp\{-ln(2)[2(\lambda-\lambda_c)/\mathrm{FWHM}]^4\}$ is used to normalize the template supplied by the user. The template must be supplied with λ (in Å) in the first column and f_λ (in arbitrary units) in the second column. Note, the ETC will not red-shift the template.

The AB magnitude is defined as $m_{AB} = -2.5logf_\nu - 48.60$, where f_ν should be given in units of erg $s^{-1}cm^{-2}$ Hz^{-1}. λ_{AB}, λ_{min}, and λ_{max} should all be given in Angstrom. The slit width and the FWHM of the Gaussian PSF should be given in arcsec. The projected pixel size is 0.14 arcsec in the UVB and VIS arms, so binning a factor of two in both directions, in order to reduce the influence of read noise, is recommended under normal seeing conditions. In the IR arm pixel binning is not possible, so the on-chip binning parameters are ignored.

The second last parameter offers a facility for doing a post-detector binning of the output S/N per (on-chip) binned pixel. It is done by convolving $(S/N)^2$ with a box of unit hight, followed by taking the square root. The length of the box must be an odd positive integer. Note that a length of 1 does nothing to the output. The total exposure time will often have to be split into N shorter sub-exposures. This is indicated by the last parameter.

SECTION A.5

An Example

As the X-shooter ETC is available via a procmail server the user must submit the input data by email. The user first receives a confirmation that the request has been accepted, and then an email containing a PostScript file with a plot of the S/N as a function of wavelength. The *subject* of the mail request must be **X-SHOOTER-ETC**, and the return email address must be given in the body of the mail. In addition the email must contain 12 parameter lines, with the parameters given in a strict order. A parameter line starts with the parameter value, followed by one or more white spaces. Each parameter line must contain the string **#;#**. The order of the parameters is specified in the following example:

- SEND MAIL TO: email address of the user
- 1800.0 #;# Exposure time of single sub-exposure in s
- T3.0 #;# Spectrum {P|B|T}{Index|T in K|FWHM in A}
- 21.5 #;# AB magnitude of source
- 3890.0 #;# Wavelength (in A) where AB mag is given
- 3754.95 #;# Lower limit wavelength in A
- 3904.95 #;# Upper limit wavelength in A
- 1.0 #;# Slit width in arcsec
- 0.7 #;# FWHM of (Gaussian) seeing in arcsec
- 1 #;# Detector binning in dispersion direction
- 2 #;# Detector binning in spatial direction
- 1 #;# Post-detector binning of signal-to-noise
- 3 #;# Number of sub-exposures used to calculate the S/N
- TEMPLATE SPECTRUM
- 3754.95 0.9955
- 3755.05 0.9917
- etc

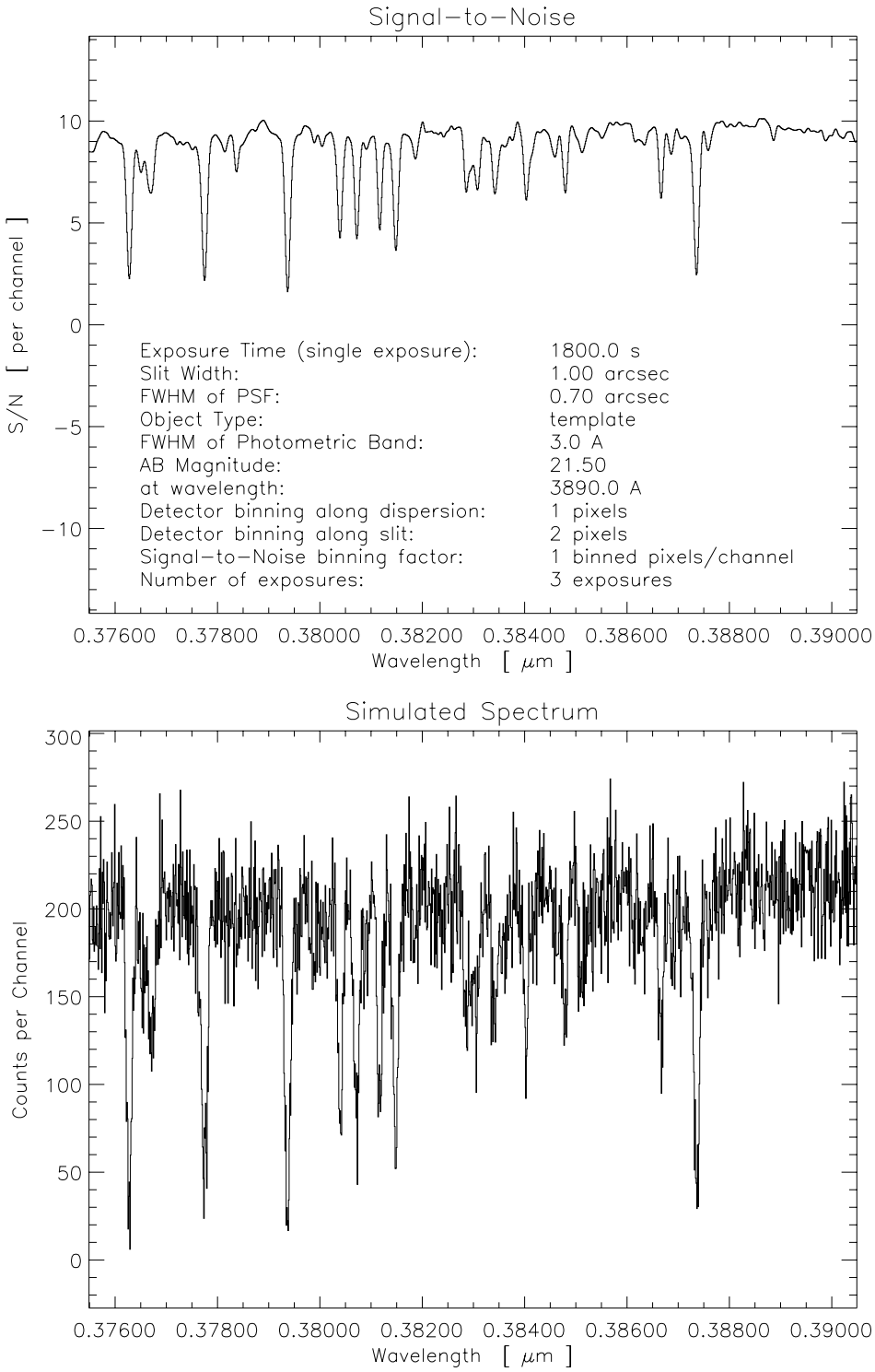

Figure A.1 Output from the X-shooter ETC, resulting from the input parameters given in the figure. The input spectrum was a simulated interval of a Lyα forest at $z \sim 2$ in the spectrum of a high redshift QSO (kindly provided by S. Bianchi).

Table A.1. Limiting Magnitudes for X-shooter

Case	U	B	V	R	I	J	H
A[a]	22.0	22.6	21.9	21.7	21.4	20.7	20.0
B[b]	25.3	26.0	25.4	25.3	24.9	24.0	23.3

[a] Limiting magnitudes per spectral resolution element. S/N = 10 for a 1 h integration in a seeing of $0\farcs7$ using a $1''$ slit. For the J and H band, exposures are split into three 20 min exposures.

[b] Limiting magnitudes for a spectrum rebinned to a resolution of 500. S/N = 5 for a total integration time of 10h, in a seeing of $0\farcs7$, using a $1''$ slit. For the U, B, V, R and I band, the exposures are split into 1 h integrations, while for the J and H band, exposures are split into 20 min exposures.

Following the 12 parameters you must append a *template spectrum* if a template type is indicated by the letter **T** in front of the second parameter (the FWHM of the photometric bandpass used to normalize the template spectrum). The line preceding the first line of the template spectrum must contain the string **TEMPLATE SPECTRUM**. All lines past this line must contain exactly two columns of ASCII numerical data, specifying the wavelength in Angstroms and the flux per wavelength in arbitrary units. The sampling of wavelengths must be uniform.

The output from the X-shooter ETC is a plot of the S/N for a spectral channel (Fig. A.1), defined as a column of (binned) pixels perpendicular to the dispersion direction, followed by a plot of a simulated spectrum. Both the S/N and the spectral counts are calculated for the sum of all sub-spectra extracted from the individual sub-exposures. The user should be aware that the S/N improves by (at least) a factor of $\sqrt{2}$ by on-chip binning (usually more, as the influence of read noise is reduced), as there is now twice the flux in the spectral channel. Because the S/N is given per spectral channel, one cannot directly compare the S/N to what you would obtain from e.g. the FORS ETC, since the spectral channels are much wider in FORS.

SECTION A.6

Limiting Magnitudes

The limiting magnitudes for a continuum source resulting from the ETC are given in Table A.1.